

FREE VIBRATION ANALYSIS OF UNIFORM OR TAPERED BEAMS
WITH TRANSVERSELY FUNCTIONALLY GRADED MATERIALS

A THESIS SUBMITTED TO
THE GRADUATE SCHOOL OF NATURAL AND APPLIED SCIENCES
OF
MIDDLE EAST TECHNICAL UNIVERSITY

BY

OKAN KOÇKAYA

IN PARTIAL FULFILLMENT OF THE REQUIREMENTS
FOR
THE DEGREE OF MASTER OF SCIENCE
IN
CIVIL ENGINEERING

FEBRUARY 2018

Approval of the thesis:

**FREE VIBRATION ANALYSIS OF UNIFORM OR TAPERED BEAMS
WITH TRANSVERSELY FUNCTIONALLY GRADED MATERIALS**

submitted by **OKAN KOÇKAYA** in partial fulfillment of the requirements for the degree of **Master of Science in Civil Engineering Department, Middle East Technical University** by,

Prof. Dr. Gülbin Dural Ünver
Dean, Graduate School of **Natural and Applied Sciences**

Prof. Dr. İsmail Özgür Yaman
Head of Department, **Civil Engineering**

Prof. Dr. Mehmet Utku
Supervisor, **Civil Engineering Dept., METU**

Prof. Dr. Afşin Sarıtaş
Co-Supervisor, **Civil Engineering Dept., METU**

Examining Committee Members

Prof. Dr. Ayşegül Askan Gündoğan
Civil Engineering Dept., METU

Prof. Dr. Mehmet Utku
Civil Engineering Dept., METU

Prof. Dr. Tekin Gültop
Civil Engineering Dept., Gazi University

Assoc. Prof. Dr. Yalın Arıcı
Civil Engineering Dept., METU

Assoc. Prof. Dr. Uğur Polat
Civil Engineering Dept., METU

Date: February 2, 2018

I hereby declare that all information in this document has been obtained and presented in accordance with academic rules and ethical conduct. I also declare that, as required by these rules and conduct, I have fully cited and referenced all material and results that are not original to this work.

Name, Last Name : Okan KOÇKAYA

Signature :

ABSTRACT

FREE VIBRATION ANALYSIS OF UNIFORM OR TAPERED BEAMS WITH TRANSVERSELY FUNCTIONALLY GRADED MATERIALS

Koçkaya, Okan

M.Sc., Department of Civil Engineering

Supervisor: Prof. Dr. Mehmet Utku

Co-Supervisor: Prof. Dr. Afşin Sarıtaş

February 2018, 106 pages

There are several analysis techniques in the literature for structural members with functionally graded material (FGM). Solutions based on theory of elasticity are the most common. Finite element approach with plate, shell or solid elements is an alternative popular solution technique. Beam elements are being recently used in the finite element approach for this purpose. Displacement (DB) and force based (FB) elements are the two main choices in this regard: while the FB method is a more recent approach, DB counterpart is the more commonly used technique. In this thesis, the proposed FB methodology for analyzing beams with FGM is verified using linear elastic free vibration analyses with comparison to the numerical results in the literature. The benchmark examples are selected solutions from the literature as well as the solution of the problem using the well-known and verified DB general purpose finite element code ANSYS. First five modal frequencies obtained using the proposed methodology are compared to the benchmark results for different cases. For the validation, uniform and tapered geometries are considered separately with homogeneous material and transversely distributed FGM. The effects of different boundary conditions and aspect ratios are taken into account.

Keywords: Functionally graded material, finite element method, beam finite element, force based method, vibration frequency

ÖZ

EKSENEL FONKSİYONEL DERECELENDİRİLMİŞ MALZEMELİ GEOMETRİSİ DEĞİŞEN YA DA DEĞİŞMEYEN KİRİŞLERİN SERBEST TİTREŞİM ANALİZİ

Koçkaya, Okan

Yüksek Lisans, İnşaat Mühendisliği Bölümü

Tez Yöneticisi: Prof. Dr. Mehmet Utku

Ortak Tez Yöneticisi: Prof. Dr. Afşin Sarıtaş

Şubat 2018, 106 sayfa

Fonksiyonel derecelendirilmiş malzeme (FDM) ile oluşturulan yapısal elemanlar için literatürde çeşitli analiz teknikleri vardır. Elastisite teorisine dayalı çözümler en yaygın olanıdır. Levha, kabuk ve katı elemanlarla sonlu elemanlar yöntemi alternatif bir popüler çözüm tekniğidir. Kiriş elemanları da son zamanlarda sonlu elemanlar yönteminde bu amaçla kullanılmaktadır. Deplasman (DB) ve kuvvet bazlı (KB) elemanlar, sonlu elemanlar yönteminde iki ana tercihtir: bu alanda KB yöntem yeni bir yaklaşım iken, DB yöntem daha sık kullanılmaktadır. Bu çalışmada, FDM ile oluşturulan kirişlerin analizi için önerilen KB metodolojisi, doğrusal elastik serbest titreşim analizleri kullanılarak literatürdeki sayısal sonuçlarla karşılaştırmalı olarak doğrulanmaktadır. Kıyaslama örnekleri, literatürdeki seçilmiş çözümlerin yanı sıra, iyi bilinen ve doğrulanmış deplasman bazlı genel amaçlı sonlu eleman kodunu kullanan ANSYS çözümlerinden oluşmaktadır. Önerilen metodoloji kullanılarak elde edilen ilk beş mod frekansı, farklı durumlar için kıyaslama sonuçları ile karşılaştırılmaktadır. Doğrulama için, değişmeyen ve değişen geometriler, homojen malzeme ve enine dağıtılmış FDM ayrı olarak göz önünde bulundurulmaktadır. Farklı sınır koşullarının ve en-boy oranlarının etkileri dikkate alınmaktadır.

Anahtar kelimeler: Fonksiyonel derecelendirilmiř malzeme, sonlu elemanlar yontemi, kiriř sonlu elemanı, kuvvet bazlı yontem, titreřim frekansı

To My Family

ACKNOWLEDGMENTS

I wish to express my profound gratitude to my supervisors Prof. Dr. Mehmet Utku and Prof. Dr. Afşin Sarıtaş for their continuous advice, support and encouragement. Their contributions are invaluable and this thesis could not have been completed without their guidance.

I would also like to express my deep gratitude to Assoc. Prof. Dr. Yalın Arıcı for his valuable suggestions and comments.

I would further like to express my gratitude to Prof. Dr. Oğuzhan Hasaebi and Prof. Dr. Yasin Dursun Sarı for their continuous support and valuable suggestions on my education career.

I would also like to thank my co-worker B. Feyza Soysal Albostan for her help whenever I needed.

I would like to acknowledge my friends Dr. Nefize Shaban, Dr. Murat Şahin, Dr. Mehmet Bakır Bozkurt, Muhammet Ali Özen, Serdar Özcan, Ersin Aktaş, Armin Taghipour, Milad Bybordiani, Mehmet Kemal Ardoęa, Utku Albostan, Reza Shabani, Salim Azak and Barıř Esen for their encouragement.

Last but not least, I must express my profound gratitude to my dear family for their understanding and endless support, especially my mother Ayşe Kokaya.

TABLE OF CONTENTS

ABSTRACT	v
ÖZ	vii
ACKNOWLEDGMENTS	x
LIST OF TABLES	xiii
LIST OF FIGURES	xv
LIST OF ABBREVIATIONS	xxii
CHAPTERS	
1. INTRODUCTION	1
1.1 GENERAL	1
1.2 LITERATURE REVIEW	3
1.3 OBJECTIVE AND SCOPE.....	4
2. MIXED BEAM ELEMENT FORMULATION	7
2.1 INTRODUCTION.....	7
2.2 KINEMATICS OF A BEAM ELEMENT	7
2.2.1 Displacement and Strain Fields.....	9
2.2.2 Coordinate Systems and Transformations	10
2.3 VARIATIONAL FORMULATION	14
2.4 FINITE ELEMENT FORMULATION AND SECTION RESPONSE	16
2.5 MATERIAL PROPERTIES.....	18
2.6 CONSISTENT MASS MATRIX.....	20
3. FREE VIBRATION ANALYSIS OF A BEAM WITH UNIFORM GEOMETRY	25

3.1	INTRODUCTION	25
3.2	VERIFICATION WITH UNIFORM GEOMETRY	26
3.2.1	Uniform Geometry with Homogeneous Material	28
3.2.1.1	The First Numerical Example.....	28
3.2.1.2	The Second Numerical Example	32
3.2.1.3	The Third Numerical Example	46
3.2.2	Uniform Geometry with Functionally Graded Materials.....	53
3.2.2.1	The Fourth Numerical Example	54
3.2.2.2	The Fifth Numerical Example	57
3.2.2.3	The Sixth Numerical Example	67
4.	FREE VIBRATION ANALYSIS OF A BEAM WITH TAPERED GEOMETRY	73
4.1	INTRODUCTION	73
4.2	VERIFICATION WITH TAPERED GEOMETRY	74
4.2.1	Tapered Geometry with Homogeneous Material	76
4.2.1.1	The Seventh Numerical Example.....	76
4.2.2	Tapered Geometry with Functionally Graded Materials.....	85
4.2.2.1	The Eighth Numerical Example	86
5.	CONCLUSIONS	97
5.1	SUMMARY.....	97
5.2	CONCLUSIONS	98
5.3	FUTURE RESEARCH DIRECTIONS	100
	BIBLIOGRAPHY	103

LIST OF TABLES

TABLES

Table 2.1 Strong and weak satisfaction of parameters in variational principles.....	14
Table 3.1 The summary of the numerical examples for beams with uniform geometry	27
Table 3.2 The properties of the uniform beam element with pure aluminum.....	29
Table 3.3 The percent differences of frequencies for calculation with two different factors, 1 and 5/6 when $n_e = 32$	32
Table 3.4 The properties of the uniform beam element with pure alumina and aluminum	33
Table 3.5 The comparison of the number of elements obtained using ANSYS and ANSYS with AMR for two different parameters with the ceramic material.....	45
Table 3.6 The difference in percent of the fundamental frequencies between ANSYS and ANSYS with AMR for three different parameters.....	46
Table 3.7 The difference in percent of the higher modes between ANSYS and ANSYS with AMR for $L/h = 5$	48
Table 3.8 The difference in percent of the higher modes between ANSYS and ANSYS with AMR for $L/h = 20$	49
Table 3.9 The properties of the uniform beam element with FGM in particular at the topmost and bottommost materials	55
Table 3.10 The properties of the uniform beam element with FGM in particular at the topmost and bottommost materials	58
Table 3.11 The properties of the uniform beam element with FGM in particular at the topmost and bottommost materials	68
Table 4.1 The summary of the numerical examples for beams with tapered geometry	75
Table 4.2 The properties of the tapered beam element with pure steel.....	77

Table 4.3 The geometric parameters of the tapered beam element with pure steel ...	77
Table 4.4 The frequency information for the first five modes, C-F beam, $L/h_R = 10$	78
Table 4.5 The properties of the tapered beam element with FGM in particular at the topmost and bottommost materials	86
Table 4.6 The geometric parameters of the tapered beam element with FGM	87
Table 4.7 The Young's modulus and the density values along the transverse direction with $k = 0.5$	88
Table 4.8 The frequency information for the higher modes with $L/h = 10$ and 20	89
Table 4.9 The frequencies obtained using FB and ANSYS, C-F beam, material FGM, aspect ratios $L/h_R = 10$, taper ratio $h_L/h_R = 2$, power law coefficient $k = 0.5$	94
Table 4.10 The frequencies obtained using FB and ANSYS, C-F beam, material FGM, aspect ratios $L/h_R = 20$, taper ratio $h_L/h_R = 2$, power law coefficient $k = 0.5$	95

LIST OF FIGURES

FIGURES

Figure 1.1 Schematic of continuously graded microstructure with metal ceramic constituents (a) Smoothly graded microstructure (b) Enlarged view and (c) Ceramic metal FGM Jha et al. [2]	2
Figure 2.1 A uniform geometry beam and the corresponding coordinates.....	9
Figure 2.2 Element forces and deformations in basic system.....	11
Figure 2.3 Element end forces and displacements in two node complete system	11
Figure 2.4 Section forces in cantilever basic system	13
Figure 2.5 Uniformly distributed element loadings in x-z directions	13
Figure 2.6 A functionally graded material in x-z plane	19
Figure 2.7 Material variations along transverse direction.....	20
Figure 3.1 A uniform geometry beam element with homogeneous material in x-z plane	28
Figure 3.2 The comparison of the fundamental frequency obtained using FB and Sina et al. [33], S-S beam, material aluminum, with increasing number of elements in the solution.....	30
Figure 3.3 The comparison of the fundamental frequency obtained using FB and ANSYS, S-S beam, material aluminum, with increasing number of elements in the solution.....	31
Figure 3.4 The comparison of the fundamental frequency obtained using FB and Şimşek [32], C-F beam, material ceramic, with increasing number of elements in the solution.....	36
Figure 3.5 The comparison of the fundamental frequency obtained using FB and Şimşek [32], C-F beam, material metal, with increasing number of elements in the solution.....	36

Figure 3.6 The comparison of the fundamental frequency obtained using FB and Şimşek [32], C-C beam, material ceramic, with increasing number of elements in the solution.....	37
Figure 3.7 The comparison of the fundamental frequency obtained using FB and Şimşek [32], C-C beam, material metal, with increasing number of elements in the solution.....	37
Figure 3.8 The comparison of the fundamental frequency obtained using FB and Şimşek [32], S-S beam, material ceramic, with increasing number of elements in the solution.....	38
Figure 3.9 The comparison of the fundamental frequency obtained using FB and Şimşek [32], S-S beam, material metal, with increasing number of elements in the solution.....	38
Figure 3.10 The comparison of the fundamental frequency obtained using FB and ANSYS, C-F beam, material ceramic, with increasing number of elements in the solution.....	39
Figure 3.11 The comparison of the fundamental frequency obtained using FB and ANSYS, C-C beam, material ceramic, with increasing number of elements in the solution.....	39
Figure 3.12 The comparison of the fundamental frequency obtained using FB and ANSYS, S-S beam, material ceramic, with increasing number of elements in the solution.....	40
Figure 3.13 The comparison of the fundamental frequency obtained using FB and Şimşek [32], material ceramic, aspect ratio $L/h=5$, with increasing number of elements in the solution.....	41
Figure 3.14 The comparison of the fundamental frequency obtained using FB and ANSYS, material ceramic, aspect ratio $L/h=5$, with increasing number of elements in the solution.....	42
Figure 3.15 The comparison of the fundamental frequency obtained using FB and Şimşek [32], material ceramic, aspect ratio $L/h=20$, with increasing number of elements in the solution.....	42

Figure 3.16 The comparison of the fundamental frequency obtained using FB and ANSYS, material ceramic, aspect ratio $L/h=20$, with increasing number of elements in the solution.....	43
Figure 3.17 The mesh refinement with +75 relevance factor for C-F and C-C beams, material ceramic, $L/h = 5$, number of elements 186	44
Figure 3.18 The mesh refinement with AMR for C-F beam, material ceramic, $L/h = 5$, left side fixed, number of elements 654	44
Figure 3.19 The mesh refinement with AMR for C-C beam, material ceramic, $L/h = 5$, number of elements 706.....	45
Figure 3.20 The comparison of the frequencies for the higher modes obtained from FB and ANSYS, C-F beam, material ceramic, aspect ratio $L/h = 5$, with increasing number of elements in the solution	47
Figure 3.21 The comparison of the frequencies for the higher modes obtained from FB and ANSYS, C-F beam, material ceramic, aspect ratio $L/h = 20$, with increasing number of elements in the solution	48
Figure 3.22 The ratio of 1 st bending mode frequency obtained from FB and ANSYS, C-F beam, material ceramic, with increasing number of elements in the solution....	50
Figure 3.23 The ratio of 2 nd bending mode frequency obtained from FB and ANSYS, C-F beam, material ceramic, with increasing number of elements in the solution....	51
Figure 3.24 The ratio of 3 rd bending mode frequency obtained from FB and ANSYS, C-F beam, material ceramic, with increasing number of elements in the solution....	51
Figure 3.25 The ratio of 4 th bending mode frequency obtained from FB and ANSYS, C-F beam, material ceramic, with increasing number of elements in the solution....	52
Figure 3.26 The ratio of 1 st axial mode frequency obtained from FB and ANSYS, C-F beam, material ceramic, with increasing number of elements in the solution	53
Figure 3.27 A uniform geometry beam element with FGM in x-z plane	54
Figure 3.28 The comparison of the fundamental frequency obtained using FB and Sina et al. [33], material FGM, number of elements $n_e = 32$, power law coefficient $k = 0.3$	56
Figure 3.29 The comparison of the fundamental frequency obtained using FB and Şimşek [32], material FGM, number of elements $n_e = 32$, power law coefficient $k = 0.3$	57

Figure 3.30 The comparison of the fundamental frequency obtained by FB and Şimşek [32], C-F beam, material FGM, aspect ratio $L/h = 5$, with increasing number of elements in the solution.....	59
Figure 3.31 The comparison of the fundamental frequency obtained by FB and Şimşek [32], C-C beam, material FGM, aspect ratio $L/h = 5$, with increasing number of elements in the solution.....	60
Figure 3.32 The comparison of the fundamental frequency obtained by FB and Şimşek [32], S-S beam, material FGM, aspect ratio $L/h = 5$, with increasing number of elements in the solution.....	60
Figure 3.33 The comparison of the fundamental frequency obtained by FB and Şimşek [32], C-F beam, material FGM, aspect ratio $L/h = 20$, with increasing number of elements in the solution.....	61
Figure 3.34 The comparison of the fundamental frequency obtained by FB and Şimşek [32], C-C beam, material FGM, aspect ratio $L/h = 20$, with increasing number of elements in the solution.....	61
Figure 3.35 The comparison of the fundamental frequency obtained by FB and Şimşek [32], S-S beam, material FGM, aspect ratio $L/h = 20$, with increasing number of elements in the solution.....	62
Figure 3.36 The comparison of the fundamental frequency obtained by FB and Şimşek [32], C-F beam, material FGM, aspect ratio $L/h = 5$, number of elements $n_e = 8$ to 32	63
Figure 3.37 The comparison of the fundamental frequency obtained by FB and Şimşek [32], C-C beam, material FGM, aspect ratio $L/h = 5$, number of elements $n_e = 8$ to 32	63
Figure 3.38 The comparison of the fundamental frequency obtained by FB and Şimşek [32], S-S beam, material FGM, aspect ratio $L/h = 5$, number of elements $n_e = 8$ to 32	64
Figure 3.39 The comparison of the fundamental frequency obtained by FB and Şimşek [32], C-F beam, material FGM, aspect ratio $L/h = 20$, number of elements $n_e = 8$ to 32	64

Figure 3.40 The comparison of the fundamental frequency obtained by FB and Şimşek [32], C-C beam, material FGM, aspect ratio $L/h = 20$, number of elements $n_e = 8$ to 32	65
Figure 3.41 The comparison of the fundamental frequency obtained by FB and Şimşek [32], S-S beam, material FGM, aspect ratio $L/h = 20$, number of elements $n_e = 8$ to 32	65
Figure 3.42 The comparison of the fundamental frequency obtained by FB and Şimşek [32], aspect ratio $L/h = 20$, power law coefficient $k = 1$, with increasing number of elements in the solution.....	66
Figure 3.43 The comparison of the fundamental frequency obtained by FB and Şimşek [32], C-F beam, power law coefficient $k = 1$, with increasing number of elements in the solution	67
Figure 3.44 The comparison of the frequencies for the higher modes obtained by FB and Şimşek [32], S-S beam, aspect ratio $L/h = 4$, power law coefficient $k = 1$, with increasing number of elements in the solution.....	69
Figure 3.45 The comparison of the frequencies for the higher modes obtained by FB and Li [34], S-S beam, aspect ratio $L/h = 4$, power law coefficient $k = 1$, with increasing number of elements in the solution	70
Figure 3.46 The comparison of the frequencies for the higher modes obtained by FB and Şimşek [32], S-S beam, aspect ratio $L/h = 4$, power law coefficient $k = 1$, number of elements $n_e = 8$ to 128.....	70
Figure 3.47 The comparison of the frequencies for the higher modes between FB and Li [34], S-S beam, aspect ratio $L/h = 4$, power law coefficient $k = 1$, number of elements $n_e = 8$ to 128	71
Figure 4.1 Tapered beam element, linear taper with homogeneous material in x-z plane	76
Figure 4.2 The comparison of the frequencies for the higher modes obtained using FB and ANSYS, C-F beam, material steel, aspect ratio $L/h_R = 10$, taper ratio $h_L / h_R = 1$, with increasing number of elements in the solution.....	79
Figure 4.3 The comparison of the frequencies for the higher modes obtained using FB and ANSYS, C-F beam, material steel, aspect ratio $L/h_R = 10$, taper ratio $h_L / h_R = 2$, with increasing number of elements in the solution.....	80

Figure 4.4 The comparison of the frequencies for the higher modes obtained using FB and ANSYS, C-F beam, material steel, aspect ratio $L/h_R = 10$, taper ratio $h_L/h_R = 3$, with increasing number of elements in the solution.....	80
Figure 4.5 The comparison of the frequencies for the higher modes obtained using FB and ANSYS, C-F beam, material steel, aspect ratio $L/h_R = 10$, taper ratio $h_L/h_R = 4$, with increasing number of elements in the solution.....	81
Figure 4.6 The comparison of the frequencies for the higher modes obtained using FB and ANSYS, C-F beam, material steel, aspect ratio $L/h_R = 10$, taper ratio $h_L/h_R = 5$, with increasing number of elements in the solution.....	81
Figure 4.7 The ratio of 1 st bending mode frequency obtained from FB and ANSYS, C-F beam, material steel, with increasing number of elements in the solution	83
Figure 4.8 The ratio of 2 nd bending mode frequency obtained from FB and ANSYS, C-F beam, material steel, with increasing number of elements in the solution	83
Figure 4.9 The ratio of 3 rd bending mode frequency obtained from FB and ANSYS, C-F beam, material steel, with increasing number of elements in the solution	84
Figure 4.10 The ratio of 4 th bending mode frequency obtained from FB and ANSYS, C-F beam, material steel, with increasing number of elements in the solution	84
Figure 4.11 The ratio of 1 st axial mode frequency obtained from FB and ANSYS, C-F beam, material steel, with increasing number of elements in the solution.....	85
Figure 4.12 A tapered geometry beam element with FGM in x-z plane.....	86
Figure 4.13 The geometric model of ANSYS with 4 laminated layers	88
Figure 4.14 The comparison of the fundamental frequency obtained using FB and ANSYS, C-F beam, number of laminated layers 4, 10 and 20	89
Figure 4.15 The comparison of the frequencies for the higher modes obtained by FB and ANSYS, C-F beam, aspect ratio $L/h = 10$, number of laminated layers 20	90
Figure 4.16 The comparison of the frequencies for the higher modes obtained by FB and ANSYS, C-F beam, aspect ratio $L/h = 20$, number of laminated layers 20	91
Figure 4.17 The ratio of 1 st bending mode frequency obtained from FB and ANSYS, C-F beam, number of laminated layers 20	92
Figure 4.18 The ratio of 2 nd bending mode frequency obtained from FB and ANSYS, C-F beam, number of laminated layers 20	92

Figure 4.19 The ratio of 3 rd bending mode frequency obtained from FB and ANSYS, C-F beam, number of laminated layers 20	93
Figure 4.20 The ratio of 4 th bending mode frequency obtained from FB and ANSYS, C-F beam, number of laminated layers 20	93
Figure 4.21 The ratio of 1 st axial mode frequency obtained from FB and ANSYS, C-F beam, number of laminated layers 20	94

LIST OF ABBREVIATIONS

2D	Two Dimensional
3D	Three Dimensional
AMR	Adaptive Mesh Refinement
C-C	Clamped-Clamped
C-F	Clamped-Free
DB	Displacement Based
FB	Force Based
FGM	Functionally Graded Material
P-P	Pinned-Pinned
S-S	Simply-Supported

CHAPTER 1

INTRODUCTION

1.1 GENERAL

Understanding material behavior is crucial to provide comfortable, secure and healthy environment for multiple generations. Hence, the role of materials in daily life is very significant. New developments in engineering help to understand material behavior and using them in several application areas improves human life quality and duration. Nowadays, with the exponential growth of research and development in biomedical industry, it is even possible to replicate some parts of the human body. To make them compatible with other parts, the functionality of human body needs to be understood well. Moreover, human body parts need to adapt to different conditions quickly in order to survive longer. Adaptation can be achieved with functionality. The use of new technological devices in medical industry shows that most of the human body parts consists of Functionally Graded Materials (FGMs) such as bones and teeth. These are under the category of organic forms of FGMs. FGMs with inorganic forms are widely used in different application areas such as the aerospace, armory, automobile, communication, defense, electronics, energy industries etc.

FGMs are special types of composite materials with continuous variation of two or more materials. Delamination problems of composite materials are avoided by the use of FGMs in several industries. Advances in manufacturing techniques reduced the manufacturing cost of FGMs leading to an increased popularity of the FGMs in recent years. From a civil engineering point of view, static and dynamic characteristics behavior of FGMs attract interest in research studies.

FGMs were divided into three types by Mahamood and Akinlabi [1] with respect to their gradient structure; i.e. chemical composition gradient, porosity gradient and microstructural gradient FGMs. The properties of beams with microstructural gradient FGM are investigated in this thesis. According to [1], microstructure is located within another material to provide gradual change during the process of solidification in order to obtain continuous gradation with FGMs. Figure 1.1 provides a continuously graded microstructure with metal and ceramic volumes.

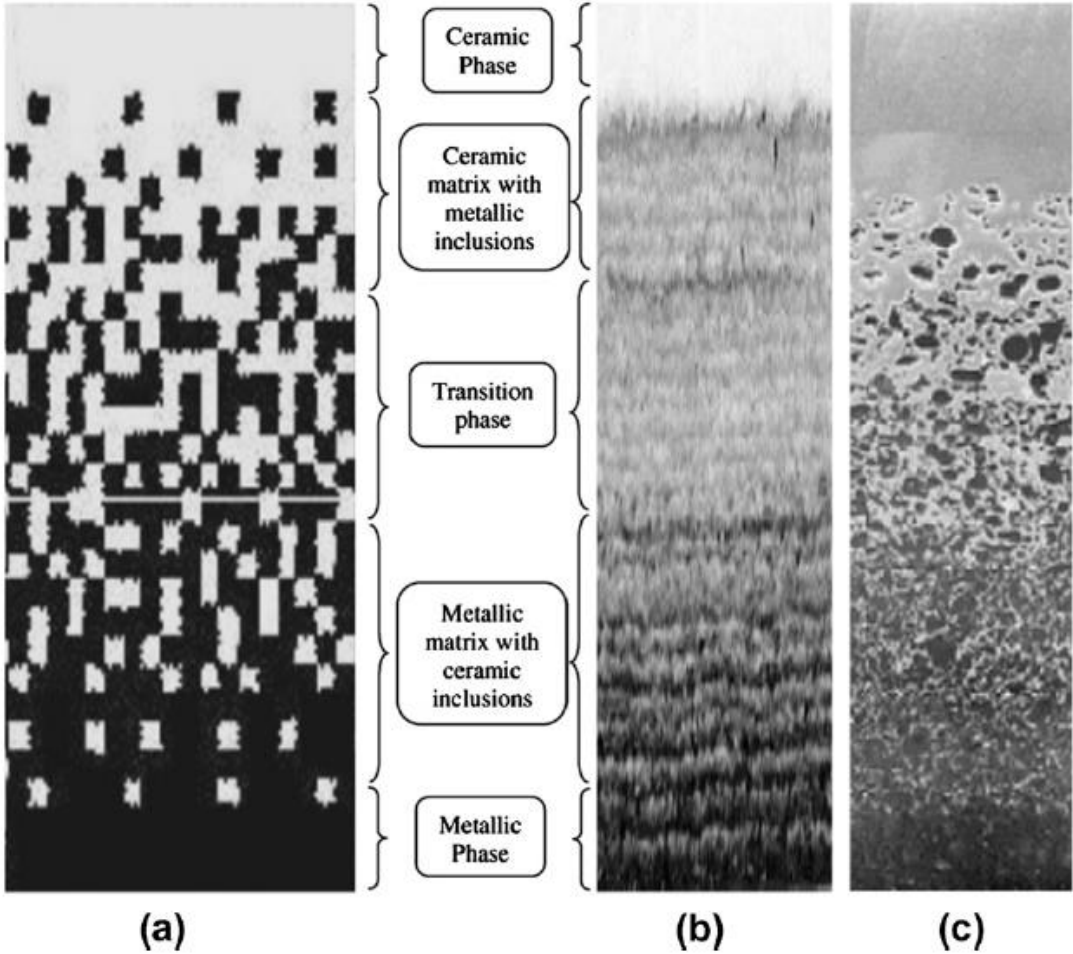


Figure 1.1 Schematic of continuously graded microstructure with metal ceramic constituents (a) Smoothly graded microstructure (b) Enlarged view and (c) Ceramic metal FGM Jha et al. [2]

1.2 LITERATURE REVIEW

There are several analysis techniques in the literature for structural members with FGM. Theory of elasticity solution methods are the most common approach. Plate, shell or solid finite element approaches are the alternative solution techniques. Other numerical methods, such as the differential quadrature method, finite difference method and mesh-free methods are also applied to the problem. A recent analysis approach is the use of beam finite element offering speed of analysis combined with the advantages of the finite element technique. This study is focused on the use of force based beam finite element especially for the case of predicting the linear elastic free vibration properties of beams. Displacement based (DB) and force based (FB) approaches are the two main choices for the beam finite element method.

The accuracy and robustness of the force based method were demonstrated by Soydaş [3] and Gürol [4]. Linear elastic free vibration analysis with uniform and tapered geometries of beams with homogeneous material was conducted by Soydaş [3]. The results obtained using force based formulation for the uniform geometry and circular section were compared to the results of ABAQUS and the explicit methods provided in Leissa [5] and Leissa and So [6] in the literature. Then, a similar comparison for rectangular section was conducted using ABAQUS and Leissa and Zhang [7] in the literature. However, Soydaş [3] only provided a comparison by using ABAQUS when tapered member was considered with both circular and rectangular sections. The implementation of FB method with FGM was presented, for the first time, by Gürol [4]. During the validation process of the linear elastic free vibration characteristics, uniform geometry was considered and results were only compared with the modal analyses outputs of ANSYS. The same method thereupon was also practiced with curved tapered geometry and homogeneous material by Dharmasiri et al [8]. A comparison of DB and FB methods were presented with limited information in [8].

Using various commercial programs for verification purposes are common in the literature. ANSYS, a powerful general purpose finite element code, is one of the most

extensively used commercial tools for validating the dynamic behavior for the FGM cases (Tornabene et al. [9], Zhu et al. [10], Batra and Jin [11], Nie and Zhong [12], Chen et al. [13], Liu et al. [14], Sarıtaş et al. [15]). It offers several advantages with respect to pre and post-processing as well as a wide variety of finite elements and solution techniques. In accordance with the literature, the validation of the analysis with FB method is going to be conducted with ANSYS in this study.

1.3 OBJECTIVE AND SCOPE

The objective of this thesis is to provide the numerical verification of linear elastic free vibration analysis results of the proposed force based beam finite element formulation by comparing them with the numerical results of the previous research in the literature and modal analysis results of ANSYS. In the verification process of the frequency results, uniform and tapered geometries are considered with homogeneous material and transversely distributed FGM separately. Additionally, in the analyses, not only the fundamental frequency but also the frequencies of higher modes are also included.

Linear elastic free vibration characteristics of tapered geometry with FGM are analyzed for the first time with the proposed mixed formulation in this thesis. Moreover, the verification of the proposed formulation given in previous research studies for the FGM case with uniform geometry is done in this thesis to show the accuracy of this formulation. Further verification of the proposed method presented in this thesis with numerical results obtained from ANSYS and previous research in the literature with homogeneous material for uniform and tapered geometries provides a valuable outcome because the numerical examples provided in this thesis include numerous parametric studies.

During the validation study, several parameters are studied in detail such as different element numbers, boundary conditions, material non-homogeneity coefficients, aspect ratios, taper ratios and different laminated layers. The dynamic behavior of the FGM beams are very important in application areas such as the aerospace, automobile,

armory industries. Consequently, free vibration behavior of FGM is required to be simulated accurately in order to understand the material behavior better. Due to the significant effects of the aforementioned parameters on the dynamic characteristics of FGM, validation presented in this work makes a valuable contribution to the literature. Furthermore, a comparison study is also conducted to highlight the effect of shear correction factor with the proposed formulation for beams with different aspect ratios.

This thesis is organized into five chapters as follows:

Chapter 2 presents an alternative finite element formulation i.e. mixed formulation for modeling the beams with varying geometry that are made of elastic functionally graded material. First, discussion on beam theories and their main differences are provided, followed by the kinematic relations for the Timoshenko beam theory. Variational and finite element formulation with section response is presented next. Finally, before concluding the chapter with the formulation for the consistent mass matrix, material properties of functionally graded material are outlined.

Chapter 3 presents the numerical verification of the proposed mixed beam element with uniform geometry under linear elastic condition. Uniform geometry with homogeneous material and functionally graded materials are verified by providing three numerical examples for each material case.

In Chapter 4, a similar verification is presented for tapered geometry with homogeneous material and functionally graded materials by providing two numerical examples for each case.

Chapter 5 presents the summary and conclusions of the study, and the directions for future research.

CHAPTER 2

MIXED BEAM ELEMENT FORMULATION

2.1 INTRODUCTION

Mixed formulation, an alternative formulation to the most commonly used displacement-based finite element method, is used in this thesis for modeling the stiffness and inertial response of planar beams with varying geometry that are made of elastic FGM. In addition to the displacement field, strain and/or stress fields are also taken into account as independent variables in the variational form of the mixed formulation elements. Before the presentation of mixed formulation, a discussion on beam theories will be provided first in this section; Euler-Bernoulli, Timoshenko and higher order beam theories, and their main differences will be outlined. Moreover, the kinematic relations for the Timoshenko beam theory will be shown in detail. Description of the basic and complete coordinate systems for the transformation of beam nodal forces and displacements are also provided. After these presentations, the three-fields Hu-Washizu functional will be explained, and the mixed formulation of the beam finite element will be outlined in setting up the stiffness matrix of a FGM beam. Finally, consistent mass matrix formulation for the FGM beam will be presented.

2.2 KINEMATICS OF A BEAM ELEMENT

In structural mechanics, beam theories are important as these help to come up with easier relations and formulations for the analysis and design of beams for not just practice but also for research purposes. Consequently, several beam theories have been developed with different physical assumptions. The underlying assumptions in beam

theories need to be considered carefully during the selection process of an appropriate beam element for the analysis of a problem at hand.

In terms of historical development, the Euler-Bernoulli beam theory is the earliest and simplest approach to the problem. Also called the classical beam theory, this theory assumes the shear deformations and strains are zero. The second theory in terms of development was proposed by Timoshenko: thus called as the Timoshenko beam theory, it considers the presence of shear deformations in the element response, but assumes that the shear strains are constant on the section. For slender elastic beams (thin beams), i.e. beams that have a large length to depth ratio, shear deformation is experimentally and furthermore analytically observed to be negligible, hence using Euler-Bernoulli or Timoshenko beam theories for thin beams does not make much difference. On the other hand, the effect of shear deformation is significant when length to depth ratio is small, e.g. for short and deep beams. For deep beams, selection of Timoshenko beam theory provides a more accurate representation of the reality, however, there is a need for a shear correction factor for the Timoshenko beam theory in order to compensate for the assumption of constant transverse shear strain through the cross section which is not the case. Choices of higher order beam theories help to overcome the need to use a shear correction factor with elastic materials, because nonuniform shear strain along transverse direction is considered with the use of higher order terms in the equations. For example, transverse shear strain with a parabolic variation was proposed as a higher order theory for laminated composite plates [16]. A detailed review of the Euler-Bernoulli, Timoshenko and the third order theory beam finite element can be found in Reddy [17].

In the next section, displacement and strain fields for a planar beam are calculated by using the Timoshenko beam theory, and then the basics for the beam finite element formulation will be presented.

2.2.1 Displacement and Strain Fields

In Timoshenko beam theory, plane cross sections are assumed to remain plane after deformation as in the case of Euler-Bernoulli beam theory, however, additionally an angle of rotation of the sections resulting from the shearing of the sections is considered. Consequently, there is an extra entry in the strain vector other than normal strain corresponding to the shear strain for a two dimensional beam element in the Timoshenko beam theory.

For planar beam analysis, the displacement field calculation is done in xz plane instead of 3D space which is shown in Figure 2.1.

$$\begin{aligned}u_x &= u(x) - z\theta(x) \\u_z &= w(x)\end{aligned}\tag{2.1}$$

where u_x and u_z are displacements in x and z directions, respectively. $\theta(x)$ is the rotation about y-axis. Furthermore, x-axis is assumed to coincide with the geometric centroid of the section.

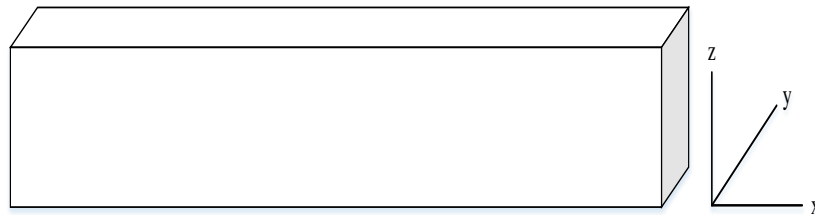


Figure 2.1 A uniform geometry beam and the corresponding coordinates

From the displacement field assumption given above, the strain field is calculated as follows:

$$\begin{aligned}\varepsilon_x &= \frac{du_x}{dx} = u'(x) - z\theta'(x) = \varepsilon_a(x) - z\kappa(x) \\ \gamma_{xz} &= \frac{du_x}{dz} + \frac{du_z}{dx} = -\theta(x) + w'(x) = \gamma(x)\end{aligned}\tag{2.2}$$

where $\varepsilon_a(x)$ is the axial strain in the longitudinal direction, γ is the shear deformation along the z-axis and $\kappa(x)$ is the curvature about the y-axis. Zero strain components are not included. Strain vector can be shown in a matrix form as:

$$\underline{\varepsilon} = \underline{a}_s \underline{e}(x) \quad \therefore \quad \begin{Bmatrix} \varepsilon_x \\ \gamma_{xz} \end{Bmatrix} = \begin{bmatrix} 1 & 0 & -z \\ 0 & 1 & 0 \end{bmatrix} \begin{Bmatrix} \varepsilon_a \\ \gamma \\ \kappa \end{Bmatrix}\tag{2.3}$$

where \underline{a}_s is the section compatibility matrix and, $\underline{e}(x)$ is the section deformation vector.

2.2.2 Coordinate Systems and Transformations

In structural analysis, selection of an efficient model helps to simplify the effort. Sometimes using a more detailed model is unnecessary because the same characteristic behavior might be obtained with a simpler model. Thus, in this thesis, two dimensional plane (xz) as shown above is considered accurate enough for the formulation of a beam element instead of casting the equations in 3D. For example, if torsional effects are not studied and the deformation of the beam mainly lies in the plane in reality, then the use of 3D formulation and analysis will just result in more computational time without any increase in accuracy.

Following this simplification, the beam kinematics and transformation relations will be further presented in the plane. There are two systems for prescribing the geometry of deformation and transformation for beam elements that are especially relevant to their formulation by using force-based approach. These two coordinate systems are the basic system and complete system. In force-based beam elements, formulation is

generated in a basic system that contains only deformation modes and it is transformed into a more general complete system, which has additionally rigid body modes of displacements. For the simplicity of the computation, selection of a basic system, which focuses on element deformations without rigid body modes of motion, is important. Cantilever beam choice provided especially an easier choice compared to the simply supported basic system popularly used in the literature, because a cantilever beam has one side fixed with no deformation on this side and the displacement field derivation is easier.

In Figure 2.2, element forces and deformations for basic system are shown as q and v , respectively. On cantilever beam, left side is fixed and deformations are only on the right side as axial displacement, transverse displacement and rotation.

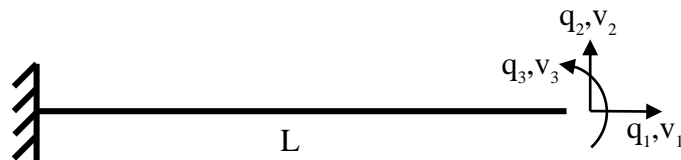


Figure 2.2 Element forces and deformations in basic system

Element end forces and displacements are shown as p and u , respectively for the complete system. In finite element formulation, the two-node element with six degrees of freedom is considered and this is shown in Figure 2.3.

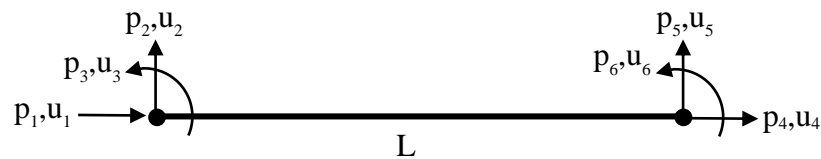


Figure 2.3 Element end forces and displacements in two node complete system

The relation between element deformations in basic system and nodal displacements in complete system is cast as follows:

$$\underline{v} = \underline{a}\underline{u} \quad \therefore \quad \begin{Bmatrix} v_1 \\ v_2 \\ v_3 \end{Bmatrix} = \begin{bmatrix} -1 & 0 & 0 & 1 & 0 & 0 \\ 0 & -1 & -L & 0 & 1 & 0 \\ 0 & 0 & -1 & 0 & 0 & 1 \end{bmatrix} \begin{Bmatrix} u_1 \\ u_2 \\ u_3 \\ u_4 \\ u_5 \\ u_6 \end{Bmatrix} \quad (2.4)$$

where \underline{v} and \underline{u} are element deformations vector in basic system and nodal displacements vector in complete system, respectively. \underline{a} is compatibility matrix used for transformation of element deformations from basic system to nodal displacements in complete system.

Above transformation can be extended for the element forces as follows:

$$\underline{p} = \underline{a}^T \underline{q} \quad \therefore \quad \begin{Bmatrix} p_1 \\ p_2 \\ p_3 \\ p_4 \\ p_5 \\ p_6 \end{Bmatrix} = \begin{bmatrix} -1 & 0 & 0 \\ 0 & -1 & 0 \\ 0 & -L & -1 \\ 1 & 0 & 0 \\ 0 & 1 & 0 \\ 0 & 0 & 1 \end{bmatrix} \begin{Bmatrix} q_1 \\ q_2 \\ q_3 \end{Bmatrix} \quad (2.5)$$

where \underline{p} and \underline{q} are nodal forces vector in complete system and element forces vector in basic system, respectively.

For the cantilever basic system shown in Figure 2.2, the section forces can be obtained from element basic forces q from statics as follows:

$$\begin{aligned} N(x) &= q_1 \\ V(x) &= q_2 \\ M(x) &= (L-x)q_2 + q_3 \end{aligned} \quad (2.6)$$

where $N(x)$ is axial force, $V(x)$ is shear force and $M(x)$ is moment about y-axis. These equations are presented in matrix and vector form in the following equations, and

furthermore these section forces are shown in Figure 2.4 at a distance x from the left node.

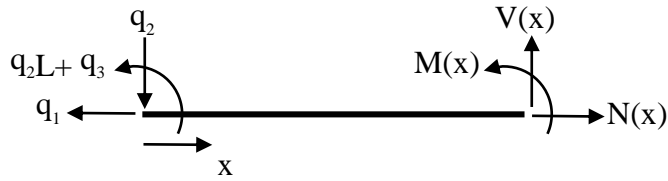


Figure 2.4 Section forces in cantilever basic system

$$\underline{s}(x) = \underline{b}(x, L) \underline{q} \quad \therefore \quad \begin{Bmatrix} N(x) \\ V(x) \\ M(x) \end{Bmatrix} = \begin{bmatrix} 1 & 0 & 0 \\ 0 & 1 & 0 \\ 0 & (L-x) & 1 \end{bmatrix} \begin{Bmatrix} q_1 \\ q_2 \\ q_3 \end{Bmatrix} \quad (2.7)$$

where $\underline{s}(x)$ is section forces vector and $\underline{b}(x, L)$ is force equilibrium matrix.

An additional section forces vector as $\underline{s}_p(x)$, which is a particular solution, is needed in $\underline{s}(x)$ when for example uniformly distributed element loadings in x and z directions are available. Force equilibrium matrix of $\underline{s}_p(x)$ is obtained by using simple static calculation similar to $\underline{b}(x, L)$ matrix for $\underline{s}(x)$.

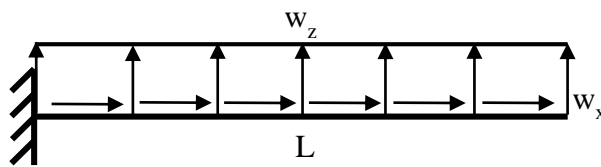


Figure 2.5 Uniformly distributed element loadings in x-z directions

$$\underline{s}(x) = \underline{b}(x, L) \underline{q} + \underline{s}_p(x) \quad \therefore \quad \underline{s}_p(x) = \begin{bmatrix} (L-x) & 0 \\ 0 & (L-x) \\ 0 & (L-x)^2 / 2 \end{bmatrix} \begin{Bmatrix} w_x \\ w_z \end{Bmatrix} \quad (2.8)$$

where w_x and w_z are uniformly distributed loads in axial and transverse directions, respectively, shown in Figure 2.5.

2.3 VARIATIONAL FORMULATION

Different variational functions with one, two or three independent fields are available in the literature. One of the most commonly used one is the principle of minimum potential energy that necessitates only displacement field as independent variable. However, Hu-Washizu variational method includes stress and strain as additional fields. Sarıtaş and Soydaş [18] provided detailed information about variational forms and Table 2.1 presents brief summary.

Table 2.1 Strong and weak satisfaction of parameters in variational principles

Varied fields	Functional name	Strong satisfaction	Weak satisfaction
\underline{u}	Potential Energy	$\underline{\varepsilon} = \nabla^s \underline{u}$ on Ω $\underline{\sigma} = \underline{\sigma}(\underline{\varepsilon})$ on Ω $\underline{u} = \underline{u}^*$ on Γ_u	$\text{div} \underline{\sigma} + \underline{b} = \underline{0}$ on Ω $\underline{t} = \underline{t}^*$ on Γ_t
$\underline{\sigma}$	Complementary Energy	$\text{div} \underline{\sigma} + \underline{b} = \underline{0}$ on Ω $\underline{\sigma} = \underline{\sigma}(\underline{\varepsilon})$ on Ω $\underline{t} = \underline{t}^*$ on Γ_t	$\underline{\varepsilon} = \nabla^s \underline{u}$ on Ω $\underline{u} = \underline{u}^*$ on Γ_u
$\underline{u}, \underline{\sigma}$	Hellinger-Reissner	$\underline{\varepsilon} = \nabla^s \underline{u}$ on Ω $\underline{u} = \underline{u}^*$ on Γ_u	$\text{div} \underline{\sigma} + \underline{b} = \underline{0}$ on Ω $\underline{\sigma} = \underline{\sigma}(\underline{\varepsilon})$ on Ω $\underline{t} = \underline{t}^*$ on Γ_t
$\underline{\sigma}, \underline{\varepsilon}$	-	$\text{div} \underline{\sigma} + \underline{b} = \underline{0}$ on Ω $\underline{t} = \underline{t}^*$ on Γ_t	$\underline{\varepsilon} = \nabla^s \underline{u}$ on Ω $\underline{\sigma} = \underline{\sigma}(\underline{\varepsilon})$ on Ω $\underline{u} = \underline{u}^*$ on Γ_u
$\underline{u}, \underline{\sigma}, \underline{\varepsilon}$	Hu-Washizu	-	$\text{div} \underline{\sigma} + \underline{b} = \underline{0}$ on Ω $\underline{\varepsilon} = \nabla^s \underline{u}$ on Ω $\underline{\sigma} = \underline{\sigma}(\underline{\varepsilon})$ on Ω $\underline{u} = \underline{u}^*$ on Γ_u $\underline{t} = \underline{t}^*$ on Γ_t

Mixed formulation elements are mostly based on either Hellinger-Reissner or Hu-Washizu functions and in this thesis, the latter is selected because of the additional independent variables in this form.

Nodal displacements \underline{u} in complete system, element forces \underline{q} in basic system and section deformations \underline{e} are independent variables used in this work for the formulation of the beam element based on Hu-Washizu variational principle. Equation (2.9) presented in [18] was also implemented in [19] and [20], and from these studies the variation of Hu-Washizu functional is written below:

$$\begin{aligned} \delta\Pi_{\text{HW}} = & \int_0^L \delta\underline{e}^T [\underline{\hat{s}}(\underline{e}(x)) - \underline{b}(x, L)\underline{q} - \underline{s}_p(x)] dx - \delta\underline{q}^T \int_0^L \underline{b}^T(x, L)\underline{e}(x) dx + \delta\underline{q}^T \underline{a}\underline{u} \\ & + \delta\underline{u}^T \underline{a}^T \underline{q} - \delta\underline{u}^T \underline{p}_{\text{app}} = 0 \end{aligned} \quad (2.9)$$

where $\underline{p}_{\text{app}}$ is applied end forces and $\underline{\hat{s}}(\underline{e}(x)) = \partial W(\underline{e}) / \partial \underline{e}$ where $W(\underline{e})$ is the strain energy function. For the dynamic case, an additional term $\delta\underline{u}^T \underline{m}\ddot{\underline{u}}$ is included at the nodes as follows:

$$\begin{aligned} \delta\Pi_{\text{HW}} = & \int_0^L \delta\underline{e}^T [\underline{\hat{s}}(\underline{e}(x)) - \underline{b}(x, L)\underline{q} - \underline{s}_p(x)] dx - \delta\underline{q}^T \int_0^L \underline{b}^T(x, L)\underline{e}(x) dx + \delta\underline{q}^T \underline{a}\underline{u} \\ & + \delta\underline{u}^T \underline{a}^T \underline{q} - \delta\underline{u}^T \underline{p}_{\text{app}} + \delta\underline{u}^T \underline{m}\ddot{\underline{u}} = 0 \end{aligned} \quad (2.10)$$

where $\ddot{\underline{u}}$ is acceleration vector. Equations (2.11), (2.12) and (2.13) need to be satisfied in order to make $\delta\Pi_{\text{HW}}$ equal to zero with arbitrary $\delta\underline{u}$, $\delta\underline{q}$ and $\delta\underline{e}$ values [15].

$$\underline{a}^T \underline{q} + \underline{m}\ddot{\underline{u}} - \underline{p}_{\text{app}} = 0 \quad \therefore \quad \underline{p} + \underline{m}\ddot{\underline{u}} \equiv \underline{p}_{\text{app}} \quad (2.11)$$

$$\underline{a}\underline{u} - \int_0^L \underline{b}^T(x, L)\underline{e}(x) dx = 0 \quad \therefore \quad \underline{v} = \underline{a}\underline{u} \equiv \int_0^L \underline{b}^T(x, L)\underline{e}(x) dx \quad (2.12)$$

$$\underline{\hat{s}}(\underline{e}(x)) - \underline{b}(x, L)\underline{q} - \underline{s}_p(x) = 0 \quad \therefore \quad \underline{\hat{s}}(\underline{e}(x)) \equiv \underline{b}(x, L)\underline{q} + \underline{s}_p(x) \quad (2.13)$$

2.4 FINITE ELEMENT FORMULATION AND SECTION RESPONSE

There are different ways to formulate the response of a beam finite element based on mixed formulation. Gürol [4] selected the principle of virtual force for formulation. Another approach was presented by Soydaş [3] and that followed a prior formulation by Molins et al. [21] and it was also based on force-based approach. An alternative method, recently provided by Sarıtaş et al. [15] is used in this study, the details of which are presented in this section.

Section deformations can be obtained by Equation (2.14) when material response is linear elastic.

$$\underline{\epsilon} = \underline{k}_s^{-1} \hat{\underline{\xi}} \quad (2.14)$$

where \underline{k}_s is section stiffness matrix. Substitution of Equation (2.14) into Equation (2.12) provides:

$$\underline{a}\underline{u} = \underline{v} = \underline{f}\underline{q} \quad \therefore \quad \underline{f} = \int_0^L \underline{b}^T(x, L) \underline{k}_s^{-1}(x) \underline{b}(x, L) dx \quad (2.15)$$

where \underline{f} is element flexibility matrix in basic system. Another substitution of Equation (2.15) into Equation (2.11) gives:

$$\underline{m}\ddot{\underline{u}} + \underline{k}\underline{u} = \underline{p}_{app} \quad \therefore \quad \underline{k} = \underline{a}^T \underline{f}^{-1} \underline{a} \quad (2.16)$$

where \underline{k} is element stiffness matrix in complete system. Section forces relation with section deformations is shown as follows:

$$\hat{\underline{\xi}} = \hat{\underline{\xi}}(\underline{\epsilon}) = \int_A \underline{a}_s^T \underline{\sigma}(\underline{\epsilon}) dA \quad \therefore \quad \underline{k}_s = \frac{\partial \hat{\underline{\xi}}}{\partial \underline{\epsilon}} = \int_A \underline{a}_s^T \frac{\partial \underline{\sigma}}{\partial \underline{\epsilon}} \underline{a}_s dA \quad (2.17)$$

where \underline{k}_s is section stiffness matrix. For linear elastic material response, a direct calculation can be achieved for section forces as follows:

$$\hat{\underline{k}}(x) = \underline{k}_{s,e}(x)\underline{e}(x) \quad \therefore \quad \underline{k}_{s,e}(x) = \int_A \underline{a}_s^T \begin{bmatrix} E(x,y) & 0 \\ 0 & G(x,y) \end{bmatrix} \underline{a}_s dA \quad (2.18)$$

where $\underline{k}_{s,e}$ is elastic section stiffness matrix. When material properties do not change in transverse direction, it can be simplified as follows:

$$\underline{k}_{s,e} = \int_A \begin{bmatrix} E & 0 & -zE \\ 0 & G & 0 \\ -zE & 0 & z^2E \end{bmatrix} dA = \begin{bmatrix} EA & 0 & -EQ \\ 0 & GA & 0 \\ -EQ & 0 & EI \end{bmatrix} \quad (2.19)$$

where A, I and Q are cross sectional area, moment of inertia about bending axis and first moment of area about bending axis, respectively. E and G are the Young's modulus and shear modulus, respectively.

If the geometric centroid is the same with axis of bending axis, Q becomes zero in the above equation.

$$\underline{k}_{s,e} = \begin{bmatrix} EA & 0 & 0 \\ 0 & GA & 0 \\ 0 & 0 & EI \end{bmatrix} \quad (2.20)$$

For tapered beams with a change of geometry in axial direction, there is a need to include an independent variable of x in the $\underline{k}_{s,e}$ matrix.

$$\underline{k}_{s,e} = \begin{bmatrix} EA(x) & 0 & -EQ(x) \\ 0 & GA(x) & 0 \\ -EQ(x) & 0 & EI(x) \end{bmatrix} \quad (2.21)$$

If higher order beam theory is not used, there is a need of shear correction factor as explained in Section 2.2 for the Timoshenko beam theory. Shear correction factor, κ_s

is multiplied with GA term in order to provide a correction for the constant shear strain assumption on the section.

2.5 MATERIAL PROPERTIES

Heterogeneous material distribution of FGM is represented by different functions such as the commonly used exponential and power laws. As can be seen in Equations (2.22) and (2.23), variations are continuous along the depth in z direction, and this type of material distribution is denoted as transversely FGM.

Exponential law equations:

$$\begin{aligned}\wp(z) &= \wp_t \exp\left(-\delta\left(1 - \frac{2z}{h}\right)\right) \\ \delta &= \frac{1}{2} \ln\left(\frac{\wp_t}{\wp_b}\right)\end{aligned}\tag{2.22}$$

Power law equation:

$$\wp(z) = (\wp_t - \wp_b) \left(\frac{z}{h} + \frac{1}{2}\right)^k + \wp_b\tag{2.23}$$

where $\wp(z)$ represents different material properties, for instance, the Young's modulus, shear modulus, coefficient of thermal expansion or the density. \wp_t and \wp_b denote material properties for the topmost layer ($z = +h/2$) and the bottommost layer ($z = -h/2$), respectively; h is the total depth of the beam; δ and k stand for the material grading indexes for exponential and power law functions, respectively. For power law equation; when $k = 0$ and $k = \infty$, $\wp(z)$ equals to \wp_t and \wp_b , respectively.

The use of the exponential law for FGM is more frequent in the fracture mechanics field while the power law is generally selected for stress analysis with FGM [22].

Moreover, the power law is used with axially FGM in which material gradation is along the longitudinal direction of the beam, i.e. in the x direction. Also it is the simplest and the most well-known function. The functions showing curvature in both the concave upward and concave downward directions is preferable [23]. However, the exponential law does not show curvature in both upward and downward directions [24]. A description of a functionally graded material in 2D plane is presented in Figure 2.6. Change of material variations with different power law coefficients is shown in Figure 2.7. It is seen that curvature in both directions are available in power law function, for example, for $k = 10$ and 0.1 , the function is concave upward and downward, respectively.

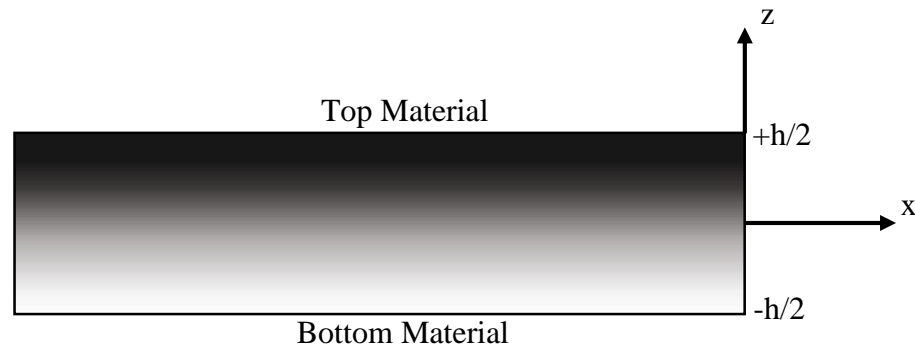


Figure 2.6 A functionally graded material in x - z plane

Besides the popular variations mentioned above, there are various material distributions that received attention in the literature such as the polynomial, trigonometric, sigmoid, modified power and the modified exponential laws functions. Polynomial, and trigonometric functions were selected in the numerical examples by Huang and Li [25] as well as a modified version of power law. The implementation of quadratic, exponential and trigonometric functions for material distribution of FGM by Sutradhar and Paulino [26] showed that material variations can be extended to more than one dimension, as far as possible, and broadened in all dimensions theoretically. Chung and Chi [27] suggested sigmoid function, which has two power law functions for two volume fractions, in order to decrease the amount of stress concentration when there is a rapid change.

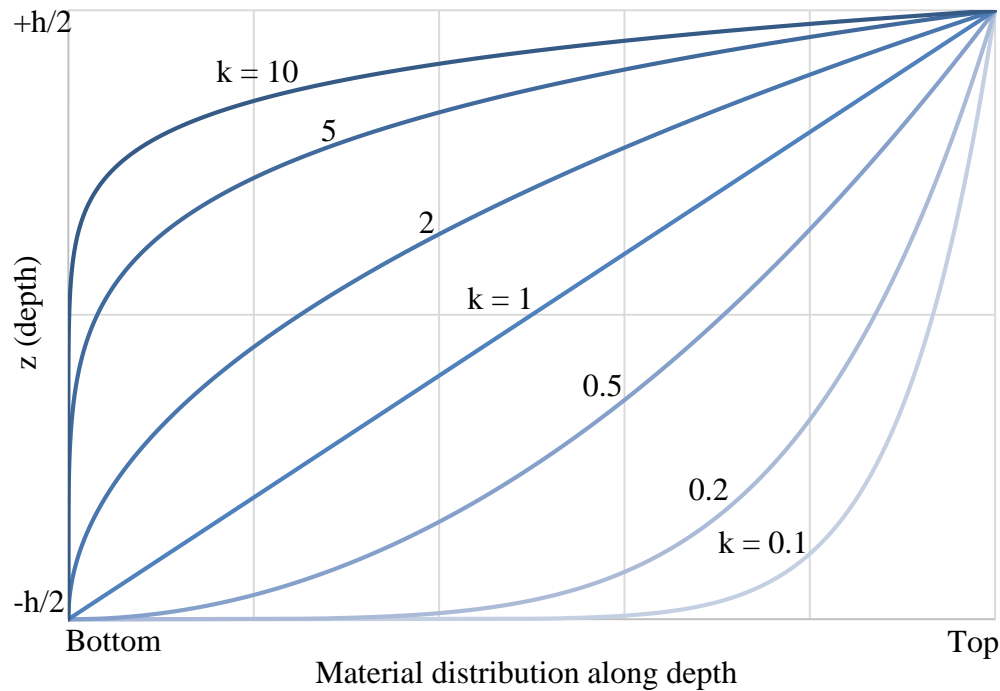


Figure 2.7 Material variations along transverse direction

2.6 CONSISTENT MASS MATRIX

Consistent mass matrix for mixed formulation is important because one of the main focus point of this thesis is the use of nonhomogeneous materials, such as functionally graded materials, for the calculation of not only stiffness properties correctly but also the inertial properties in a consistent and accurate fashion. Due to the use of the above mixed formulation approach, a similar underlying formulation should be provided for the computation of the mass matrix. However, there was no need for the prescription of displacement field along element length in obtaining the stiffness matrix as in the prior section. This was due to the fact that the force field was used in setting up flexibility matrix of the element, after which its inverse provided the stiffness matrix. Due to the absence of displacement field from prior derivation, the derivation of the displacement field becomes necessary. However, a more elaborate and consistently accurate approach can be obtained by the use of the virtual force method as given in

[21]. This approach, the unit dummy load method, was successfully applied in the mixed formulation in [28].

In this thesis, the mass matrix derivation previously presented for more typical beam applications will be provided for the analysis of uniform or tapered beam geometries that contain homogeneous or heterogeneous materials. For the proposed formulation, consistent mass matrix does not specifically require the need of displacement shape functions for each different case to account for the nonuniform geometry or a heterogeneous material. With a displacement-based approach, it would require a cumbersome derivation of displacement field approximation for the calculation of the stiffness and the mass matrix, and this is greatly simplified with the use of mixed approach.

The mass matrix calculation also uses the same cantilever beam basic system and force field functions as used before for the stiffness matrix, and therefore this derivation is consistent with the prior effort.

The section mass matrix is computed as follows:

$$\underline{\mathbf{m}}_s(\mathbf{x}) = \int_A \underline{\mathbf{a}}_s^T \rho(\mathbf{x}, \mathbf{y}, \mathbf{z}) \underline{\mathbf{a}}_s dA \quad (2.24)$$

where $\underline{\mathbf{a}}_s$ is the section compatibility matrix shown earlier in Equation (2.3) and ρ is density. It is assumed that the density does not vary through the normal to xz -plane, i.e. y -axis.

The section stiffness matrix is rewritten here again as:

$$\underline{\mathbf{k}}_s(\mathbf{x}) = \int_A \underline{\mathbf{a}}_s^T \begin{bmatrix} \mathbf{E}(\mathbf{z}) & 0 \\ 0 & \mathbf{G}(\mathbf{z}) \end{bmatrix} \underline{\mathbf{a}}_s dA \quad (2.25)$$

As previously mentioned in Section 2.2.2, there are two nodes in complete system and each node has 3 degrees of freedom. Consequently, the size of the element mass matrix is 6x6.

$$\underline{\mathbf{m}} = \begin{bmatrix} \underline{\mathbf{m}}_{00} & \underline{\mathbf{m}}_{0L} \\ \underline{\mathbf{m}}_{L0} & \underline{\mathbf{m}}_{LL} \end{bmatrix} \quad (2.26)$$

Entries of element mass matrix are calculated as:

$$\underline{\mathbf{m}}_{LL} = \underline{\mathbf{f}}^{-1} \int_0^L \underline{\mathbf{b}}^T(\mathbf{x}, L) \underline{\mathbf{k}}_s^{-1}(\mathbf{x}) \left(\int_x^L \underline{\mathbf{b}}(\mathbf{x}, \xi) \underline{\mathbf{m}}_s(\xi) \underline{\mathbf{f}}_p(\xi) \underline{\mathbf{f}}^{-1} d\xi \right) d\mathbf{x} \quad (2.27)$$

$$\underline{\mathbf{m}}_{L0} = \underline{\mathbf{f}}^{-1} \int_0^L \underline{\mathbf{b}}^T(\mathbf{x}, L) \underline{\mathbf{k}}_s^{-1}(\mathbf{x}) \left(\int_x^L \underline{\mathbf{b}}(\mathbf{x}, \xi) \underline{\mathbf{m}}_s(\xi) (\underline{\mathbf{b}}^T(0, \xi) - \underline{\mathbf{f}}_p(\xi) \underline{\mathbf{f}}^{-1} \underline{\mathbf{b}}^T(0, L)) d\xi \right) d\mathbf{x} \quad (2.28)$$

$$\underline{\mathbf{m}}_{L0} = \underline{\mathbf{m}}_{0L}^T = -\underline{\mathbf{b}}(0, L) \underline{\mathbf{m}}_{LL} + \int_0^L \underline{\mathbf{b}}(0, \mathbf{x}) \underline{\mathbf{m}}_s(\mathbf{x}) \underline{\mathbf{f}}_p(\mathbf{x}) \underline{\mathbf{f}}^{-1} d\mathbf{x} \quad (2.29)$$

$$\underline{\mathbf{m}}_{00} = -\underline{\mathbf{b}}(0, L) \underline{\mathbf{m}}_{L0} + \int_0^L \underline{\mathbf{b}}(0, \mathbf{x}) \underline{\mathbf{m}}_s(\mathbf{x}) (\underline{\mathbf{b}}^T(0, \mathbf{x}) - \underline{\mathbf{f}}_p(\mathbf{x}) \underline{\mathbf{f}}^{-1} \underline{\mathbf{b}}^T(0, L)) d\mathbf{x} \quad (2.30)$$

where $\underline{\mathbf{f}}$ and $\underline{\mathbf{f}}_p$ are element flexibility matrix and partial flexibility matrix, respectively. Subscripts on entries of element mass matrix as 0 and L represent left end node and right end node, respectively. Furthermore, $\underline{\mathbf{f}}$ is calculated in Equation (2.15) and $\underline{\mathbf{f}}_p$ is computed as follows:

$$\underline{\mathbf{f}}_p(\mathbf{x}) = \int_0^{\mathbf{x}} \underline{\mathbf{b}}^T(\xi, \mathbf{x}) \underline{\mathbf{k}}_s^{-1}(\mathbf{x}) \underline{\mathbf{b}}(\xi, L) d\xi \quad (2.31)$$

In Equations (2.27) and (2.28), $\underline{\mathbf{b}}(\mathbf{x}, \xi)$ was written as $\underline{\mathbf{b}}^T(\mathbf{x}, \xi)$ mistakenly in [15] and [29]. Moreover, $\underline{\mathbf{b}}(\xi, L)$, which is equal to $\underline{\mathbf{b}}(\xi, \mathbf{x}) \underline{\mathbf{b}}(\mathbf{x}, L)$, was presented as $\underline{\mathbf{b}}(\xi, \mathbf{x})$ in

Equation (2.31). Additionally, $\underline{m}_{L0} = \underline{m}_{0L}^T$ was given erroneously without the transpose of the matrix on the right side of the equal sign in Equation (2.29) in the same articles.

According to Saritaş et al. [15], a comparison of mass matrices obtained with the proposed mixed formulation and the displacement based formulation provided by Chakraborty et al. [24] yielded identical results for uniform geometry FGM. On the other hand, for the tapered geometry, the former method presented more accurate results compared to the latter one.

In dynamic solutions, an alternative method to the use of consistent mass matrix is the use of the lumped mass matrix. For heterogeneous materials, such as the FGMs, it is not reasonable to use lumped mass matrix for the representation of the inertia in the model because the lumped mass matrix does not include the effects of shear deformation and rotational inertia. Consequently, there is a need for a continuous mass matrix to obtain more accurate results, other than masses specified at certain lumped locations.

CHAPTER 3

FREE VIBRATION ANALYSIS OF A BEAM WITH UNIFORM GEOMETRY

3.1 INTRODUCTION

In this chapter, the proposed 2D beam element with uniform geometry will be analyzed for linear elastic free vibration with various boundary conditions for the homogeneous or heterogeneous material distribution. Heterogeneous material distribution with FGM is selected in transverse direction since most of the research studies in the literature focus on such a material distribution for the FGM members. To be more specific, power law and exponential law functions are used to provide continuous material variation in the z direction for FGM. In addition, the technical terms of force based method and mixed formulation are used interchangeably.

The proposed mixed formulation analyses are conducted with MATLAB software [30]. Moreover, ANSYS [31], a powerful general purpose finite element code, is used in 2D to validate the proposed formulation in addition to the benchmark comparisons available in the literature. ANSYS results are more realistic for real life problems than the proposed formulation due to the assumptions used in the proposed method to increase efficiency, however, these results come at the significant cost of using the software and advanced computational requirements. Accordingly, the proposed method, which can be implemented efficiently for different geometric and material variations with simple modifications, is an accurate and robust alternative to the displacement based methods as well as the cumbersome closed form solutions. Further verification of the proposed method with numerical results obtained from ANSYS and previous research will fill the gap in the literature.

In the next sections, various parametric studies for the beam finite element will be carried out for different number of elements, boundary conditions, material non-homogeneity coefficients and aspect ratios (L/h). The outcomes of ANSYS and the use of adaptive mesh refinement option with ANSYS will additionally be presented as another parametric study. Before this presentation, discussion on the uniform geometry is provided first. Next, numerical examples with homogeneous and FGM material distributions will be presented.

3.2 VERIFICATION WITH UNIFORM GEOMETRY

The mixed formulation beam element with uniform geometry and homogeneous material for linear elastic free vibration was first analyzed by Soydaş [3] and the same method thereupon was applied for the FGM by Gürol [4]. However, the verification of the proposed formulation with the previous research for the homogeneous material case is not sufficient. For validation of the FGM case, especially with regards to the accuracy of this approach, a verification to the benchmark results is required. For the benchmark results; highly cited works by Şimşek [32], Sina et al. [33] and Li [34] are selected.

In the next section, three numerical examples will be provided for uniform geometry beams with homogeneous material distribution case. After this presentation, FGM for uniform geometry beams will next be presented for another three numerical examples. In Table 3.1, the summary of the numerical examples with uniform geometry beams is presented.

Table 3.1 The summary of the numerical examples for beams with uniform geometry

Free Vibration Analysis of a Uniform Geometry Beam																							
Uniform Geometry with Homogeneous Material	Uniform Geometry with Functionally Graded Materials																						
The First Example	The Fourth Example																						
<table border="1" style="width: 100%; border-collapse: collapse;"> <tr><td style="width: 30%;">Frequency</td><td style="text-align: center;">Fundamental</td></tr> <tr><td>Comparison</td><td style="text-align: center;">ANSYS and Sina et al. [33]</td></tr> <tr><td>Boundary Condition</td><td style="text-align: center;">S-S</td></tr> <tr><td>Aspect Ratio</td><td style="text-align: center;">10, 30, 100</td></tr> <tr><td>Material</td><td style="text-align: center;">Aluminum</td></tr> </table>	Frequency	Fundamental	Comparison	ANSYS and Sina et al. [33]	Boundary Condition	S-S	Aspect Ratio	10, 30, 100	Material	Aluminum	<table border="1" style="width: 100%; border-collapse: collapse;"> <tr><td style="width: 30%;">Frequency</td><td style="text-align: center;">Fundamental</td></tr> <tr><td>Comparison</td><td style="text-align: center;">Şimşek [32] and Sina et al. [33]</td></tr> <tr><td>Boundary Condition</td><td style="text-align: center;">C-F, C-C, S-S</td></tr> <tr><td>Aspect Ratio</td><td style="text-align: center;">10, 30, 100</td></tr> <tr><td>Material</td><td style="text-align: center;">Alumina (Ceramic), Aluminum (Metal)</td></tr> <tr><td>Power Law Coefficient</td><td style="text-align: center;">0.3</td></tr> </table>	Frequency	Fundamental	Comparison	Şimşek [32] and Sina et al. [33]	Boundary Condition	C-F, C-C, S-S	Aspect Ratio	10, 30, 100	Material	Alumina (Ceramic), Aluminum (Metal)	Power Law Coefficient	0.3
Frequency	Fundamental																						
Comparison	ANSYS and Sina et al. [33]																						
Boundary Condition	S-S																						
Aspect Ratio	10, 30, 100																						
Material	Aluminum																						
Frequency	Fundamental																						
Comparison	Şimşek [32] and Sina et al. [33]																						
Boundary Condition	C-F, C-C, S-S																						
Aspect Ratio	10, 30, 100																						
Material	Alumina (Ceramic), Aluminum (Metal)																						
Power Law Coefficient	0.3																						
The Second Example	The Fifth Example																						
<table border="1" style="width: 100%; border-collapse: collapse;"> <tr><td style="width: 30%;">Frequency</td><td style="text-align: center;">Fundamental</td></tr> <tr><td>Comparison</td><td style="text-align: center;">ANSYS and Şimşek [32]</td></tr> <tr><td>Boundary Condition</td><td style="text-align: center;">C-F, C-C, S-S</td></tr> <tr><td>Aspect Ratio</td><td style="text-align: center;">5, 20</td></tr> <tr><td>Material</td><td style="text-align: center;">Alumina (Ceramic), Aluminum (Metal)</td></tr> </table>	Frequency	Fundamental	Comparison	ANSYS and Şimşek [32]	Boundary Condition	C-F, C-C, S-S	Aspect Ratio	5, 20	Material	Alumina (Ceramic), Aluminum (Metal)	<table border="1" style="width: 100%; border-collapse: collapse;"> <tr><td style="width: 30%;">Frequency</td><td style="text-align: center;">Fundamental</td></tr> <tr><td>Comparison</td><td style="text-align: center;">Şimşek [32]</td></tr> <tr><td>Boundary Condition</td><td style="text-align: center;">C-F, C-C, S-S</td></tr> <tr><td>Aspect Ratio</td><td style="text-align: center;">5, 20</td></tr> <tr><td>Material</td><td style="text-align: center;">Alumina (Ceramic), Aluminum (Metal)</td></tr> <tr><td>Power Law Coefficient</td><td style="text-align: center;">0.2, 0.5, 1, 2, 5, 10</td></tr> </table>	Frequency	Fundamental	Comparison	Şimşek [32]	Boundary Condition	C-F, C-C, S-S	Aspect Ratio	5, 20	Material	Alumina (Ceramic), Aluminum (Metal)	Power Law Coefficient	0.2, 0.5, 1, 2, 5, 10
Frequency	Fundamental																						
Comparison	ANSYS and Şimşek [32]																						
Boundary Condition	C-F, C-C, S-S																						
Aspect Ratio	5, 20																						
Material	Alumina (Ceramic), Aluminum (Metal)																						
Frequency	Fundamental																						
Comparison	Şimşek [32]																						
Boundary Condition	C-F, C-C, S-S																						
Aspect Ratio	5, 20																						
Material	Alumina (Ceramic), Aluminum (Metal)																						
Power Law Coefficient	0.2, 0.5, 1, 2, 5, 10																						
The Third Example	The Sixth Example																						
<table border="1" style="width: 100%; border-collapse: collapse;"> <tr><td style="width: 30%;">Frequency</td><td style="text-align: center;">Higher modes</td></tr> <tr><td>Comparison</td><td style="text-align: center;">ANSYS</td></tr> <tr><td>Boundary Condition</td><td style="text-align: center;">C-F</td></tr> <tr><td>Aspect Ratio</td><td style="text-align: center;">5, 20</td></tr> <tr><td>Material</td><td style="text-align: center;">Alumina (Ceramic), Aluminum (Metal)</td></tr> </table>	Frequency	Higher modes	Comparison	ANSYS	Boundary Condition	C-F	Aspect Ratio	5, 20	Material	Alumina (Ceramic), Aluminum (Metal)	<table border="1" style="width: 100%; border-collapse: collapse;"> <tr><td style="width: 30%;">Frequency</td><td style="text-align: center;">Higher modes</td></tr> <tr><td>Comparison</td><td style="text-align: center;">Şimşek [32] and Li [34]</td></tr> <tr><td>Boundary Condition</td><td style="text-align: center;">S-S</td></tr> <tr><td>Aspect Ratio</td><td style="text-align: center;">4</td></tr> <tr><td>Material</td><td style="text-align: center;">Aluminum, Steel</td></tr> <tr><td>Power Law Coefficient</td><td style="text-align: center;">1</td></tr> </table>	Frequency	Higher modes	Comparison	Şimşek [32] and Li [34]	Boundary Condition	S-S	Aspect Ratio	4	Material	Aluminum, Steel	Power Law Coefficient	1
Frequency	Higher modes																						
Comparison	ANSYS																						
Boundary Condition	C-F																						
Aspect Ratio	5, 20																						
Material	Alumina (Ceramic), Aluminum (Metal)																						
Frequency	Higher modes																						
Comparison	Şimşek [32] and Li [34]																						
Boundary Condition	S-S																						
Aspect Ratio	4																						
Material	Aluminum, Steel																						
Power Law Coefficient	1																						

3.2.1 Uniform Geometry with Homogeneous Material

The first two numerical examples in this section are focused on the fundamental frequency. The third example will spotlight frequencies of the higher modes in the modal analysis.

A uniform geometry beam element with homogeneous material in x-z plane is shown in Figure 3.1.

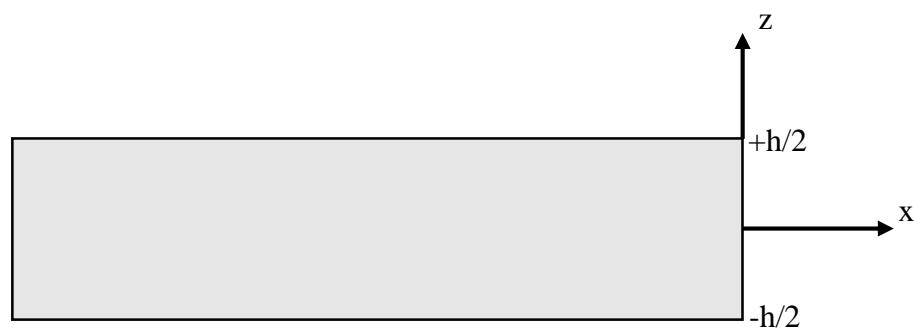


Figure 3.1 A uniform geometry beam element with homogeneous material in x-z plane

3.2.1.1 The First Numerical Example

In the first numerical example, the fundamental frequency obtained using the proposed formulation is compared with ANSYS in 2D and the solutions provided by Sina et al. [33]. In the latter approach, Timoshenko beam theory was used. The same model which was used by Sina et al. [33] is reproduced here for the case of Simply Supported (S-S) beam with pure aluminum for different L/h ratios as 10, 30, 100.

The properties of the first numerical example are shown in Table 3.2 where E , ρ , ν , κ_s are the Young's modulus, density, Poisson's ratio and the shear correction factor, respectively.

Table 3.2 The properties of the uniform beam element with pure aluminum

Boundary Condition	Aspect Ratio (L/h)	Homogeneous Material	E (GPa)	ρ (kg / m ³)	ν	κ_s
S-S	10	Aluminum	70	2700	0.23	5/6
	30					
	100					

The non-dimensional fundamental frequency was presented in [33] as follows:

$$\omega = \bar{\omega}L^2 \sqrt{\frac{\int_{-h/2}^{h/2} \rho dz}{h^2 \int_{-h/2}^{h/2} E dz}} \quad (3.1)$$

where $\bar{\omega}$, h , L are natural frequency, total depth and total length, respectively.

A comparison of the fundamental frequencies for three different aspect ratios is shown in Figure 3.2 where n_e is the number of elements used in the current modal analysis and ω_{FB} is the non-dimensional frequency obtained with the use of the proposed method in this thesis, where FB stands for the force based method or also called as the mixed formulation. The proposed FB method has varying frequency values as the number of elements changes as 1, 2, 4 and 8. However, in the paper by Sina et al. [33], there was only one frequency result specified for each aspect ratio, which was actually obtained by solving the differential equations through a finite difference scheme. Therefore, different frequency values for each number of elements obtained from the proposed method is compared with single value reported by [33] in Figure 3.2. The vertical axis is normalized as $\omega_{FB}/\omega_{Sina}$ where denominator represents for the non-dimensional frequency of the study by Sina et al. [33] and the scale for the horizontal axis is selected logarithmic with base 2 since the number of elements is increased as the power of 2. Furthermore, as a result of normalization process, when the ratio on the vertical axis becomes 1.00, a perfect match is obtained. When the ratio is larger

than 1, it means that the frequency value of FB is larger than the results from Sina et al. [33] and for the opposite scenario, FB is smaller than [33].

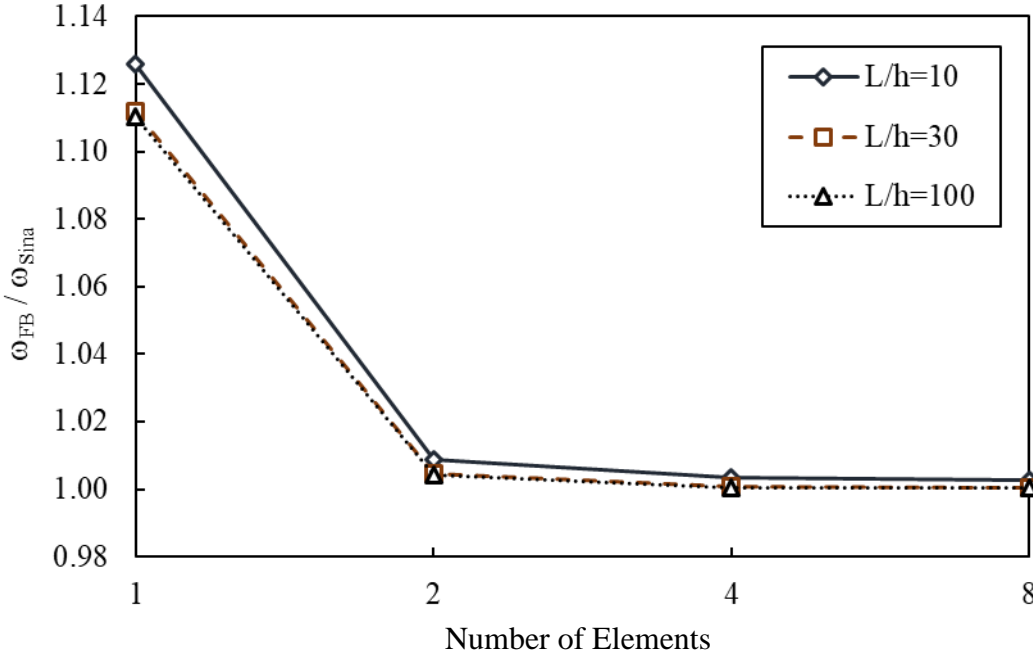


Figure 3.2 The comparison of the fundamental frequency obtained using FB and Sina et al. [33], S-S beam, material aluminum, with increasing number of elements in the solution

A similar comparison of the fundamental frequency obtained by the proposed method and ANSYS results is given in Figure 3.3 where ω_{ANSYS} symbolizes for frequency obtained from ANSYS in 2D. The same normalization procedure is applied between the frequencies of the FB method for different number of elements and one frequency result from ANSYS software for each different aspect ratio. In the analysis of ANSYS, 2D behavior is formed using plane stress model with the quadrilateral dominant method. This method contains triangular and rectangular finite elements in the mesh discretization and the selection is controlled by the program. The number of elements used for the first numerical example is 195, 228 and 276 for the different L/h ratios of 10, 30 and 100, respectively.

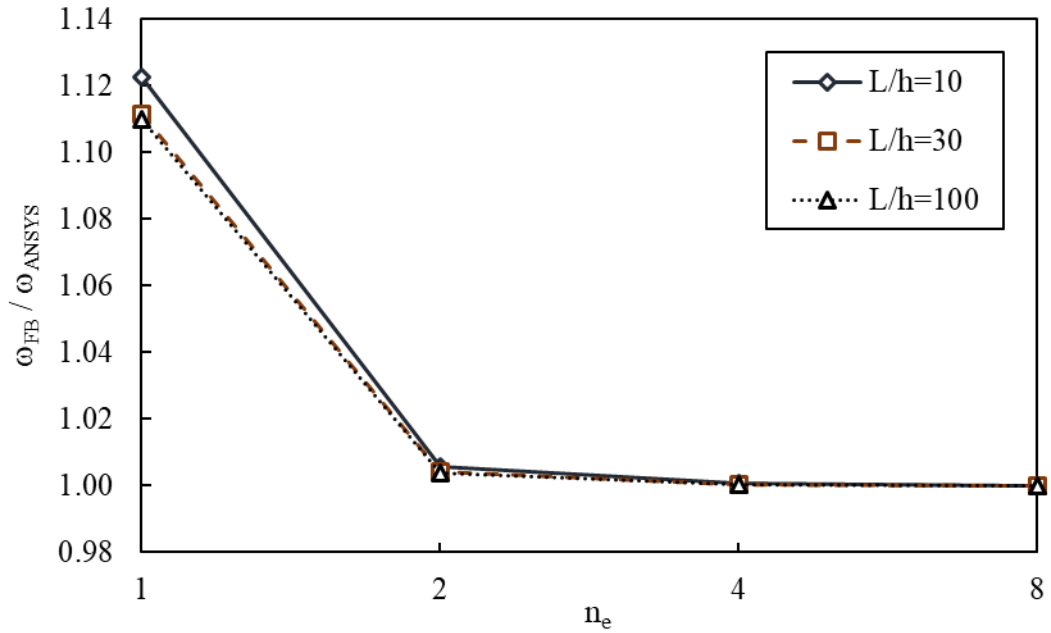


Figure 3.3 The comparison of the fundamental frequency obtained using FB and ANSYS, S-S beam, material aluminum, with increasing number of elements in the solution

In Figure 3.2 and Figure 3.3, the number of elements for the finite element analysis with the proposed formulation is presented for 1, 2, 4 and 8 to catch the trend easily because the behavior continues very similar for 16 and 32 elements compared to 4 elements. Additionally, the ratio converges to 1.00 for all aspect ratios and converges to 1.000 except for aspect ratio 10 after 4 finite elements in Figure 3.2.

A careful examination of Figure 3.2 and Figure 3.3 reveal that the FB method provides somewhat closer frequency values to the modal analysis results of ANSYS software than Sina et al. [33]. Since the results from ANSYS are more realistic for real life problems for the homogeneous material case, the proposed method is more successful than Sina et al. [33] in both the thick and thin beam cases. Additionally, when the number of elements increases, the ratios on the vertical axis converge to 1.00 quickly in both figures. For example, Figure 3.3 shows that $n_e = 2$ provides fairly enough accuracy and for $n_e = 4$, the FB method presents precise solutions up to three decimal

points for all three aspect ratios. It can also be concluded that for smaller aspect ratios i.e. thick beams, the difference is more significant especially in Figure 3.2.

In this numerical example, shear correction factor is specified as 5/6. However, in order to highlight the effect of shear correction factor for different aspect ratios, a comparison study has been conducted. The comparison of the fundamental frequency obtained using FB method for three aspect ratios is presented in Table 3.3 in the form of the percent differences of frequencies for calculation with two different factors, 1 and 5/6 when $n_e = 32$ as calculated using Equation (3.2). It can be observed that when the aspect ratios get smaller, the difference increases, this means that for short and deep beams, the influence of shear deformation is more significant as mentioned in Section 2.2.

Table 3.3 The percent differences of frequencies for calculation with two different factors, 1 and 5/6 when $n_e = 32$

Aspect Ratio (L/h)	Difference (%)
10	0.195
30	0.022
100	0.002

$$\frac{|\omega_{\text{FB}, \kappa_s=1} - \omega_{\text{FB}, \kappa_s=5/6}|}{\omega_{\text{FB}, \kappa_s=5/6}} \times 100 \quad (3.2)$$

3.2.1.2 The Second Numerical Example

In the second numerical example, the fundamental frequency obtained using the proposed formulation is compared with Şimşek [32] and ANSYS in 2D. Two different materials, i.e., alumina and aluminum, were used in [32] with different boundary conditions corresponding to the clamped-free (C-F), clamped-clamped (C-C) and pinned-pinned (P-P) cases. For the consistency in this work, S-S terminology is used

instead of P-P in the numerical examples, because the beam is actually free to move in the axial direction. Alumina and aluminum were referred to as ceramic and metal, respectively, in [32]. Two aspect ratios, 5 and 20 are used in this work.

The properties of the second numerical example with pure alumina and aluminum are tabulated in Table 3.4, where E , ρ , ν , κ_s are the Young's modulus, density, Poisson's ratio and the shear correction factor, respectively.

Table 3.4 The properties of the uniform beam element with pure alumina and aluminum

Boundary Conditions	Aspect Ratios (L/h)	Homogeneous Material	E (GPa)	ρ (kg / m ³)	ν	κ_s
C-F	5	Ceramic (Alumina)	380	3960	0.3	5/6
C-C						
S-S		Metal (Aluminum)	70	2702		

The non-dimensional fundamental frequency was presented in [32] as follows:

$$\lambda = \frac{\omega L^2}{h} \sqrt{\frac{\rho_m}{E_m}} \quad (3.3)$$

where λ , ω are non-dimensional and natural frequencies, ρ_m and E_m represents density and Young's modulus of aluminum, h and L are total depth and total length, respectively. Additionally, in Equation (3.3), the left side of formula was written incorrectly as λ^2 instead of λ in [32].

The comparison of the fundamental frequencies between the FB method and [32] for all the above cases is presented in Figures 3.4 to 3.9. The results from the FB method

is compared with the frequencies obtained with ANSYS in 2D in Figures 3.10 to 3.12.

There are four different parameters which need to be considered in the validation of the proposed method: the boundary conditions, aspect ratio, two particular materials (ceramic, metal) and the number of elements. Additionally, the outcomes of ANSYS and the use of AMR option with ANSYS are presented as another parametric study as given in Table 3.5 and Table 3.6.

As mentioned in the first numerical example, increasing number of finite elements are used with the FB method. The scale for the horizontal axis is selected logarithmic. The frequency obtained from the different number of elements with the FB method is also compared with frequency value reported in [32] and the frequency obtained in ANSYS in 2D. In this example, C-F is the first boundary condition that is used with the ceramic material in Figure 3.4 and with metal in Figure 3.5 for the comparison between FB and [32]. The C-C and S-S beams sequentially follow the C-F beams with the same order.

For Figures 3.4 to 3.9, the most easily noticed point is that the behavior follows a similar pattern with ceramic and metal for all three different boundary conditions. In fact, the ratios of the frequencies between FB and [32] with ceramic and metal are the same at least for three decimal points. Further inspection of the figures for the comparison of the frequencies between FB and [32] shows that for beams with $L/h = 5$, which represents short and deep beams, the ratio converges slower than for beams with $L/h = 20$. However, the proposed method is precise even for $n_e = 4$ with $L/h = 5$ because the ratios become 1 with zeros up to three decimal points with C-F beam and two decimal points with C-C and S-S beams.

In Figure 3.6 and Figure 3.7, there are no data points for one element because the proposed method cannot capture the fundamental frequency when $n_e = 1$ for the C-C boundary condition. On the other hand, this shortcoming can be overcome when the fixed end on the right side is released on the horizontal axis. Moreover, the frequency

values obtained from the proposed method stays exactly the same even though it is free to translate on the horizontal direction. Figure 3.6 and Figure 3.7 show that for the C-C beams when $L/h = 5$, the fundamental frequency ratios converge to a value that is slightly less than 1.00. This means that the FB results are lower than the results of [32] for the C-C beams.

For the comparison between FB and ANSYS, the C-F ceramic beam is studied first. The C-C and S-S conditions are investigated later. Figures for the metal case for all three boundary conditions are not presented for the sake of brevity as the results follow the same trend for the metal and ceramic cases.

According to Figure 3.8 and Figure 3.12, the behavior of the proposed FB method is identical for the S-S beam when compared with [32] and ANSYS, however, there is a difference for the C-F and C-C beam boundary conditions between the two approaches. The difference becomes more significant for the C-C beam than C-F beam. In ANSYS, the clamped boundary conditions provide exact fixity, while the beam elements only provide fixity on a single point at the end. Thus, for short and deep beams, the results of the beam element solution diverge from the ANSYS results. Moreover, since the C-C beam has fixed supports on both sides, the difference is more than the C-F beam which has only one fixed support; the results presented in the figures are thus compatible with this argument. Consequently, the most precise results are obtained with the S-S beam and the precision of the S-S beam is also corroborated by the results of the first numerical example.

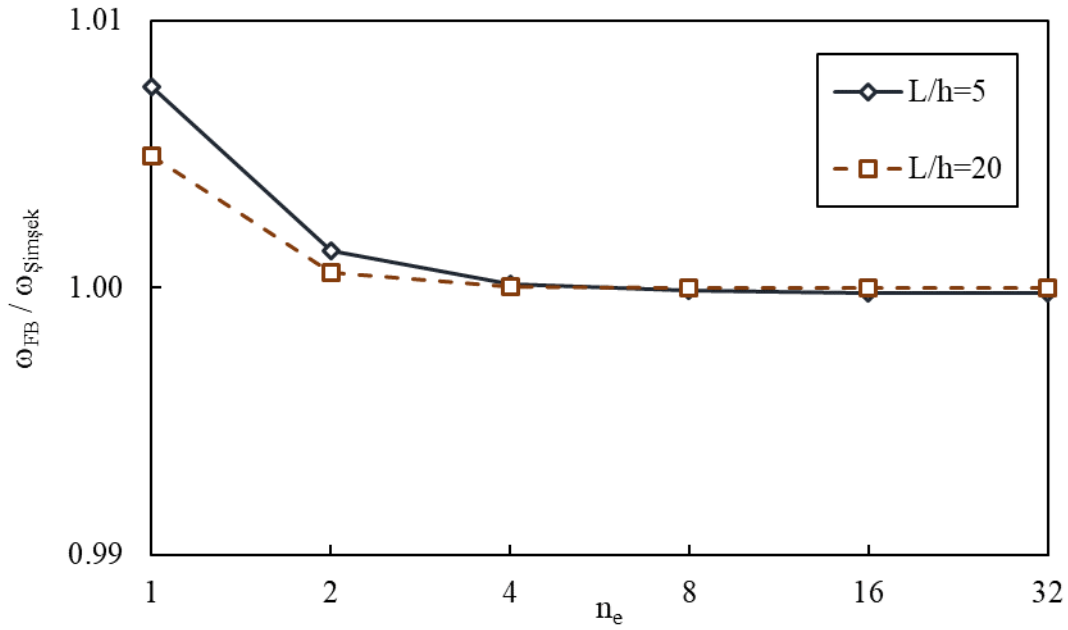


Figure 3.4 The comparison of the fundamental frequency obtained using FB and Şimşek [32], C-F beam, material ceramic, with increasing number of elements in the solution

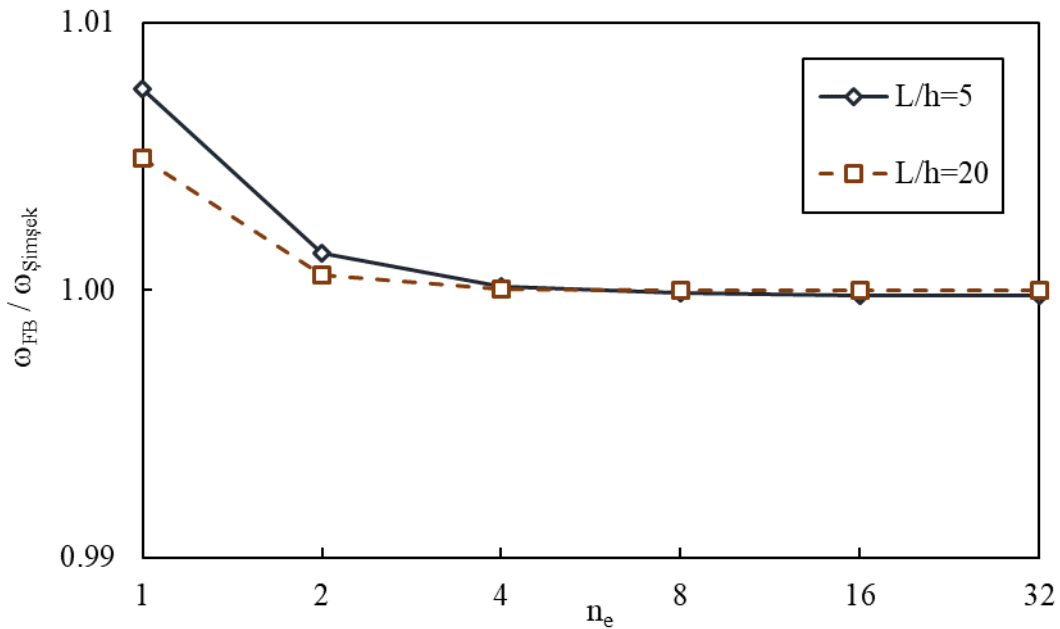


Figure 3.5 The comparison of the fundamental frequency obtained using FB and Şimşek [32], C-F beam, material metal, with increasing number of elements in the solution

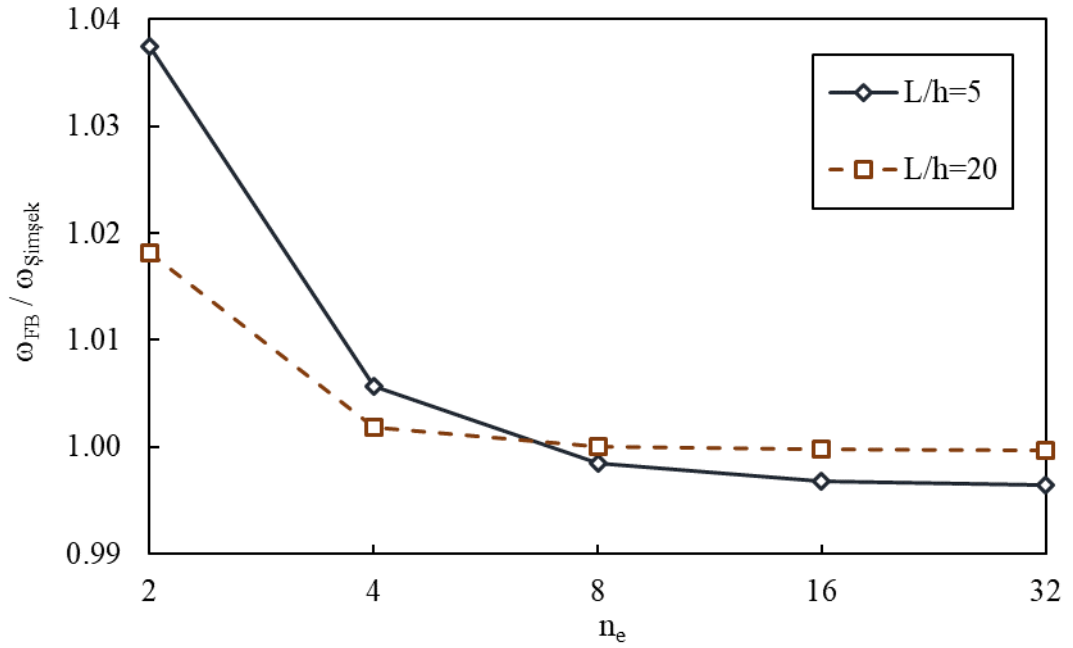


Figure 3.6 The comparison of the fundamental frequency obtained using FB and Şimşek [32], C-C beam, material ceramic, with increasing number of elements in the solution

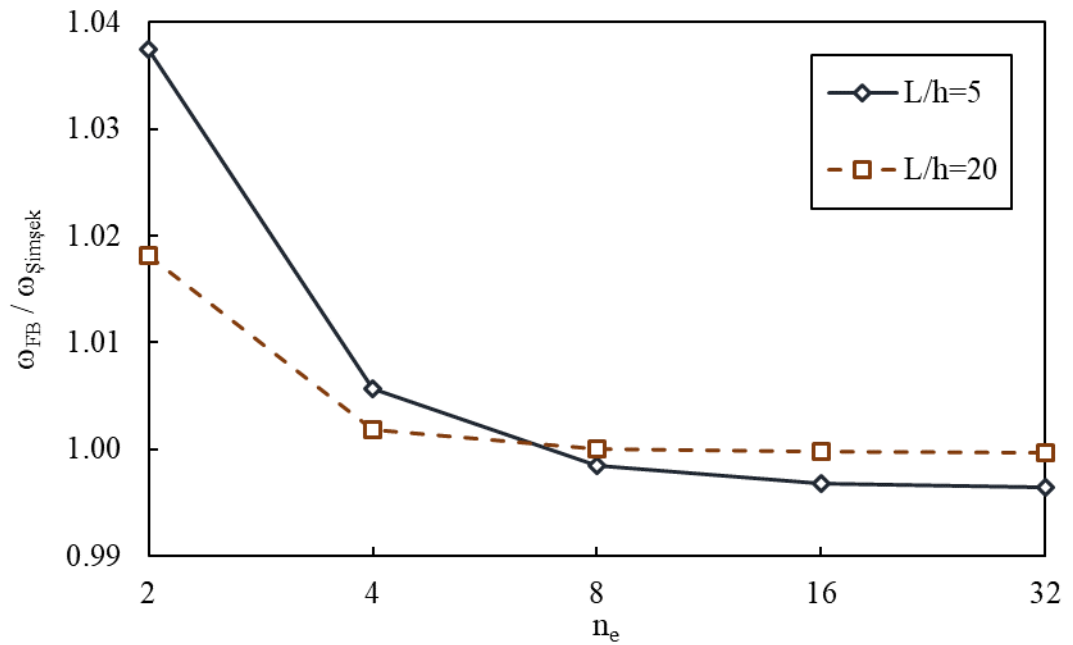


Figure 3.7 The comparison of the fundamental frequency obtained using FB and Şimşek [32], C-C beam, material metal, with increasing number of elements in the solution

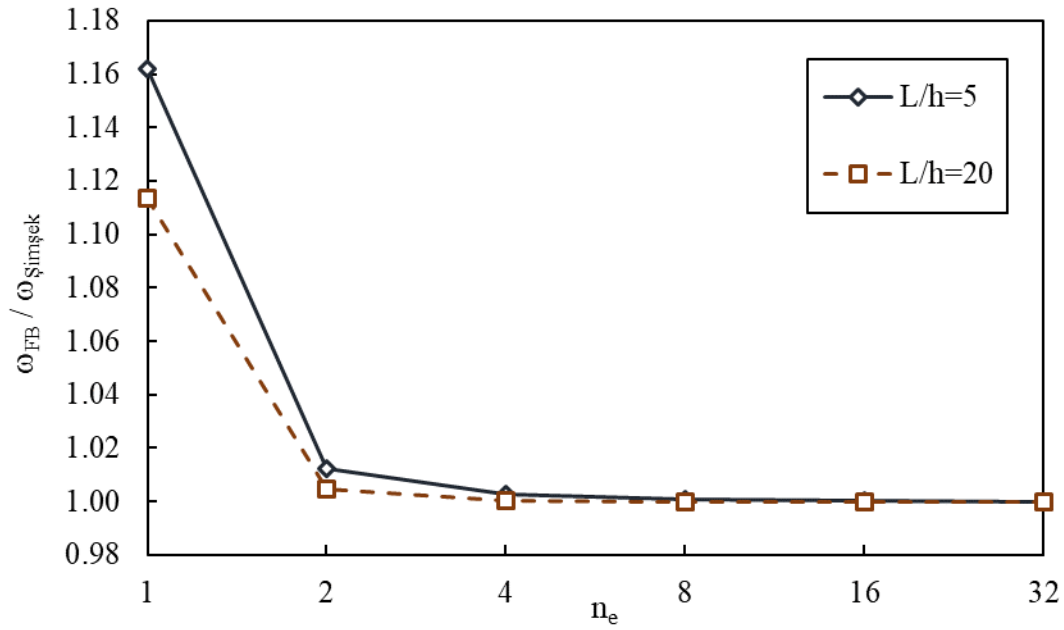


Figure 3.8 The comparison of the fundamental frequency obtained using FB and Şimşek [32], S-S beam, material ceramic, with increasing number of elements in the solution

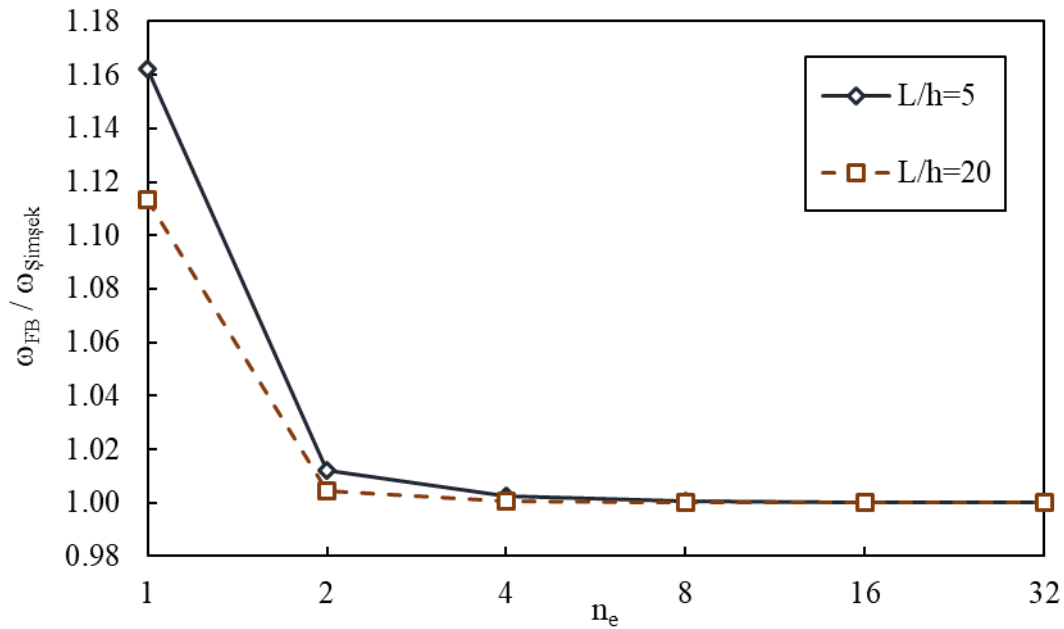


Figure 3.9 The comparison of the fundamental frequency obtained using FB and Şimşek [32], S-S beam, material metal, with increasing number of elements in the solution

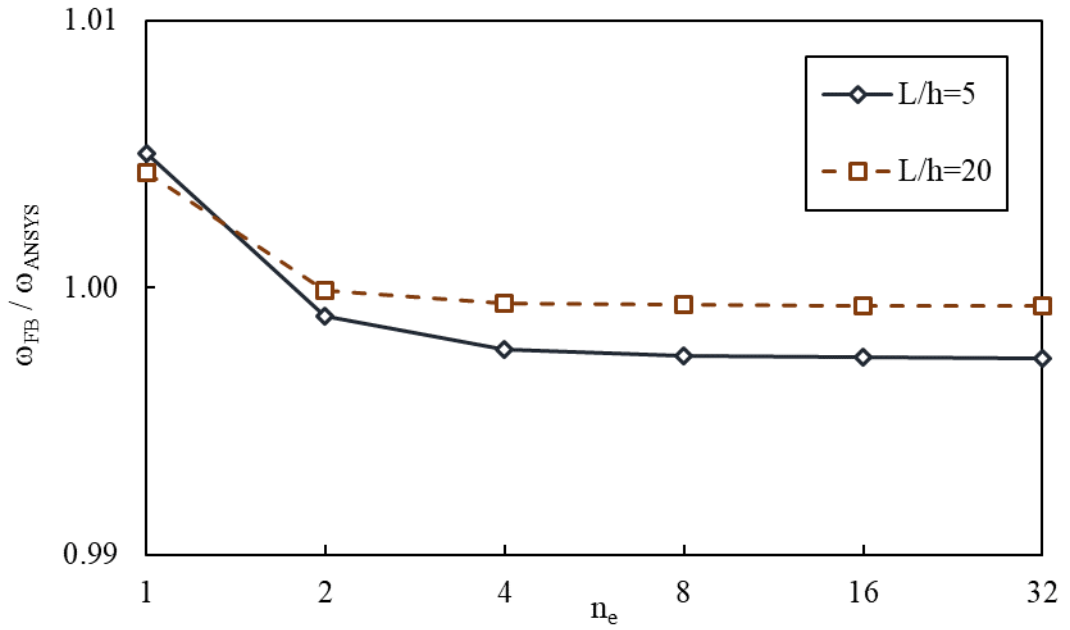


Figure 3.10 The comparison of the fundamental frequency obtained using FB and ANSYS, C-F beam, material ceramic, with increasing number of elements in the solution

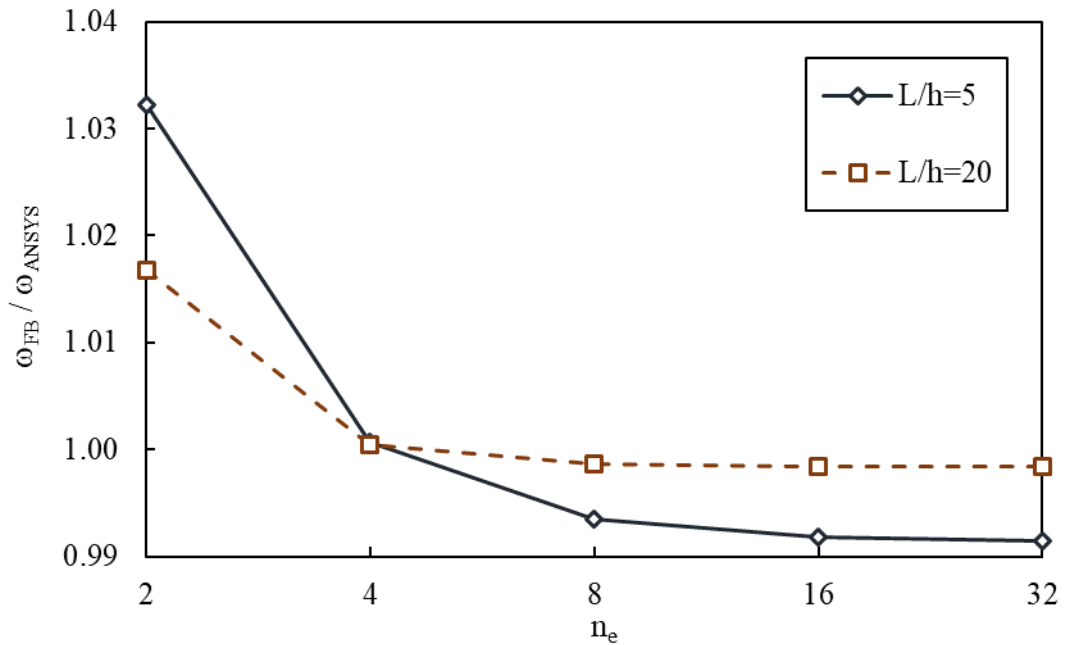


Figure 3.11 The comparison of the fundamental frequency obtained using FB and ANSYS, C-C beam, material ceramic, with increasing number of elements in the solution

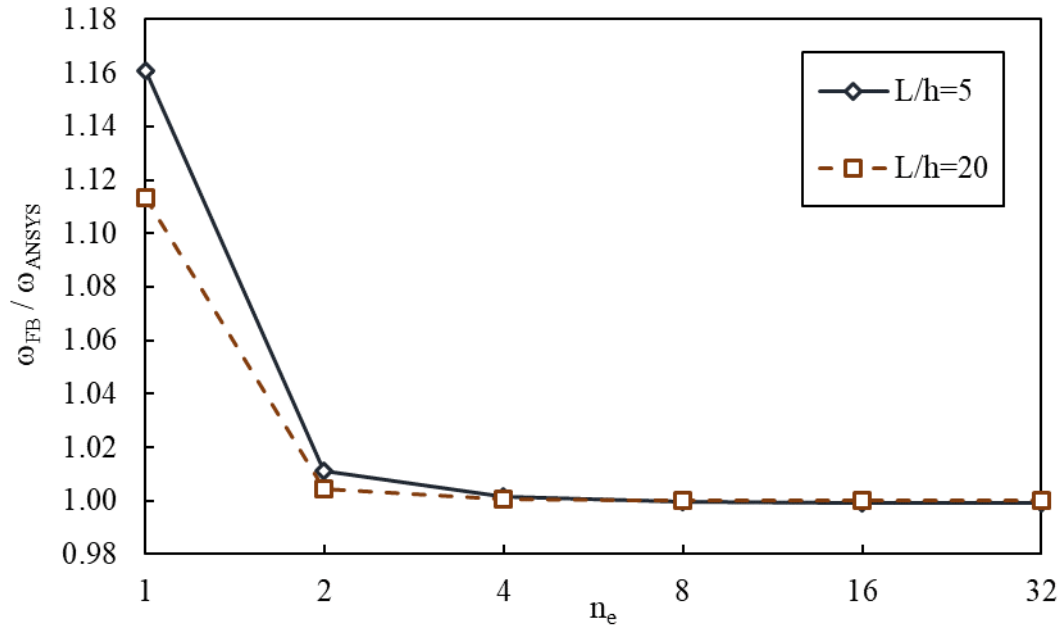


Figure 3.12 The comparison of the fundamental frequency obtained using FB and ANSYS, S-S beam, material ceramic, with increasing number of elements in the solution

A careful examination of all the presented figures shows that the ratios with regard to the [32] and ANSYS solution converge faster for $L/h = 20$ case than the $L/h = 5$ counterpart, because the latter one represents thick beams which require the use of higher order beam theories. Constant shear deformation assumption is not good enough for FB when compared to the ANSYS solution, because the ANSYS model represents real beam characteristics better than the proposed method. The shortcoming of the proposed method is due to the thick beams. It can be explained with the provision of fixity on a single point at the end. Consequently, the boundary condition effects get more significant when $L/h = 5$. The same explanation is also valid with the C-F and C-C beams. When the C-C case and $L/h = 5$ aspect ratio are used together, the boundary conditions affect the solution at the maximum level.

A better comparison of the proposed method with different boundary conditions is provided in Figures 3.13 to 3.16 for each aspect ratio with the ceramic material. In

order to highlight on the convergence of the ratios of the FB and the compared solutions, the number of elements in the plot is started from two instead of one.

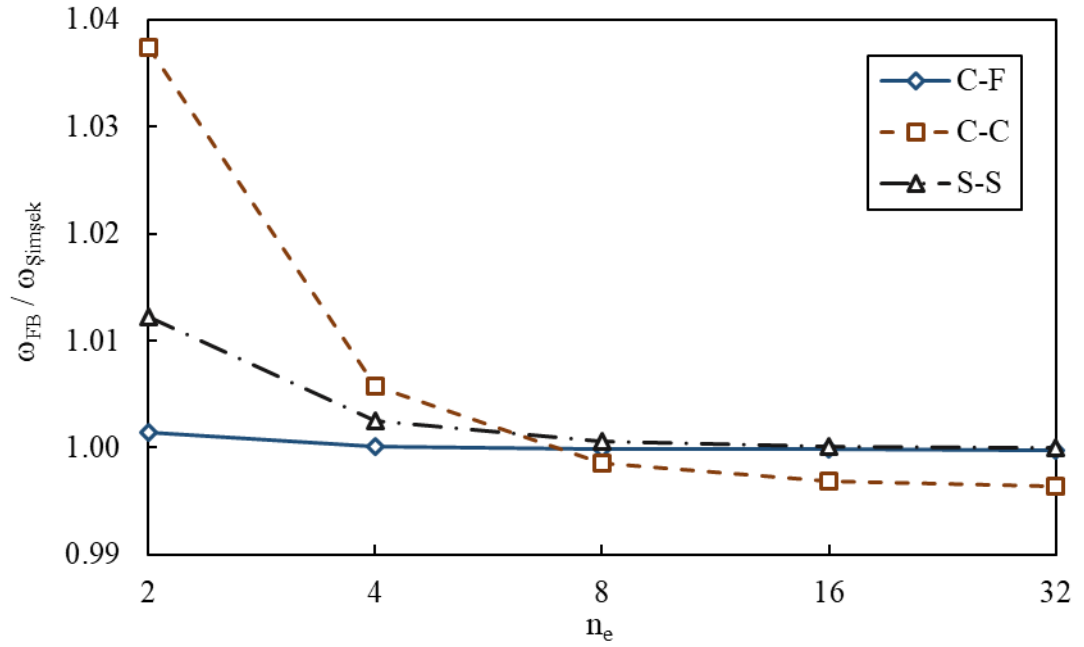


Figure 3.13 The comparison of the fundamental frequency obtained using FB and Şimşek [32], material ceramic, aspect ratio $L/h=5$, with increasing number of elements in the solution

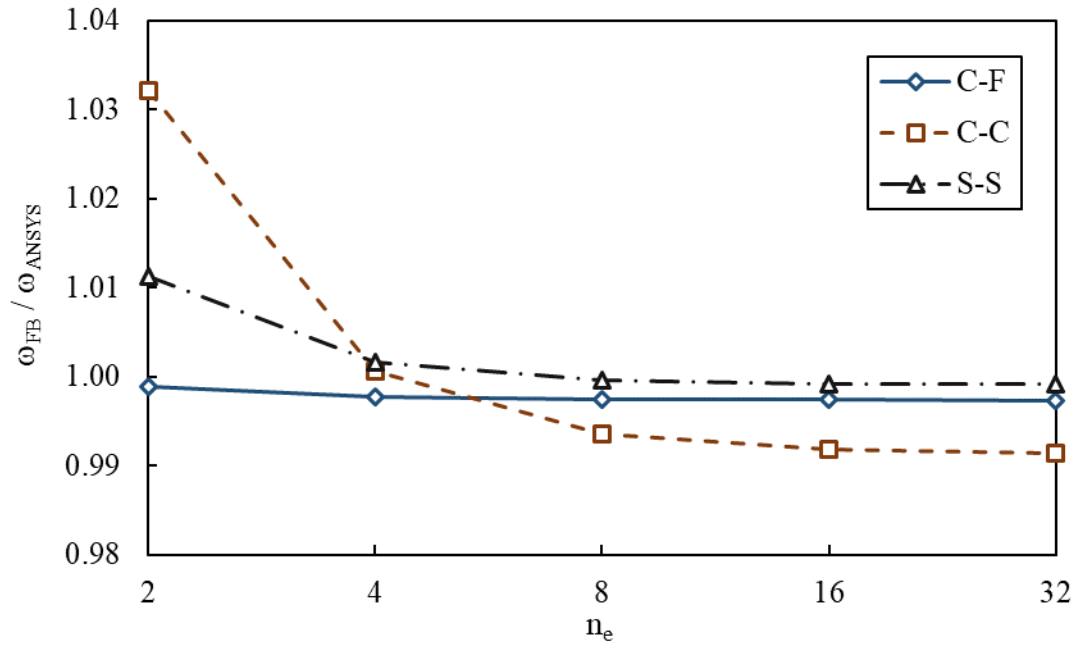


Figure 3.14 The comparison of the fundamental frequency obtained using FB and ANSYS, material ceramic, aspect ratio $L/h=5$, with increasing number of elements in the solution

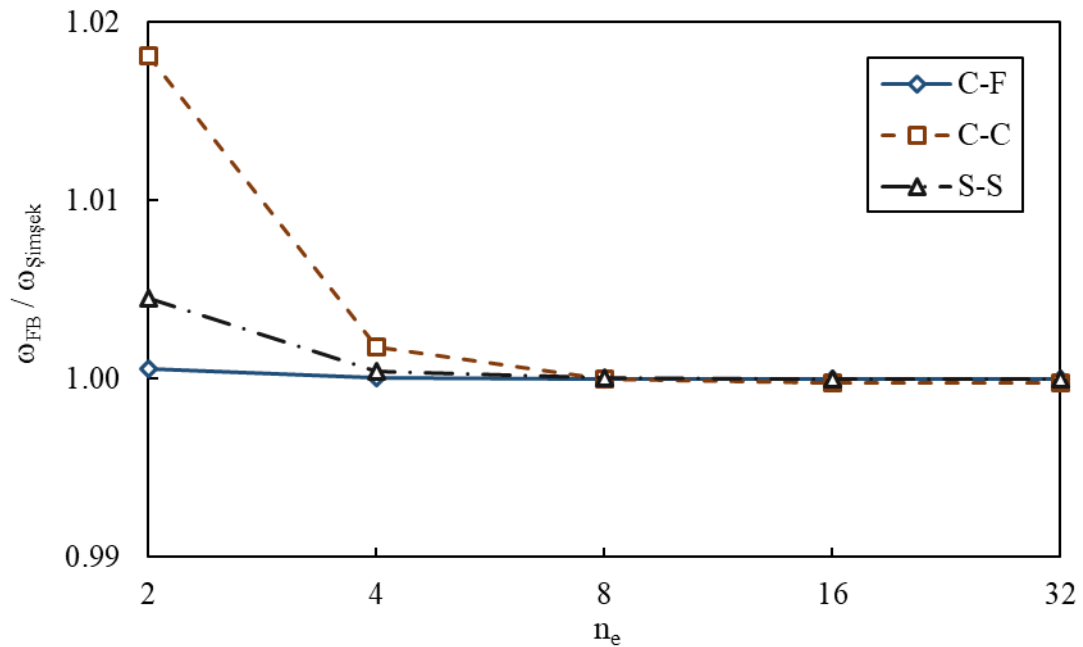


Figure 3.15 The comparison of the fundamental frequency obtained using FB and Şimşek [32], material ceramic, aspect ratio $L/h=20$, with increasing number of elements in the solution

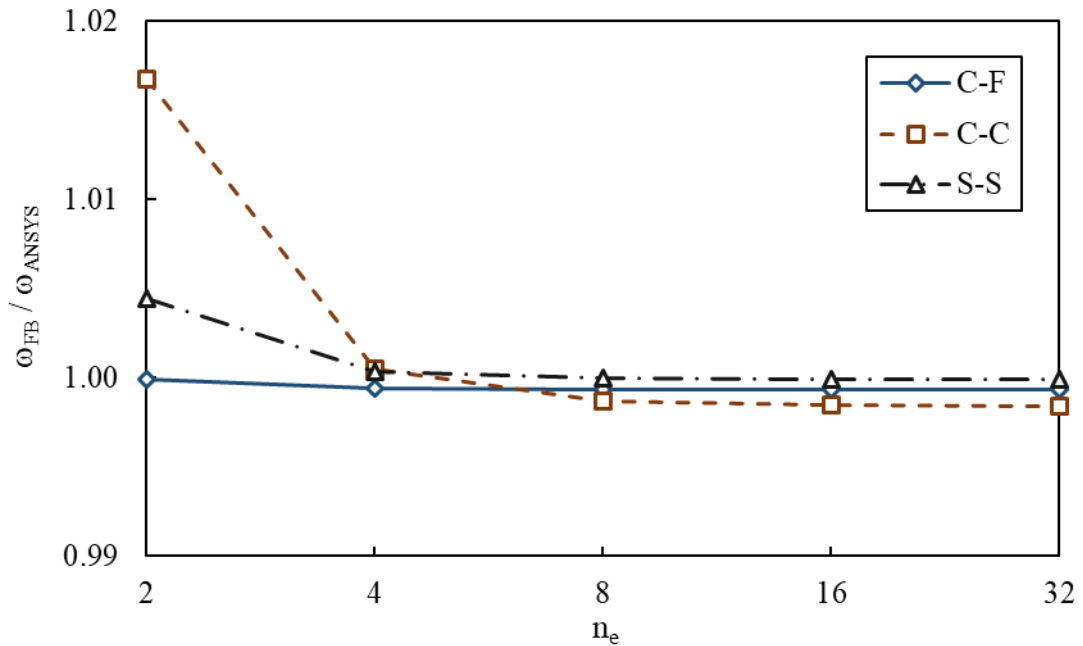


Figure 3.16 The comparison of the fundamental frequency obtained using FB and ANSYS, material ceramic, aspect ratio $L/h=20$, with increasing number of elements in the solution

Another parametric study is conducted comparing ANSYS results with its counterpart utilizing the Adaptive Mesh Refinement (AMR) option with ANSYS. AMR is an iterative convergence option tool which automatically refines the mesh until the user defined limits, such as the number of iterations or the error limit, are reached. The advantage of this additional option is that the refinement is only provided on a particular area for a specific result instead of the entire area. The selection of the refined area is identified automatically by an adaptive solver engine for the requirement of a specific result and the specific result in this example is total deformation. Before performing adaptive convergence, an initial mesh refinement needs to be defined and the fineness of the mesh is controlled by changing the relevance factor. This factor is in the range of -100 and +100. A relevance factor of +100 provides the highest accuracy, on the other hand, -100 is used for the highest speed. Higher accuracy is obtained with a finer mesh discretization, however, the advantage of a coarse mesh is being faster than fine mesh discretization.

In Table 3.5 and Table 3.6, the models of ANSYS with a relevance factor +75 which is initially discretized as a fine mesh and ANSYS with AMR option are compared. In these comparisons, different boundary conditions, aspect ratios and materials are considered in order to show that the results differentiate with respect to different mesh discretization and the model is as good as how it represents the real life cases. In ANSYS, 2D behavior is formed using plane stress model with triangular/quadrilateral elements with quadratic approximation. This element, PLANE183, consists of the mixture of triangular and quadrilateral finite elements and the selection is controlled by the program with two degrees of freedom at each node: the translations in the x and z directions. Figures 3.17 to 3.19 present different mesh discretization samples for C-F and C-C beams to show how the model is refined.

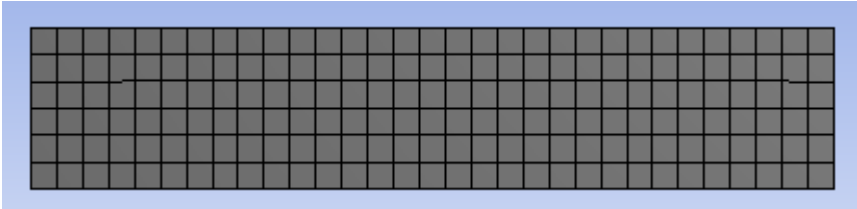


Figure 3.17 The mesh refinement with +75 relevance factor for C-F and C-C beams, material ceramic, $L/h = 5$, number of elements 186

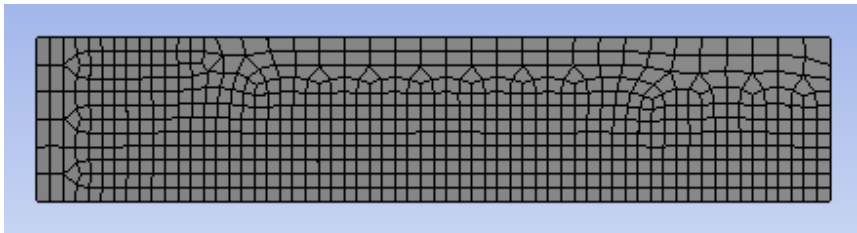


Figure 3.18 The mesh refinement with AMR for C-F beam, material ceramic, $L/h = 5$, left side fixed, number of elements 654

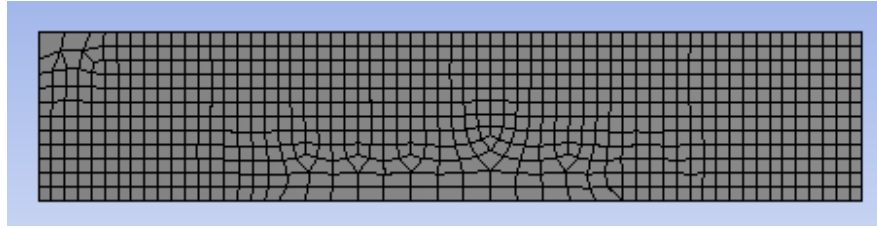


Figure 3.19 The mesh refinement with AMR for C-C beam, material ceramic, $L/h = 5$, number of elements 706

The number of elements and the difference (in percent) of the fundamental frequency are presented in Table 3.5 and Table 3.6, respectively. As can be observed in Table 3.5, the maximum number of elements for the mesh refinement is required for the C-C beam case when $L/h=5$. This is expected since there are two fixed sides on a thick beam. Thus, a more refined mesh discretization is necessary to reach the minimum convergence limit.

Table 3.5 The comparison of the number of elements obtained using ANSYS and ANSYS with AMR for two different parameters with the ceramic material

Boundary Conditions	Number of Elements			
	$L/h = 5$		$L/h = 20$	
	ANSYS	ANSYS with AMR	ANSYS	ANSYS with AMR
C-F	186	654	186	625
C-C	186	706	186	625

In Table 3.6, the difference in percentage is very small between two materials when the other conditions are the same and two iterations are enough to obtain more refined results with AMR for these models because the geometric model initially has finer mesh discretization of ANSYS even before AMR. However, the maximum value is again observed with C-C beam for $L/h = 5$ and this supports the conclusion from Table 3.5.

Table 3.6 The difference in percent of the fundamental frequencies between ANSYS and ANSYS with AMR for three different parameters

Boundary Conditions	Difference (%)			
	L/h = 5		L/h = 20	
	Ceramic	Metal	Ceramic	Metal
C-F	0.018	0.019	0.013	0.015
C-C	0.040	0.035	0.032	0.031

The last numerical example for the uniform geometry case with homogeneous material will be presented in the next section. Higher mode frequencies will be provided for the first time for the case of homogeneous material.

3.2.1.3 The Third Numerical Example

In the third numerical example, the frequencies of the higher modes obtained by the proposed method are compared with the ANSYS results. Material properties are identical to the second example, i.e. pure alumina and aluminum, with one boundary condition case, namely C-F condition.

As the results are similar for both materials, they are only presented for the ceramic case. The comparison of the frequencies for the higher modes obtained using FB and ANSYS with the C-F beam having aspect ratios of 5 and 20 are shown in Figure 3.20 and Figure 3.21, respectively. As it is not possible to capture mode 4 and 5 with one element using the proposed method, no data is presented for these modes when $n_e = 1$. For the C-F beams, one element can only capture three modes while for two elements, six modes can be obtained.

In Figure 3.20 and Figure 3.21, the scales of the vertical and horizontal axes are the same with the previous examples. The only different parameter is the aspect ratios as 5 and 20 in the aforementioned figures. When comparing the results for the aspect ratios of 5 and 20, it should be mentioned that the results cannot be compared directly according to the mode number alone. For example, mode 3 in Figure 3.20 is the first

axial mode whereas mode 3 in Figure 3.21 is the third bending mode. Therefore, the former needs to be compared with mode 4 in Figure 3.21, since that is the first axial mode. Each mode is compared individually for the two different aspect ratios in detail in Figures 3.22 to 3.26.

From Figure 3.20 and Figure 3.21, it can be concluded that all five frequency ratios obtained from the higher modes converge to 1.00, when the number of elements increases. This observation shows that the proposed method is also successful for the higher modes. Moreover, the results for the 1st bending and 1st axial modes converge to 1.00 faster than the higher modes because it is more difficult to obtain the higher modes. This can be explained by the fact that the effects of boundary conditions are higher for the higher modes compared to the fundamental frequency (Manik [35]).

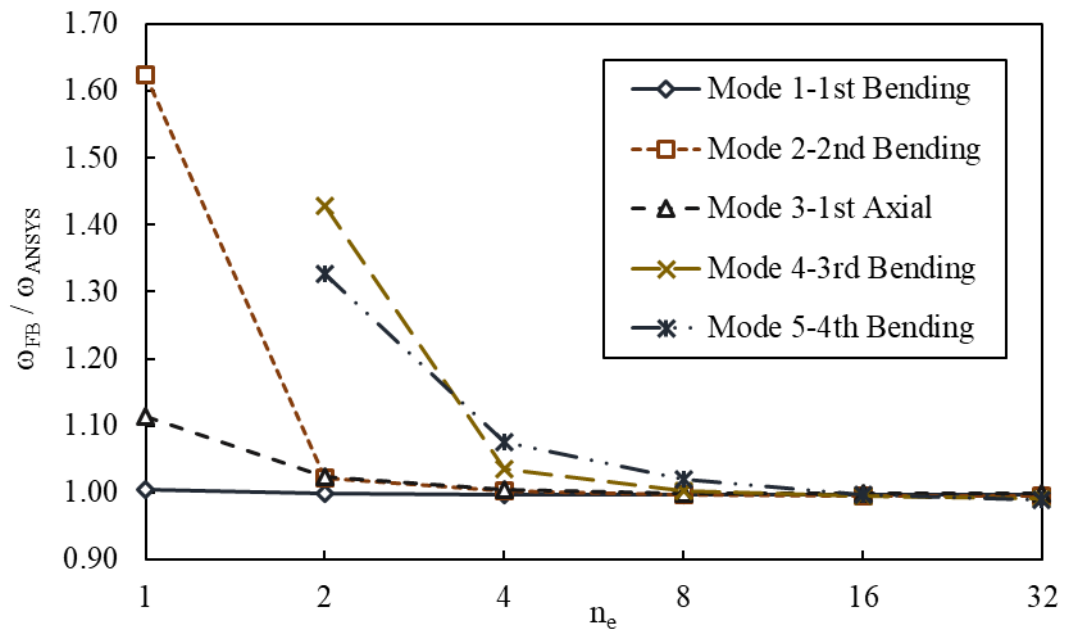


Figure 3.20 The comparison of the frequencies for the higher modes obtained from FB and ANSYS, C-F beam, material ceramic, aspect ratio $L/h = 5$, with increasing number of elements in the solution

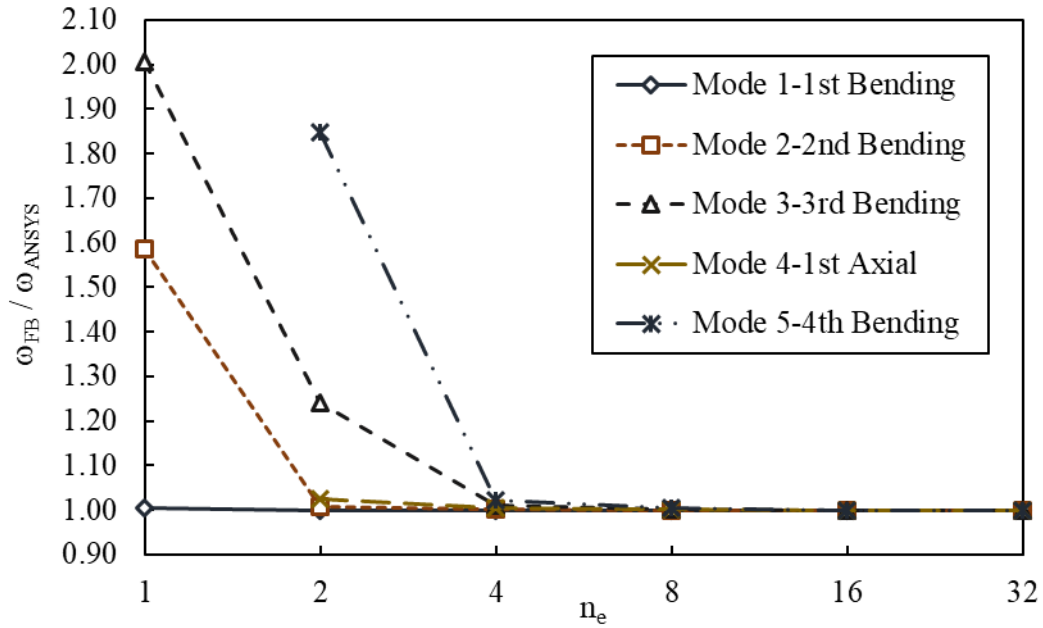


Figure 3.21 The comparison of the frequencies for the higher modes obtained from FB and ANSYS, C-F beam, material ceramic, aspect ratio $L/h = 20$, with increasing number of elements in the solution

ANSYS results are compared to their counterparts with the AMR option in Table 3.7 and Table 3.8 for beams with aspect ratios 5 and 20, respectively.

Table 3.7 The difference in percent of the higher modes between ANSYS and ANSYS with AMR for $L/h = 5$

	Mode	C-F	
		$L/h = 5$	
	Axial: A	Difference (%)	
	Bending: B	Ceramic	Metal
Mode 1	B	0.018	0.019
Mode 2	B	0.024	0.023
Mode 3	A	0.006	0.004
Mode 4	B	0.026	0.024
Mode 5	B	0.023	0.025

Difference in percent among the ANSYS and ANSYS with AMR solutions is obtained as below:

$$\frac{|\omega_{\text{ANSYS}} - \omega_{\text{ANSYS,AMR}}|}{\omega_{\text{ANSYS,AMR}}} \times 100 \quad (3.4)$$

Table 3.8 The difference in percent of the higher modes between ANSYS and ANSYS with AMR for L/h = 20

	Mode	C-F	
		L/h = 20	
	Axial: A	Difference (%)	
	Bending: B	Ceramic	Metal
Mode 1	B	0.013	0.015
Mode 2	B	0.016	0.016
Mode 3	B	0.021	0.020
Mode 4	A	0.008	0.005
Mode 5	B	0.031	0.024

After examination of Table 3.7 and Table 3.8, it is observed that the difference is smaller with the 1st bending and 1st axial modes than higher modes. In general, the difference is slight because the mesh discretization is selected with finer refinement obtained using +75 relevance factor which also provides high accuracy in ANSYS 2D without AMR.

From Figures 3.22 to 3.25, the ratios of the frequency obtained from the proposed methodology to the ANSYS results are presented for the first four modes. The most accurate one is the 1st bending mode as expected from the investigation of the fundamental frequency ratios in the first and second numerical examples. The ratio converges to 1 for the L/h = 20 case, however, for the L/h = 5 case, the ratio gets closer to 1, then diverge from this point when more than eight finite elements are used. One reason is due to the limitation of the Timoshenko beam theory using constant shear correction factor which is especially not true for thick beams. Consequently, the results for L/h = 5 can be improved by the use of higher order beam theories instead of the

Timoshenko beam theory. Another reason for the divergence is the assumption of the proposed method at the fixed end as explained in the second numerical example.

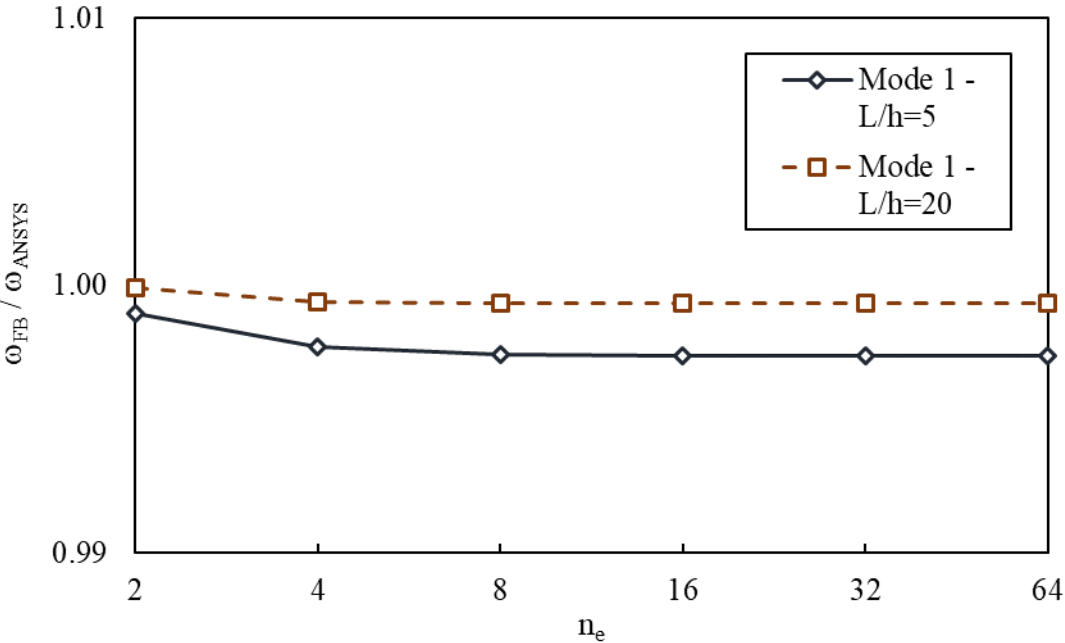


Figure 3.22 The ratio of 1st bending mode frequency obtained from FB and ANSYS, C-F beam, material ceramic, with increasing number of elements in the solution

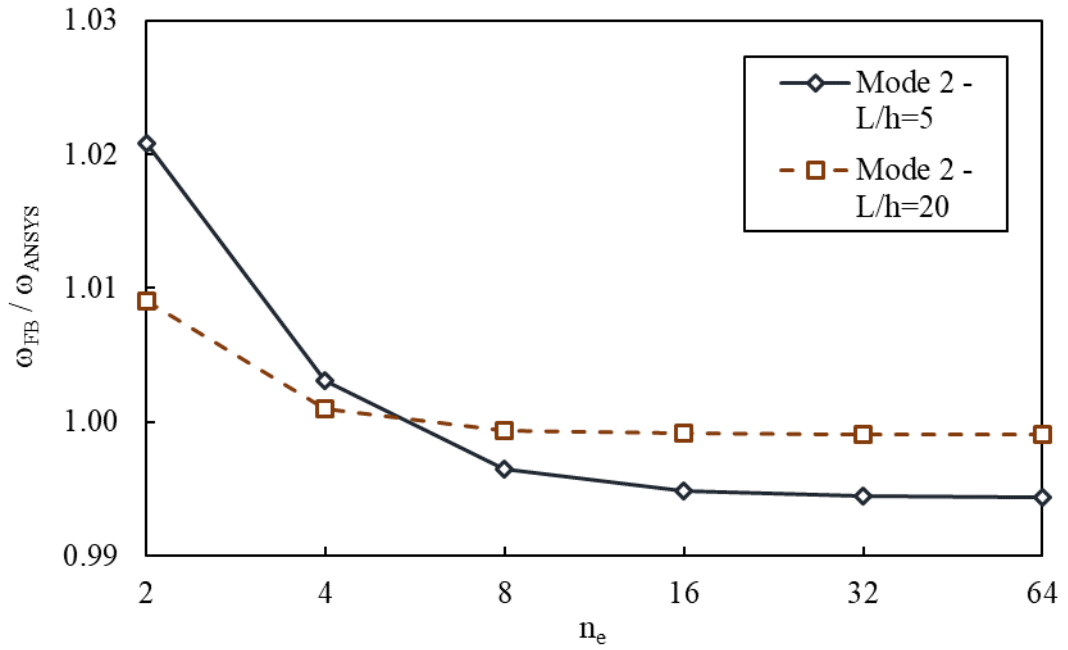


Figure 3.23 The ratio of 2nd bending mode frequency obtained from FB and ANSYS, C-F beam, material ceramic, with increasing number of elements in the solution

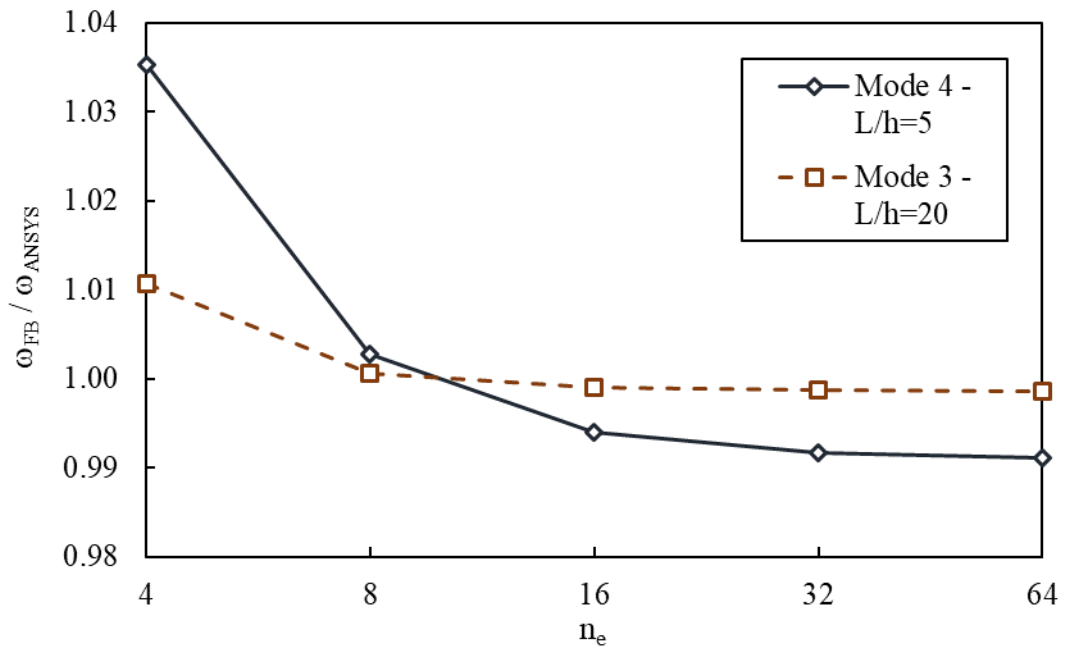


Figure 3.24 The ratio of 3rd bending mode frequency obtained from FB and ANSYS, C-F beam, material ceramic, with increasing number of elements in the solution

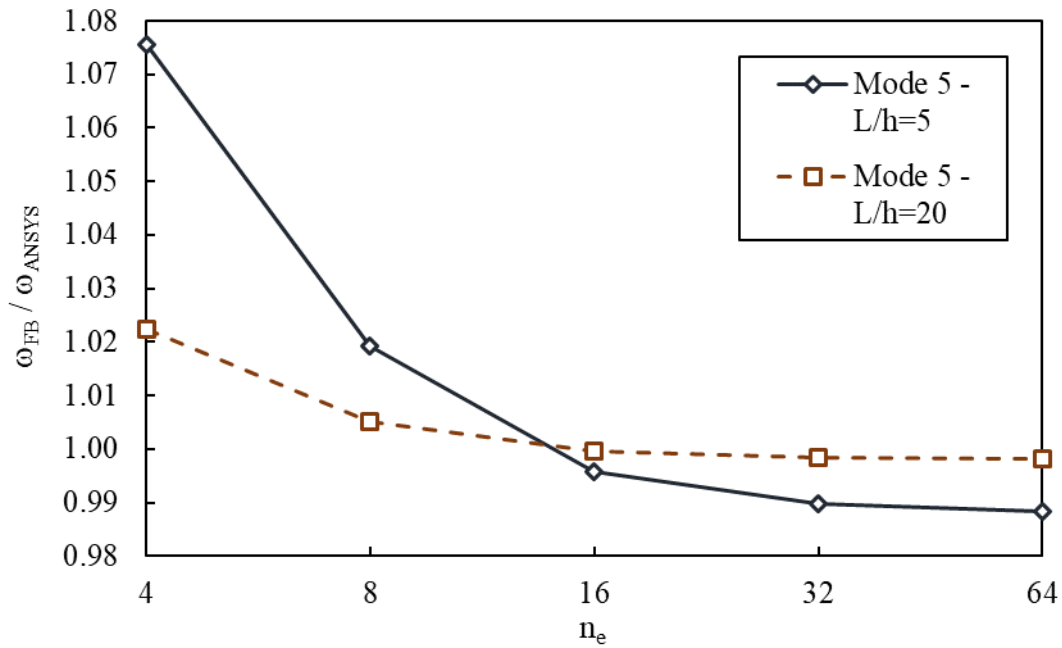


Figure 3.25 The ratio of 4th bending mode frequency obtained from FB and ANSYS, C-F beam, material ceramic, with increasing number of elements in the solution

In Figure 3.26, the ratio of the frequencies as obtained from the two methods for the 1st axial mode is presented. For aspect ratios of 5 and 20, the ratios follow a parallel trend for increasing number of elements. The ratios converge to values very close to 1 for both aspect ratios. As expected, the case with $L/h = 20$ gets a little closer to 1 than compared to the case with $L/h = 5$.

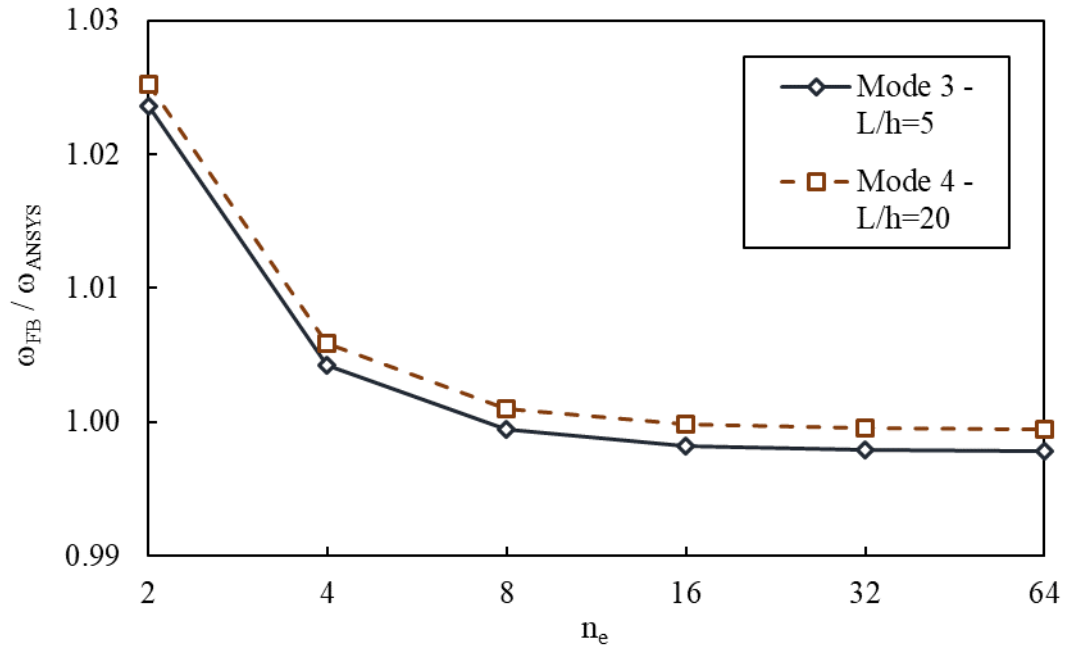


Figure 3.26 The ratio of 1st axial mode frequency obtained from FB and ANSYS, C-F beam, material ceramic, with increasing number of elements in the solution

In the next section, uniform geometry will be modelled with FGM instead of homogeneous material and another three numerical examples will be provided using the FGM.

3.2.2 Uniform Geometry with Functionally Graded Materials

In this section, power law function is used to represent continuous heterogeneous material distribution with FGM along the transverse direction. Formula for power law is outlined in Equation (2.23) where k stands for the material grading index. The effect of k on the material distribution is provided in Figure 2.7.

A uniform geometry beam element with FGM in x - z plane is presented in Figure 3.27.

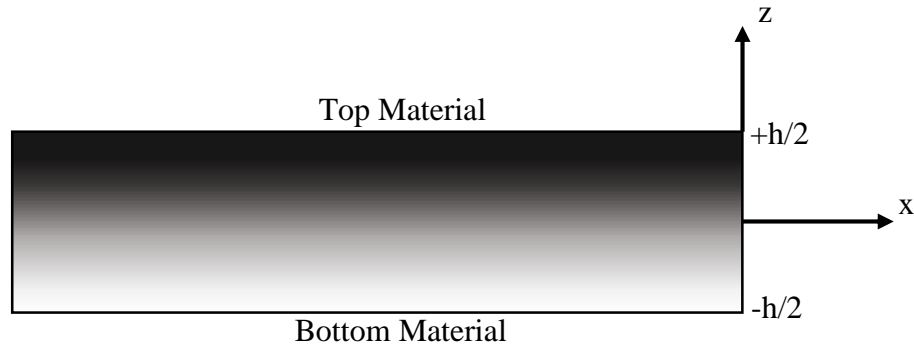


Figure 3.27 A uniform geometry beam element with FGM in x-z plane

In this section, three numerical examples will be presented with FGM. The first two will focus on fundamental frequency, and the higher modes will be investigated in the last example.

3.2.2.1 The Fourth Numerical Example

In the fourth numerical example, the fundamental frequency obtained from the proposed methodology is compared with results from Sina et al. [33] and Şimşek [32]. Timoshenko beam theory is selected to make results compatible with [33]. FGM is composed of two materials with a power law coefficient of $k = 0.3$ with different boundary conditions and aspect ratios. In this example, the topmost material alumina and bottommost material aluminum are addressed as ceramic and metal, respectively.

The properties of FGM used in this case are tabulated in Table 3.9 where E , ρ , ν , κ_s , k are the Young's modulus, density, Poisson's ratio, shear correction factor and the power law coefficient, respectively.

Table 3.9 The properties of the uniform beam element with FGM in particular at the topmost and bottommost materials

Boundary Conditions	Aspect Ratios (L/h)	FGM Materials		E (GPa)	ρ (kg / m ³)	ν	κ_s
		Top	Bottom				
C-F	10	Top	Alumina	380	3800	0.23	5/6
C-C	30	Bottom	Aluminum	70	2700		
S-S	100	k = 0.3					

The non-dimensional fundamental frequency is selected the same as in Equation (3.1).

In this example, for the transversely FGM of the beam, E and ρ are assumed to vary along the transverse direction by using Equation (2.23) with a power law coefficient of 0.3 as mentioned in Table 3.9, while the Poisson's ratio ν is taken constant. Delale and Erdoğan [36] explained that the effect of ν is not significant on the stress intensity factors, thus leading to the assumption of a single ν for the section. Xiang and Yang [37] also suggested that ν can be taken as a constant value to provide simplicity in calculations. Moreover, Li [34] concluded that as the variation of ν is not significant in practice, it can be taken constant for both materials. It is also noticed that ν was taken constant along the transverse direction by Şimşek [32].

In Figure 3.28 and Figure 3.29, the ratios of the fundamental frequency between the proposed FB method and those of Sina et al. [33] and Şimşek [32], respectively, are presented. In this example, a linear scale is selected for the vertical axis as in the previous examples, however, in the horizontal axis, the scale is provided logarithmic with base 10 instead of 2 to be able to outline three aspect ratios of 10, 30 and 100 clearly. The results from the proposed method is only shown for $n_e = 32$ with $k = 0.3$, for different boundary conditions and aspect ratios. Although $n_e = 4$ with FB provides results that are close enough to these methods, $n_e = 32$ is selected in order to focus on the precision of the proposed method and the convergence rate when the aspect ratio increases.

The proposed method with the C-C beam behaves very close to the cases with other boundary conditions when compared with Şimşek even for the slender beams. Figure 3.28 and Figure 3.29 show that the FB method converges to the results presented by Sina and Şimşek when the aspect ratio increases. Moreover, Fb approach provides precise results in line with Şimşek. The proposed method is acceptably precise and robust when used with the functionally graded materials.

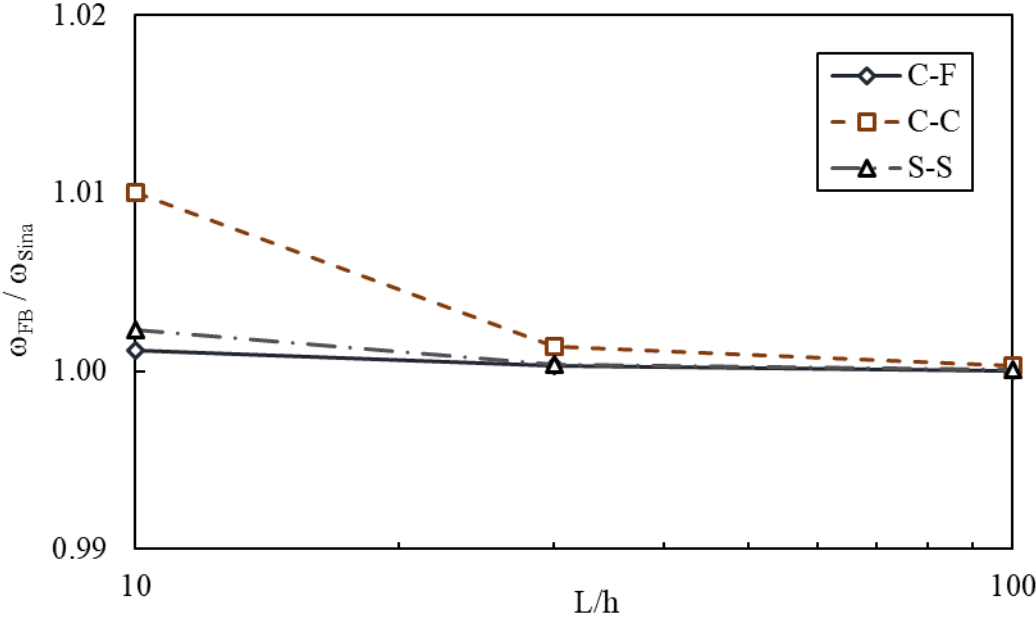


Figure 3.28 The comparison of the fundamental frequency obtained using FB and Sina et al. [33], material FGM, number of elements $n_e = 32$, power law coefficient $k = 0.3$

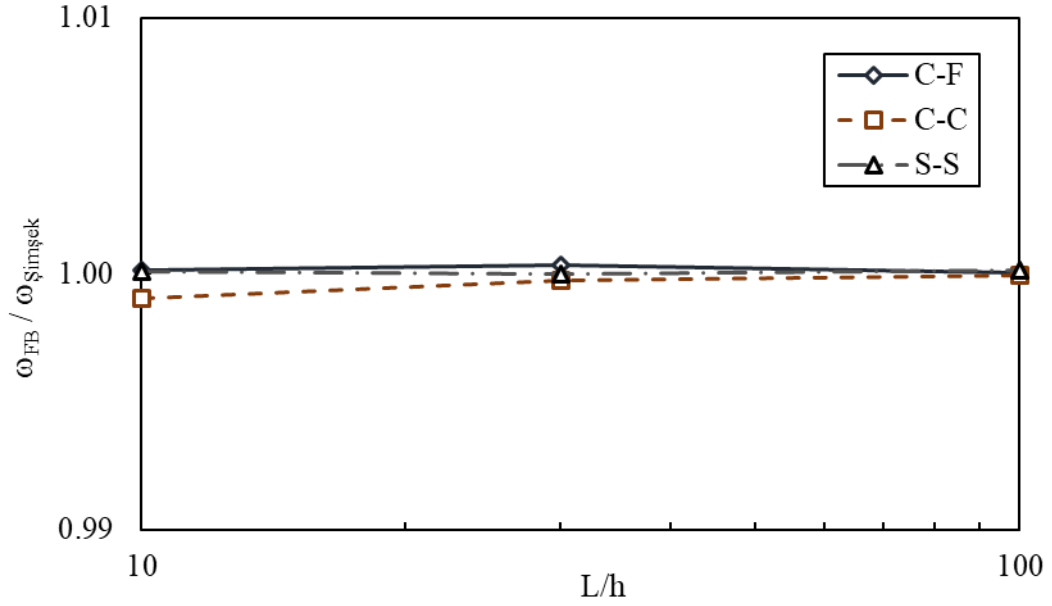


Figure 3.29 The comparison of the fundamental frequency obtained using FB and Şimşek [32], material FGM, number of elements $n_e = 32$, power law coefficient $k = 0.3$

3.2.2.2 The Fifth Numerical Example

In the fifth numerical example, the fundamental frequency obtained using the proposed formulation is compared with Şimşek [32] by using Timoshenko beam theory with various boundary conditions, aspect ratios and especially numerous power law coefficients.

In order to understand the effect of the power law coefficient, it is strongly advised to revisit Section 2.5 and examine Figure 2.7 showing the material variation along the transverse direction. When k equals to zero, material becomes pure alumina as indicated by Equation (2.23). Pure aluminum is obtained when k goes to infinity. In this example, the topmost and the bottommost materials are assumed as alumina and aluminum, respectively.

The properties of FGM used in this numerical example are tabulated in Table 3.10 where E , ρ , ν , κ_s , k are the Young's modulus, density, Poisson's ratio, shear correction factor and the power law coefficient, respectively. The non-dimensional fundamental frequency is selected the same as in Equation (3.3).

Table 3.10 The properties of the uniform beam element with FGM in particular at the topmost and bottommost materials

Boundary Conditions	Aspect Ratios (L/h)	FGM Materials		E (GPa)	ρ (kg / m ³)	ν	κ_s
C-F	5	Top	Alumina	380	3960	0.3	5/6
C-C		Bottom	Aluminum	70	2702		
S-S		k = 0.2 / 0.5 / 1 / 2 / 5 / 10					

The new parameter for FGM is the power law coefficient and it is the main focus point for Figures 3.30 to 3.41. The first three figures are presented for $L/h = 5$ with three different boundary conditions in the order of C-F, C-C and S-S. Additionally, another three figures follow with the same properties for $L/h = 20$ condition. In these figures, three decimal points are selected on the vertical axis since it is difficult to notice each legend for six different power law coefficients with one less decimal point. Moreover, semi-logarithmic graph presentation is also applied.

In Figure 3.31 and Figure 3.34, the boundary condition is C-C, therefore it is not possible to catch frequencies with a single element. However, as mentioned in the second numerical example, with an additional horizontal translational release on the right end, the frequencies can be obtained for this case. Furthermore, when the values are compared with cases with more than one element, it is observed that they stay exactly the same even for the FGM case.

Figures 3.30 to 3.35 show for various power law coefficients, different boundary conditions and aspect ratios, the ratios of the fundamental frequency from the proposed solution and the benchmark case converge to one.

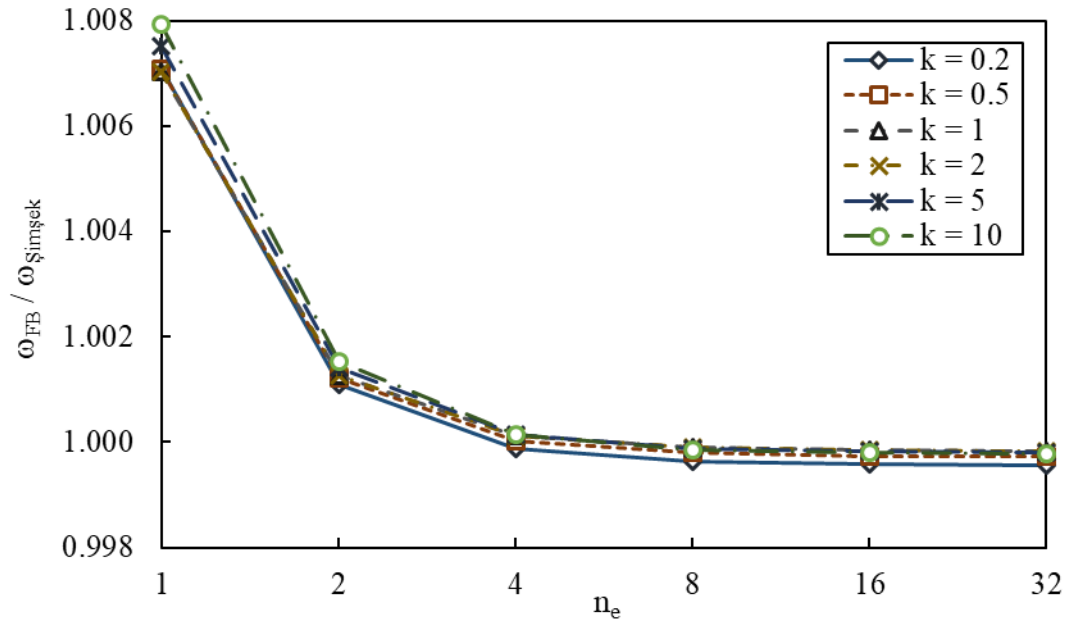


Figure 3.30 The comparison of the fundamental frequency obtained by FB and Şimşek [32], C-F beam, material FGM, aspect ratio $L/h = 5$, with increasing number of elements in the solution

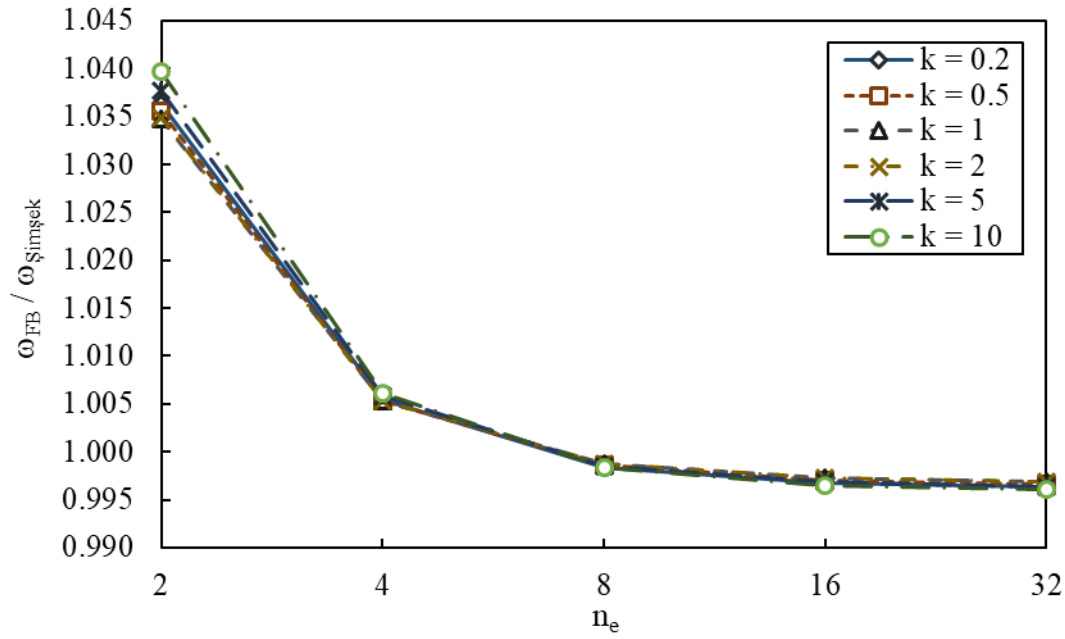


Figure 3.31 The comparison of the fundamental frequency obtained by FB and Şimşek [32], C-C beam, material FGM, aspect ratio $L/h = 5$, with increasing number of elements in the solution

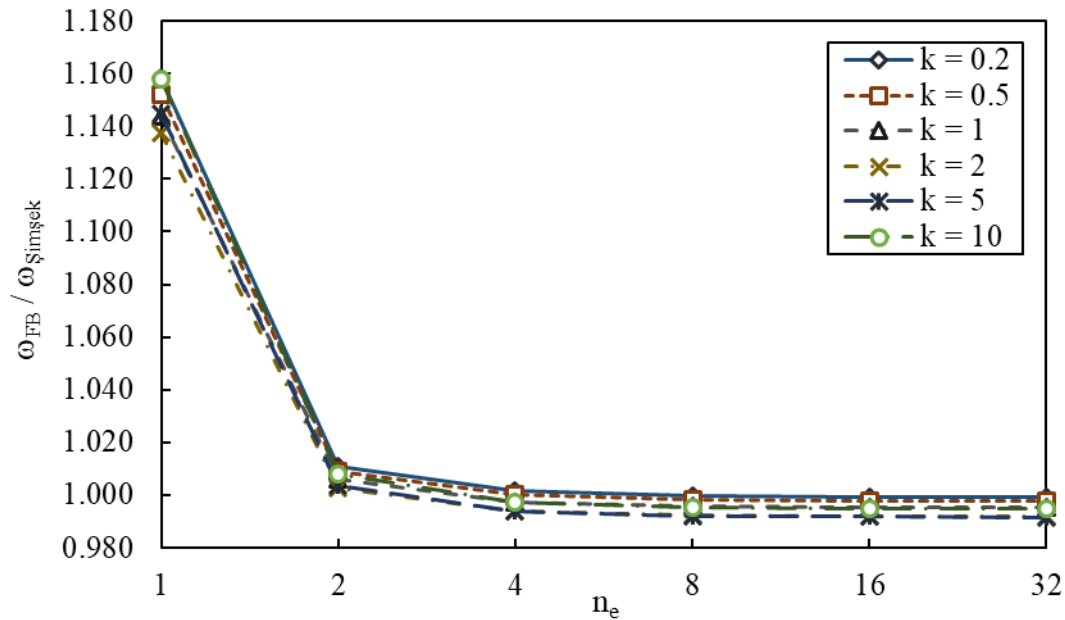


Figure 3.32 The comparison of the fundamental frequency obtained by FB and Şimşek [32], S-S beam, material FGM, aspect ratio $L/h = 5$, with increasing number of elements in the solution

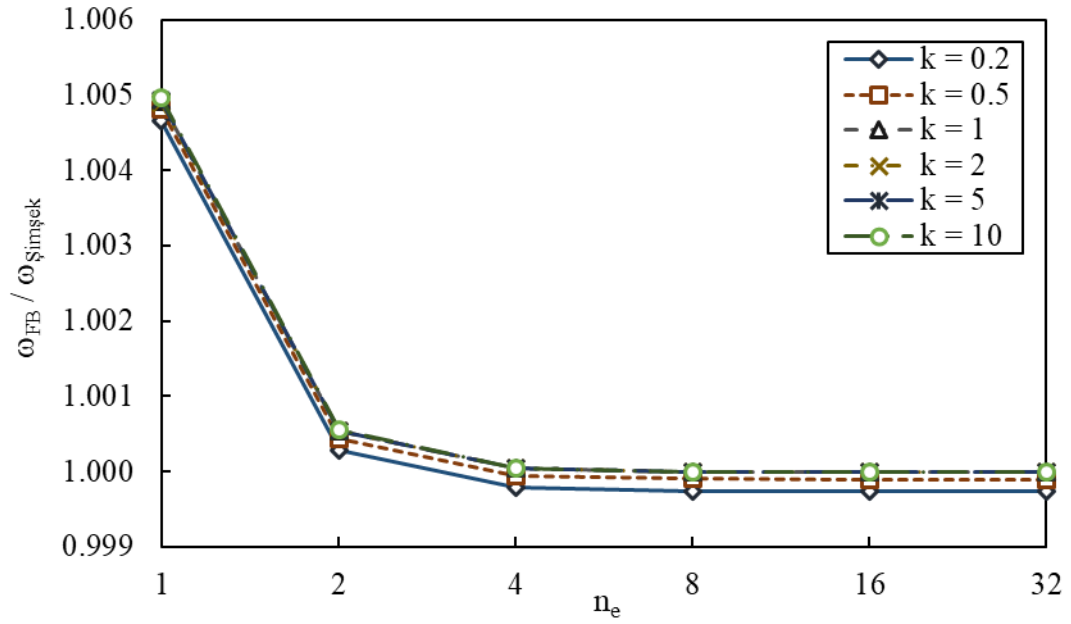


Figure 3.33 The comparison of the fundamental frequency obtained by FB and Şimşek [32], C-F beam, material FGM, aspect ratio $L/h = 20$, with increasing number of elements in the solution

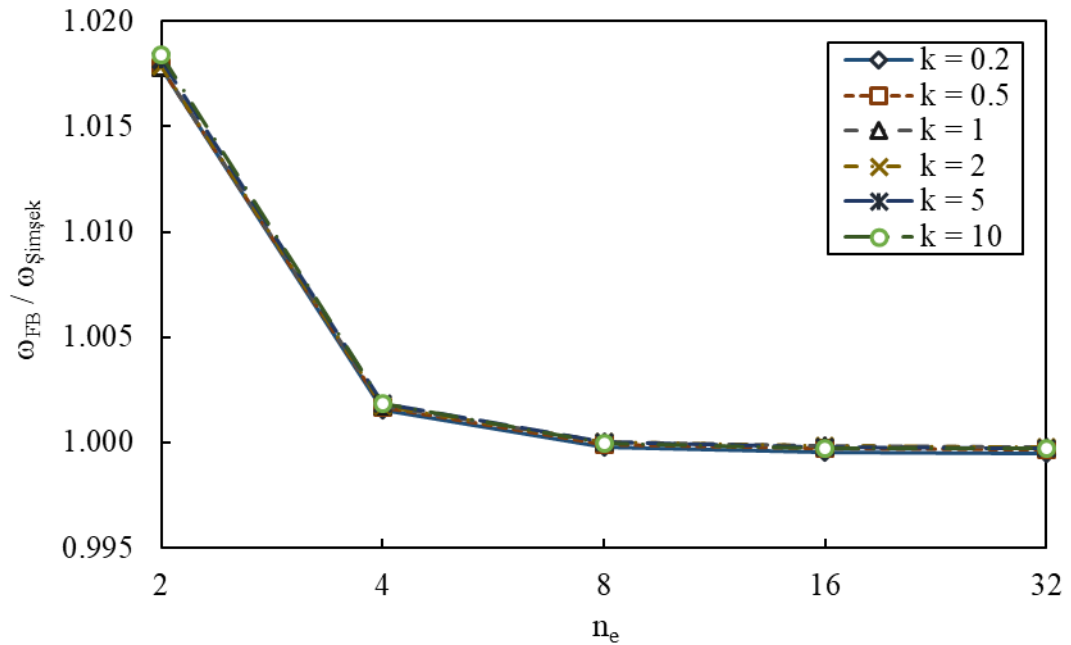


Figure 3.34 The comparison of the fundamental frequency obtained by FB and Şimşek [32], C-C beam, material FGM, aspect ratio $L/h = 20$, with increasing number of elements in the solution

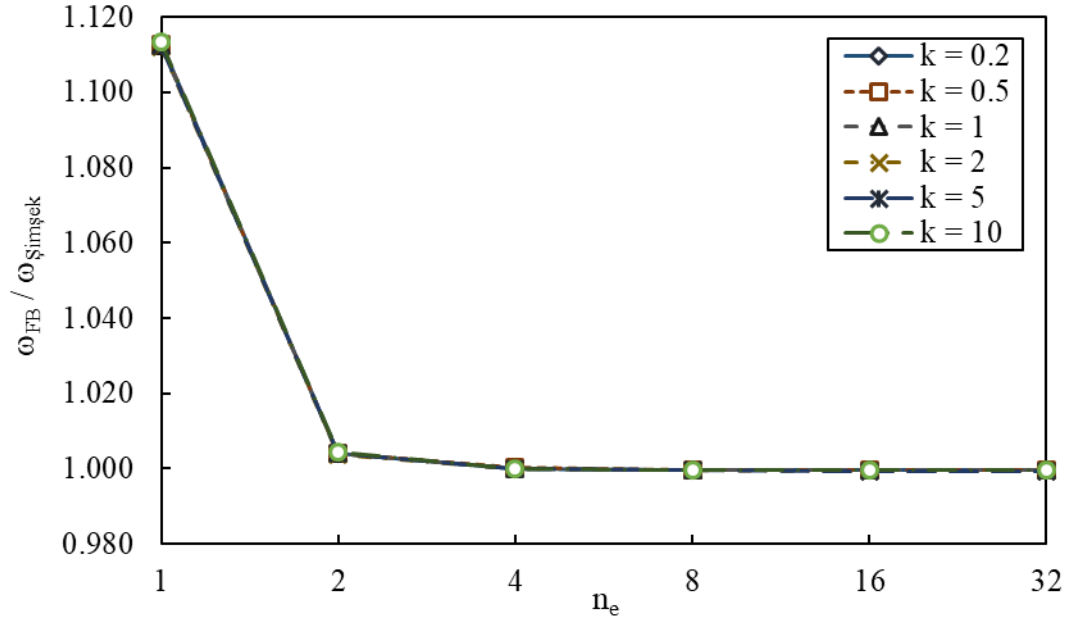


Figure 3.35 The comparison of the fundamental frequency obtained by FB and Şimşek [32], S-S beam, material FGM, aspect ratio $L/h = 20$, with increasing number of elements in the solution

A more detailed observation can be done with the presentation of the same ratios from Figures 3.36 to 3.41 with the origin point on the x-axis selected as 8. For the case with C-F beam with $L/h = 20$, horizontal lines are observed when $n_e = 8$: this means that the convergence of results are obtained before 8 elements

After careful examination, it can be deduced that the conclusions obtained from the previous examples with homogeneous and FGM cases are still valid, i.e., when the aspect ratio is larger, the rate of convergence is faster than smaller aspect ratios and mostly with better accuracy. Moreover, the convergence rate is the slowest with the C-C beam condition as expected. On the other hand, it should also be noted that the convergence of the FB solution for the S-S beam in this example is worse than the previous cases with S-S beam in the 1st, 2nd and 4th examples.

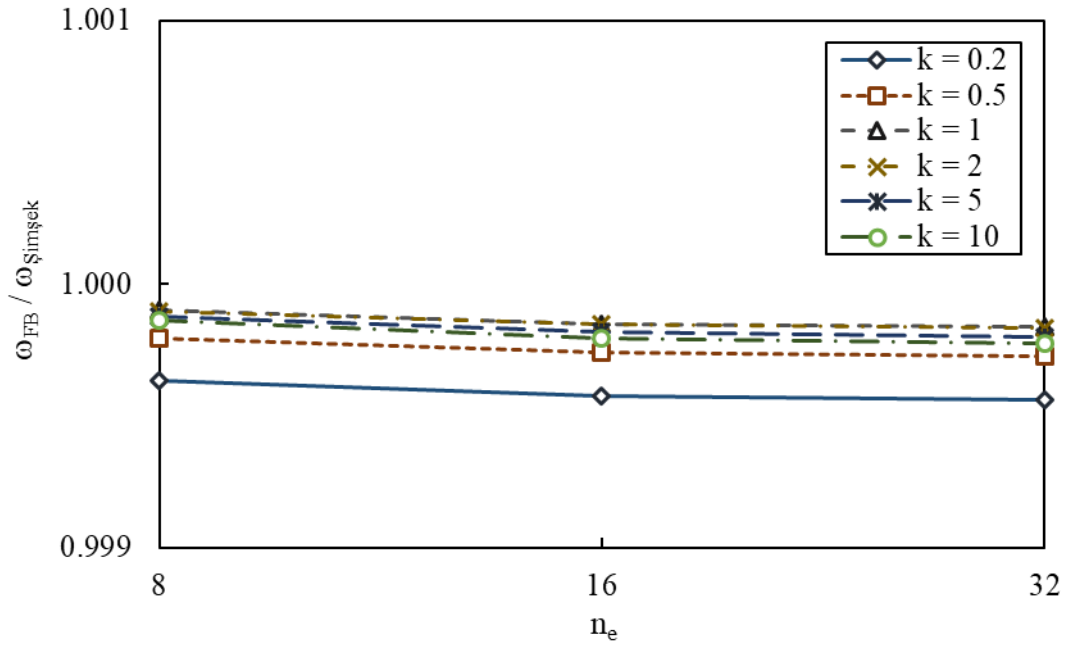


Figure 3.36 The comparison of the fundamental frequency obtained by FB and Şimşek [32], C-F beam, material FGM, aspect ratio $L/h = 5$, number of elements $n_e = 8$ to 32

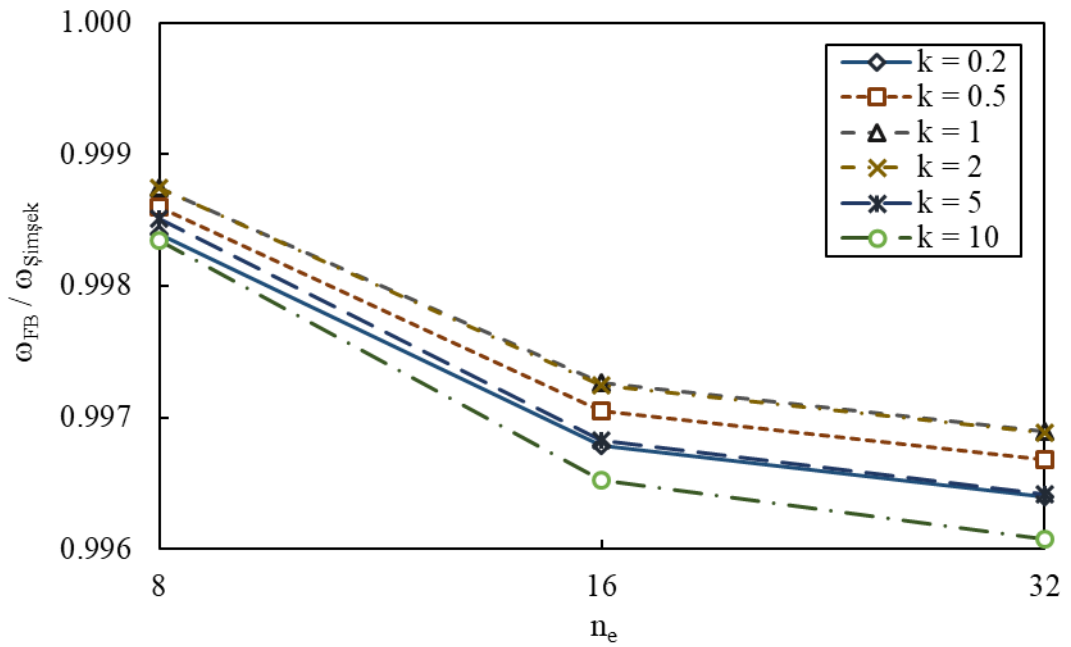


Figure 3.37 The comparison of the fundamental frequency obtained by FB and Şimşek [32], C-C beam, material FGM, aspect ratio $L/h = 5$, number of elements $n_e = 8$ to 32

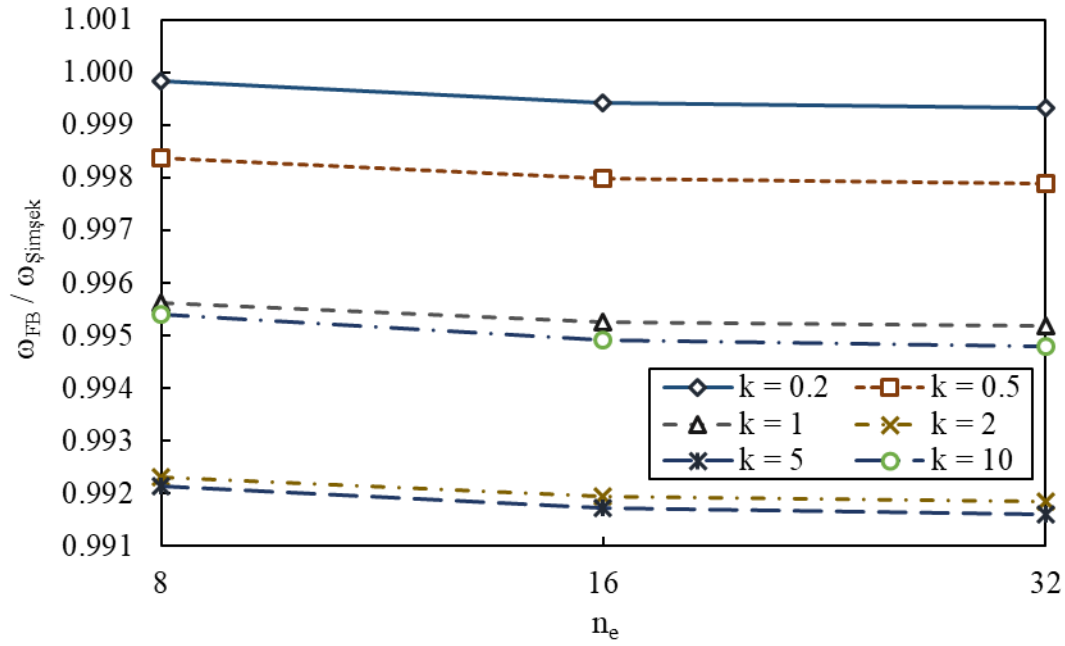


Figure 3.38 The comparison of the fundamental frequency obtained by FB and Şimşek [32], S-S beam, material FGM, aspect ratio $L/h = 5$, number of elements $n_e = 8$ to 32

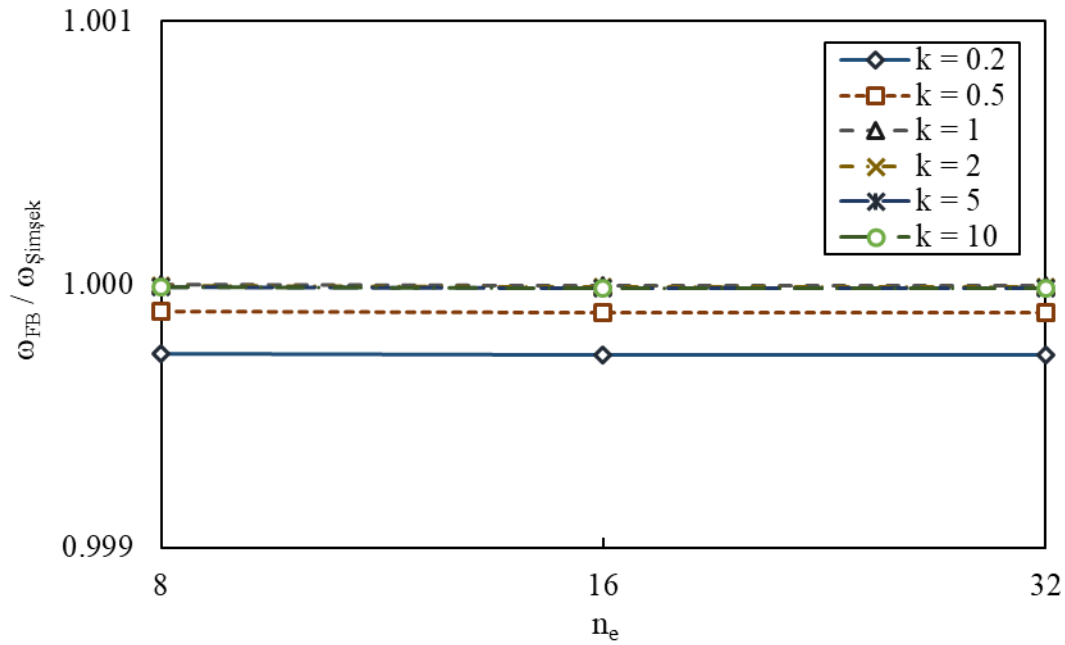


Figure 3.39 The comparison of the fundamental frequency obtained by FB and Şimşek [32], C-F beam, material FGM, aspect ratio $L/h = 20$, number of elements $n_e = 8$ to 32

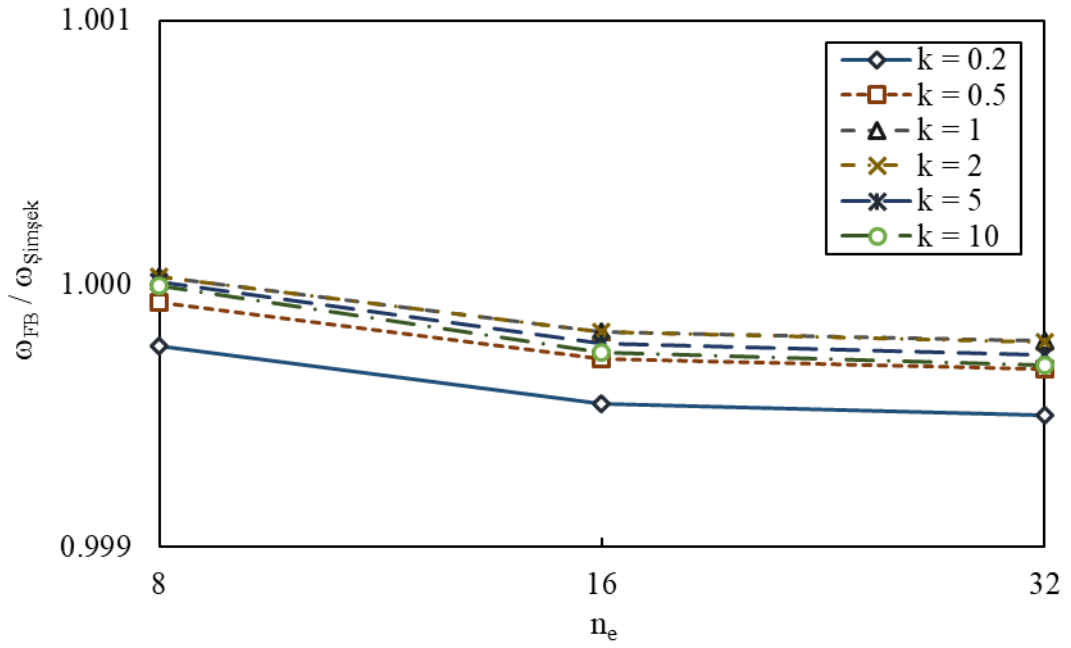


Figure 3.40 The comparison of the fundamental frequency obtained by FB and Şimşek [32], C-C beam, material FGM, aspect ratio $L/h = 20$, number of elements $n_e = 8$ to 32

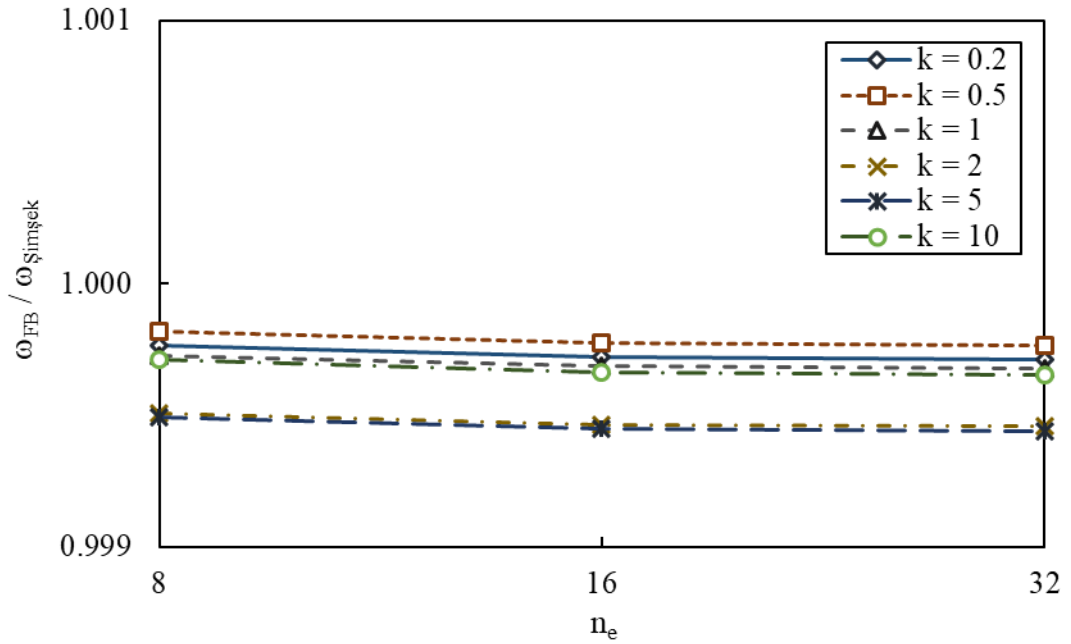


Figure 3.41 The comparison of the fundamental frequency obtained by FB and Şimşek [32], S-S beam, material FGM, aspect ratio $L/h = 20$, number of elements $n_e = 8$ to 32

The results of two additional parametric studies are presented in Figure 3.42 and Figure 3.43. The former figure is focused on the effect of different boundary conditions while the effect of aspect ratios is compared in the latter chart. In both figures, a linear material variation is assumed in the transverse direction, i.e. $k = 1$.

In Figure 3.42, the results from the proposed method is compared to the solutions from [32] for $L/h = 20$ and $k = 1$ for three boundary conditions. As can be seen, the result from the C-C beam is the slowest to converge to the results from [32]; the fastest one is the counterpart for the C-F beam.

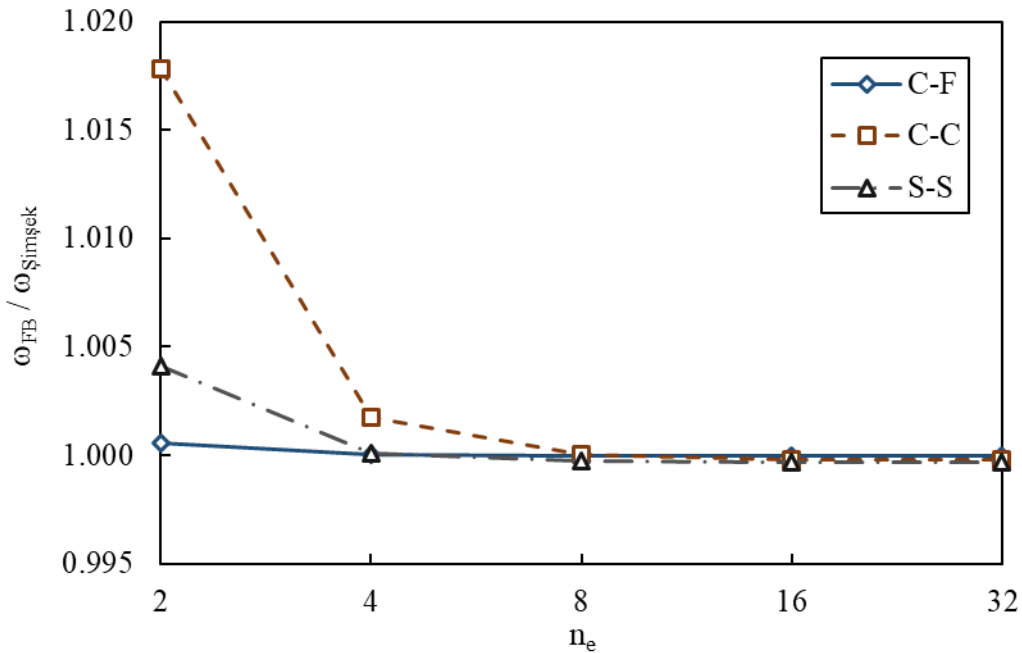


Figure 3.42 The comparison of the fundamental frequency obtained by FB and Şimşek [32], aspect ratio $L/h = 20$, power law coefficient $k = 1$, with increasing number of elements in the solution

In Figure 3.43, the result from the proposed method is compared to [32] for the C-F case with $k = 1$ for two different aspect ratios. The comparison shows that for slender beams (in this case, selected as $L/h = 20$), convergence of the results is obtained faster than the thick beams with $L/h = 5$.

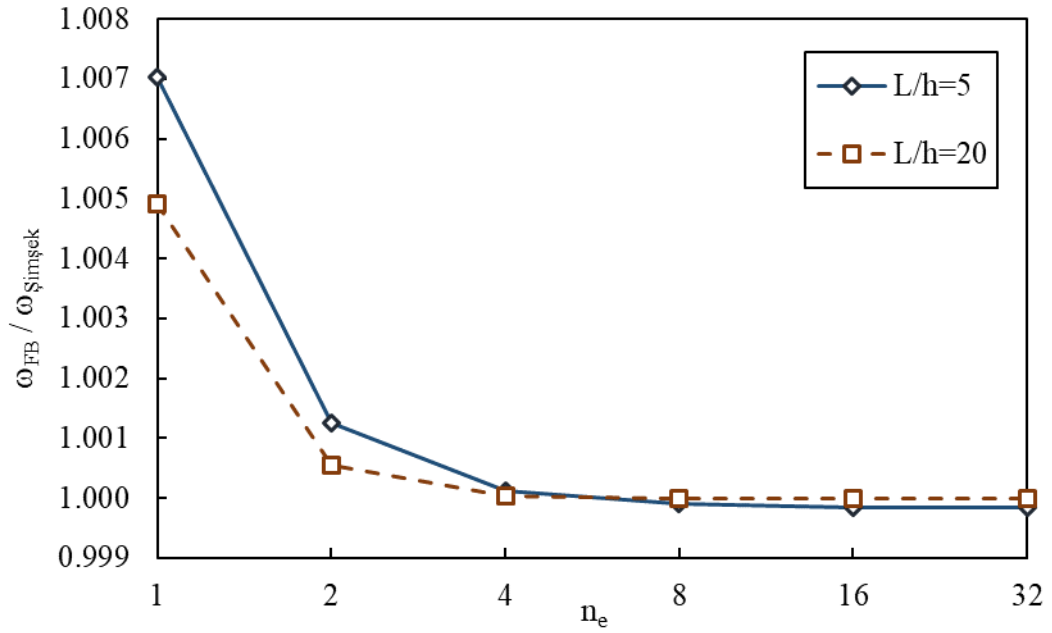


Figure 3.43 The comparison of the fundamental frequency obtained by FB and Şimşek [32], C-F beam, power law coefficient $k = 1$, with increasing number of elements in the solution

3.2.2.3 The Sixth Numerical Example

In the sixth numerical example, the frequencies of the higher modes obtained with the proposed method are compared with the results from Şimşek [32] and Li [34] for the FGM. Only S-S boundary condition is considered in the analysis.

The properties of FGM for the sixth numerical example are tabulated in Table 3.11 where E , ρ , ν , κ_s , k are the Young's modulus, density, Poisson's ratio, shear correction factor and the power law coefficient, respectively. The non-dimensional fundamental frequency is selected the same as in Equation (3.3).

Table 3.11 The properties of the uniform beam element with FGM in particular at the topmost and bottommost materials

Boundary Conditions	Aspect Ratios (L/h)	FGM Materials		E (GPa)	ρ (kg / m ³)	ν	κ_s
S-S	4	Top	Aluminum	70	2707	0.3	0.867
		Bottom	Steel	210	7850		
		k = 1					

The shear correction factor is taken from [34] in order to conduct the analyses with the same properties. The shear correction factor, κ_s , is given as follows:

$$\kappa_s = \frac{5(1+\nu)}{6+5\nu} \quad (3.5)$$

In Figure 3.44 and Figure 3.45, the comparisons of the frequencies for the higher modes are presented for the FB versus Şimşek [32] and FB versus Li [34], respectively. The first five frequencies are presented for the verification of the proposed method. In this example, linear and logarithmic scales are selected in the vertical and horizontal axes, respectively. According to Figure 3.44 and Figure 3.45, the ratios for the higher modes with the FGM converge to 1 in both graphs when the number of elements increases. These trends with FGM are similar to the trends in the third numerical example with the homogeneous material case for the higher modes. It should be noted that these figures should be compared to Figure 3.20 in the third numerical example due to the similarity in their aspect ratios. To sum up, the proposed method provides precise results for the higher mode frequencies not only with homogeneous material, but also with FGM when the number of elements is selected wisely.

Figure 3.44 and Figure 3.45 appear very similar to each other. In order to highlight the differences, the ratios between the FB and other models are presented in Figure 3.46 and Figure 3.47 with 8, 16, 32, 64 and 128 elements on the horizontal axis. These figures provide a better opportunity to catch the points where the ratios converge. It can be deduced that for the modes 1 and 5, FB versus Şimşek results are more in line

compared to FB versus Li. On the other hand, the latter one provides closer results to 1 for the modes 2, 3 and 4. As mentioned before, the general trend in Figure 3.44 and Figure 3.45 is for the ratios of predicted frequencies from the FB and comparison model to converge to 1. It should be noted that for the higher modes, it is more difficult to obtain a perfect match than as in the case of the fundamental frequency.

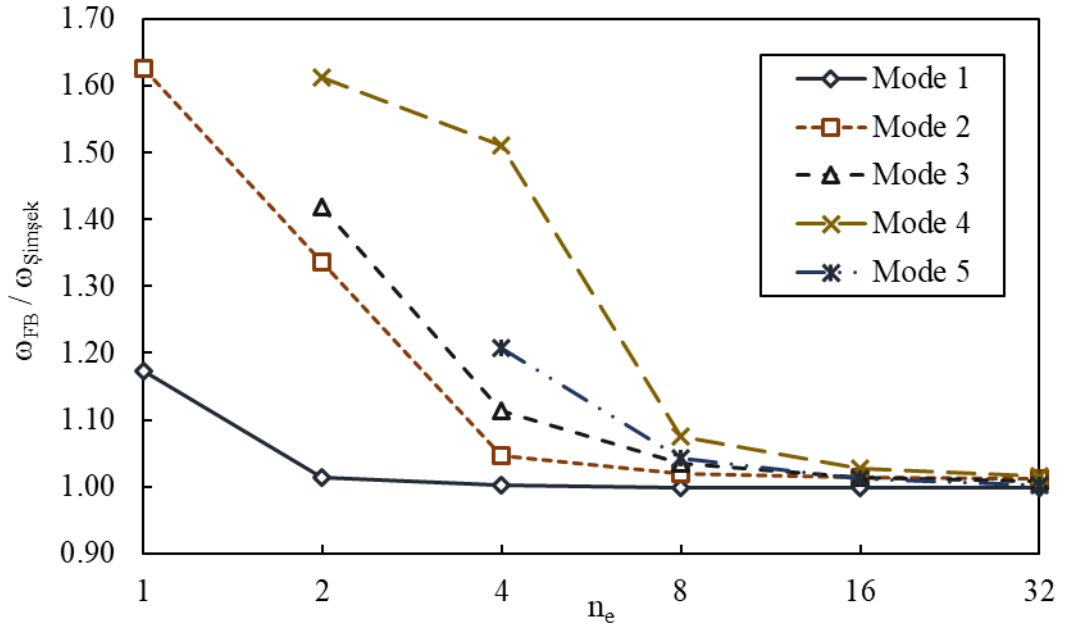


Figure 3.44 The comparison of the frequencies for the higher modes obtained by FB and Şimşek [32], S-S beam, aspect ratio $L/h = 4$, power law coefficient $k = 1$, with increasing number of elements in the solution

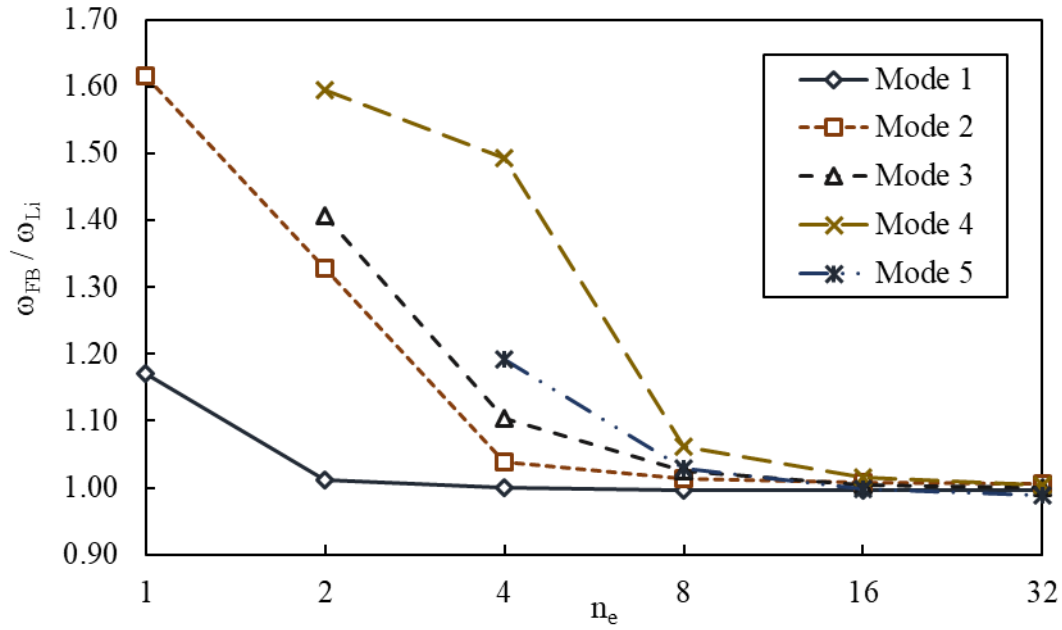


Figure 3.45 The comparison of the frequencies for the higher modes obtained by FB and Li [34], S-S beam, aspect ratio $L/h = 4$, power law coefficient $k = 1$, with increasing number of elements in the solution

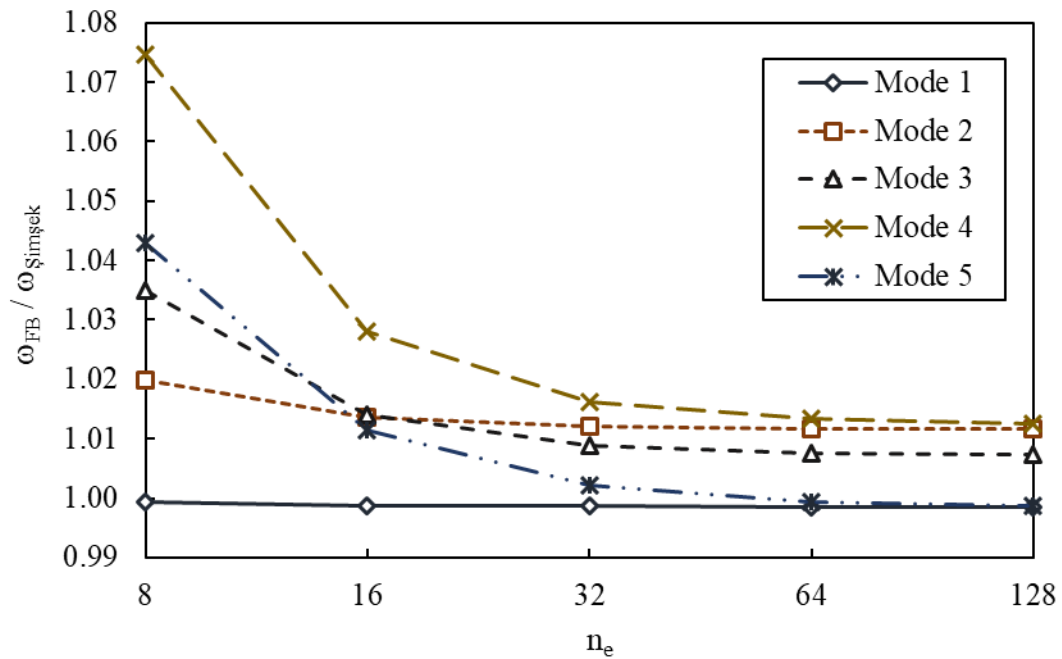


Figure 3.46 The comparison of the frequencies for the higher modes obtained by FB and Şimşek [32], S-S beam, aspect ratio $L/h = 4$, power law coefficient $k = 1$, number of elements $n_e = 8$ to 128

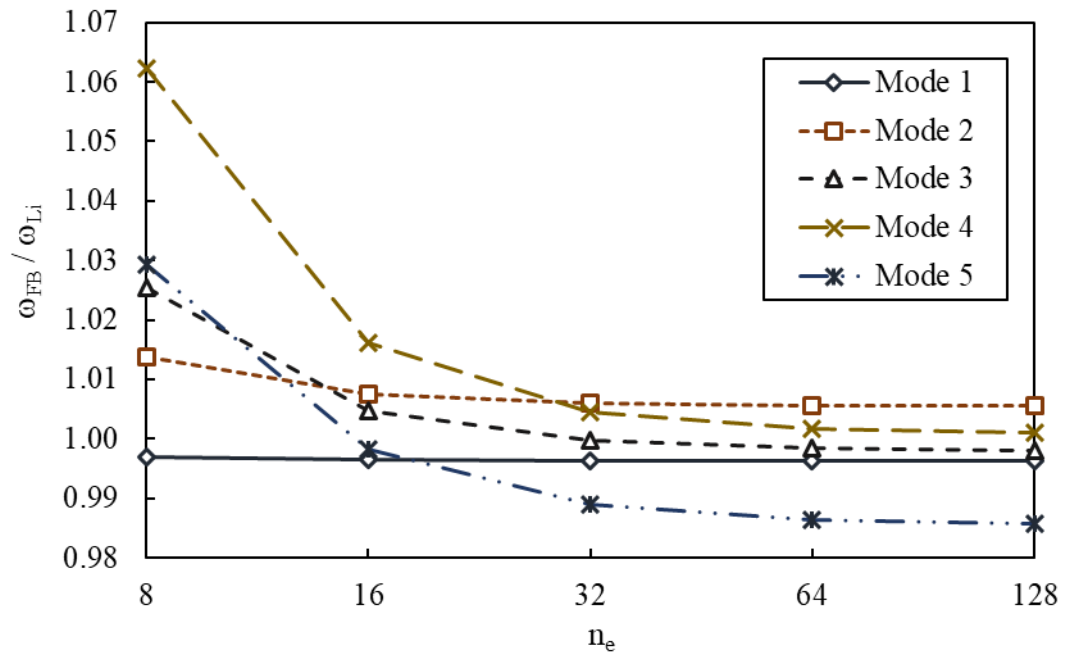


Figure 3.47 The comparison of the frequencies for the higher modes between FB and Li [34], S-S beam, aspect ratio $L/h = 4$, power law coefficient $k = 1$, number of elements $n_e = 8$ to 128

In the next chapter, the analyses of a more complex geometry with homogeneous and the functionally graded material will be presented. Two numerical examples will be provided for the verification of the proposed method for the case of tapered geometry.

CHAPTER 4

FREE VIBRATION ANALYSIS OF A BEAM WITH TAPERED GEOMETRY

4.1 INTRODUCTION

In this chapter, the proposed 2D beam element with tapered geometry will be analyzed for linear elastic free vibration of beams with the C-F boundary condition for the homogeneous or heterogeneous material distribution. Heterogeneous material distribution with functionally graded material is selected in transverse direction since most of the previous research in the literature focus on such a material distribution for the FGM members. To be more specific, power law and exponential law functions are mainly used to provide continuous material variation in the z direction for FGM. The change of depth will be modeled as a linear decreasing function in the plane in the proposed frame element formulation for simulating the tapered geometry. It should be noted that the terms force based method and mixed formulation are again used interchangeably in the following text.

The proposed mixed formulation analyses are conducted with MATLAB software. Moreover, ANSYS is used in 2D to validate the proposed formulation as presented in Chapter 3.1. Although ANSYS results are more realistic with homogeneous material distribution for real life problems, modeling of phasing material in ANSYS (such as FGM) with continuous distribution in the material properties is difficult. FGM can only be modelled with laminated layers which do not represent the continuous material variation of the FGM case accurately; however, accuracy can be improved when the number of laminated layers increases. Consequently, the solutions of vibration characteristics from laminated beam analyses in ANSYS and the proposed beam formulation with power law coefficient can be compared for the tapered FGM beams.

Tapered beam has a more complex geometry than uniform beam. Due to the cumbersome closed form solutions, the use of the displacement based methods gets more complicated even without the FGM case, i.e. the homogeneous material case. On the other hand, the proposed method, which can be implemented efficiently for different geometric and material variations with simple modifications, is an uncomplicated approach with accuracy and robustness provided even for a tapered beam with FGM. Further verification of the proposed method with ANSYS results will fill the gap in the literature.

In the next sections, various parametric studies for the beam finite element will be carried out for different number of elements, aspect ratios (L/h), taper ratios and different laminated layers. Before this presentation, discussion on the tapered geometry is provided first. Next, numerical examples with homogeneous and FGM material distributions will be presented.

4.2 VERIFICATION WITH TAPERED GEOMETRY

The mixed formulation beam element with tapered geometry and homogeneous material for linear elastic free vibration was previously presented by Soydaş [3] and the same method thereupon was applied for the homogeneous material by Dharmasiri et al [8]. However, the verification of the proposed formulation for the homogeneous material case is not sufficient. For the FGM, especially with regards to the accuracy of this approach, a verification is required. The free vibration characteristics of a beam with tapered geometry with FGM are analyzed for the first time with the proposed mixed formulation in this thesis.

The formulation of the proposed method with tapered geometry is first verified by modeling the tapered geometry to replicate a uniform geometry case, setting the same depth values at the ends of the analyzed beam members. For this case, the codes

developed for the tapered geometry beam perfectly matched the results obtained in Chapter 3 for the uniform geometry case. On the other hand, when the geometry is changed to the tapered case, it is observed that the computation time increases excessively during the symbolic integration part of the consistent mass matrix calculated with the force-based approach. This is due to the linearly varying depth values resulting in additional complexities in the symbolic integration process in MATLAB, for each finite element. Accordingly, the MATLAB script has been optimized to obtain reasonable durations since the computation time is an important parameter.

In the next section, the first example provided is tapered geometry beams with homogeneous material distribution case. Then, results for tapered geometry beams with FGM will be presented as another numerical example. In Table 4.1, the summary of the numerical examples with tapered geometry beams is presented.

Table 4.1 The summary of the numerical examples for beams with tapered geometry

Free Vibration Analysis of a Tapered Geometry Beam																															
Tapered Geometry with Homogeneous Material	Tapered Geometry with Functionally Graded Materials																														
<table border="1" style="width: 100%; border-collapse: collapse; text-align: center;"> <thead> <tr> <th colspan="2" style="padding: 5px;">The Seventh Example</th> </tr> </thead> <tbody> <tr> <td style="padding: 5px;">Frequency</td> <td style="padding: 5px;">Higher modes</td> </tr> <tr> <td style="padding: 5px;">Comparison</td> <td style="padding: 5px;">ANSYS</td> </tr> <tr> <td style="padding: 5px;">Boundary Condition</td> <td style="padding: 5px;">C-F</td> </tr> <tr> <td style="padding: 5px;">Aspect Ratio</td> <td style="padding: 5px;">10</td> </tr> <tr> <td style="padding: 5px;">Taper Ratio</td> <td style="padding: 5px;">1, 2, 3, 4, 5</td> </tr> <tr> <td style="padding: 5px;">Material</td> <td style="padding: 5px;">Steel</td> </tr> </tbody> </table>	The Seventh Example		Frequency	Higher modes	Comparison	ANSYS	Boundary Condition	C-F	Aspect Ratio	10	Taper Ratio	1, 2, 3, 4, 5	Material	Steel	<table border="1" style="width: 100%; border-collapse: collapse; text-align: center;"> <thead> <tr> <th colspan="2" style="padding: 5px;">The Eighth Example</th> </tr> </thead> <tbody> <tr> <td style="padding: 5px;">Frequency</td> <td style="padding: 5px;">Higher modes</td> </tr> <tr> <td style="padding: 5px;">Comparison</td> <td style="padding: 5px;">ANSYS</td> </tr> <tr> <td style="padding: 5px;">Boundary Condition</td> <td style="padding: 5px;">C-F</td> </tr> <tr> <td style="padding: 5px;">Aspect Ratio</td> <td style="padding: 5px;">10, 20</td> </tr> <tr> <td style="padding: 5px;">Taper Ratio</td> <td style="padding: 5px;">2</td> </tr> <tr> <td style="padding: 5px;">Material</td> <td style="padding: 5px;">Alumina (Ceramic), Aluminum (Metal)</td> </tr> <tr> <td style="padding: 5px;">Power Law Coefficient</td> <td style="padding: 5px;">0.5</td> </tr> </tbody> </table>	The Eighth Example		Frequency	Higher modes	Comparison	ANSYS	Boundary Condition	C-F	Aspect Ratio	10, 20	Taper Ratio	2	Material	Alumina (Ceramic), Aluminum (Metal)	Power Law Coefficient	0.5
The Seventh Example																															
Frequency	Higher modes																														
Comparison	ANSYS																														
Boundary Condition	C-F																														
Aspect Ratio	10																														
Taper Ratio	1, 2, 3, 4, 5																														
Material	Steel																														
The Eighth Example																															
Frequency	Higher modes																														
Comparison	ANSYS																														
Boundary Condition	C-F																														
Aspect Ratio	10, 20																														
Taper Ratio	2																														
Material	Alumina (Ceramic), Aluminum (Metal)																														
Power Law Coefficient	0.5																														

4.2.1 Tapered Geometry with Homogeneous Material

The numerical example in this section is focused on the frequencies of the higher modes with the first five frequencies in the modal analysis.

A linearly decreasing tapered geometry beam element with homogenous material in x-z plane is shown in Figure 4.1.

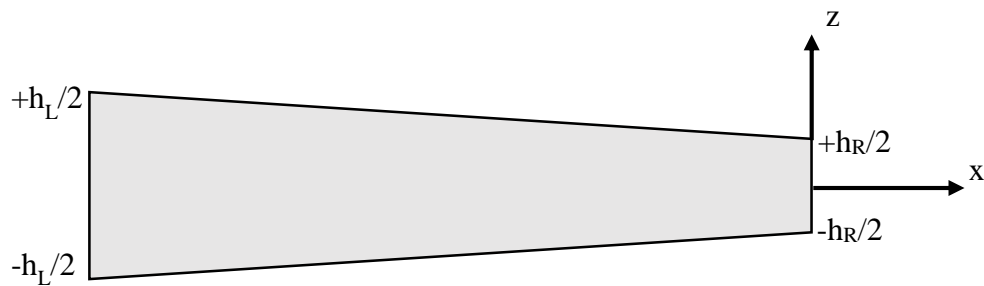


Figure 4.1 Tapered beam element, linear taper with homogeneous material in x-z plane

4.2.1.1 The Seventh Numerical Example

In the seventh numerical example, the frequencies of the higher modes obtained by the proposed method are compared with the ANSYS results. The boundary condition is selected only as the C-F case with homogeneous material (steel) and an aspect ratio of 10. The properties of the beam element are shown in Table 4.2 where E , ρ , ν , κ_s are the Young's modulus, density, Poisson's ratio and the shear correction factor, respectively.

Table 4.2 The properties of the tapered beam element with pure steel

Boundary Condition	Aspect Ratio	Homogeneous Material	E (GPa)	ρ (kg / m ³)	ν	κ_s
C-F	10	Steel	210	7850	0.3	5/6

In Table 4.3, the geometric parameters of the tapered beam element with pure steel are presented. In this geometric model, various taper ratios are obtained by changing the depth of the left side which is fixed. Linearly decreasing rate of change is considered for taper ratio i.e. h_L/h_R . Additionally, aspect ratio is calculated by dividing h_R into length and it is considered constant in this example. The value for the aspect ratio is intentionally selected small to experience difficulties since it is concluded in Chapter 3 that when aspect ratio is small, convergence rate and accuracy is slower than that in slender beam. As a result, investigation of accuracy with a difficult scenario for the proposed method helps to prove robustness of the method firmly.

Table 4.3 The geometric parameters of the tapered beam element with pure steel

Length (m)	Depth (m)		Taper Ratio	Aspect Ratio
	h_L	h_R		
1	0.1	0.1	1	10
	0.2		2	
	0.3		3	
	0.4		4	
	0.5		5	

The frequency information for the first five modes for the C-F beams with aspect ratio 10 is tabulated in Table 4.4. The characteristics of the modes are identical for the considered five different taper ratios.

Table 4.4 The frequency information for the first five modes, C-F beam, $L/h_R = 10$

	Axial: A
	Bending: B
Mode 1	B
Mode 2	B
Mode 3	A
Mode 4	B
Mode 5	B

In Figures 4.2 to 4.6, the comparison of the frequencies for higher modes between FB and ANSYS with the C-F beam is provided for five different taper ratios. In each figure, five different modes are considered. After this presentation, from Figures 4.7 to 4.10, the first four bending modes are compared for five different taper ratios. The comparison of the 1st axial mode is provided in Figure 4.11. Since it is not possible to capture Mode 4 and Mode 5 with one element by using the proposed method, there is no data presented for these modes when $n_e = 1$ in Figure 4.9 and Figure 4.10. Semi-logarithmic graph presentation is again used in this numerical example. It should be noted that a taper ratio of 1 corresponds to a uniform geometry as presented in Figure 4.2. It is shown to examine a comparison of uniform and tapered geometries in the same numerical example.

From Figures 4.2 to 4.6, a trend is observed with taper ratio. This trend shows that when the taper ratio increases, the frequency ratios converge at slightly lower rate compared to the smaller taper ratio, however, they do not diverge. The most accurate results are obtained by uniform geometry as would be expected and the least accurate one is with the taper ratio of 5. It is also an expected scenario, since in the C-F beam, the left side is fixed: when the taper ratio increases, the depth at the fixed end also increases. Therefore, ANSYS with multiple finite elements at the end captures the clamped boundary condition better; as mentioned before FB beam elements use an assumption and consider fixity only on a single point at the end. It is also interesting to note that the proposed formulation converges very close to 1.00, regardless of the

simplification effects. Furthermore, in all five cases, eight elements with the proposed method is in good agreement with ANSYS even for the higher modes.

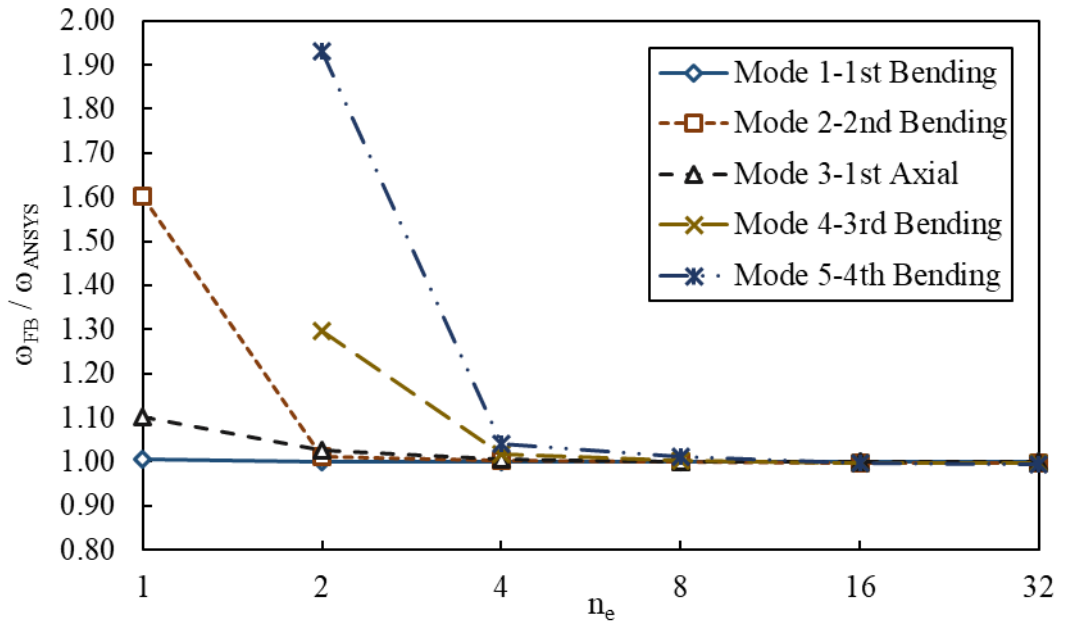


Figure 4.2 The comparison of the frequencies for the higher modes obtained using FB and ANSYS, C-F beam, material steel, aspect ratio $L/h_R = 10$, taper ratio $h_L/h_R = 1$, with increasing number of elements in the solution

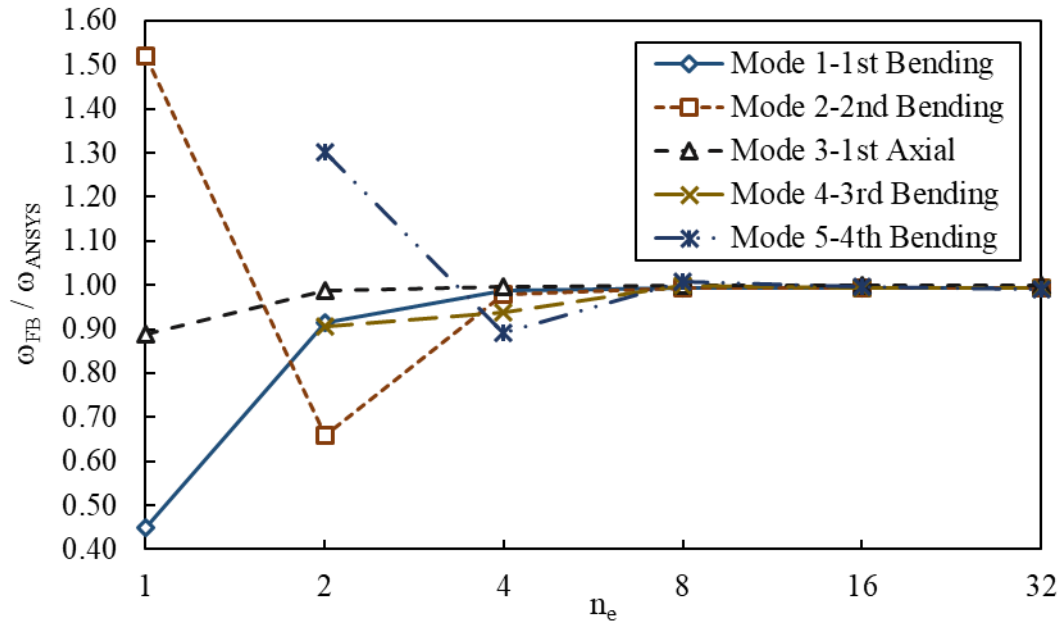


Figure 4.3 The comparison of the frequencies for the higher modes obtained using FB and ANSYS, C-F beam, material steel, aspect ratio $L/h_R = 10$, taper ratio $h_L/h_R = 2$, with increasing number of elements in the solution

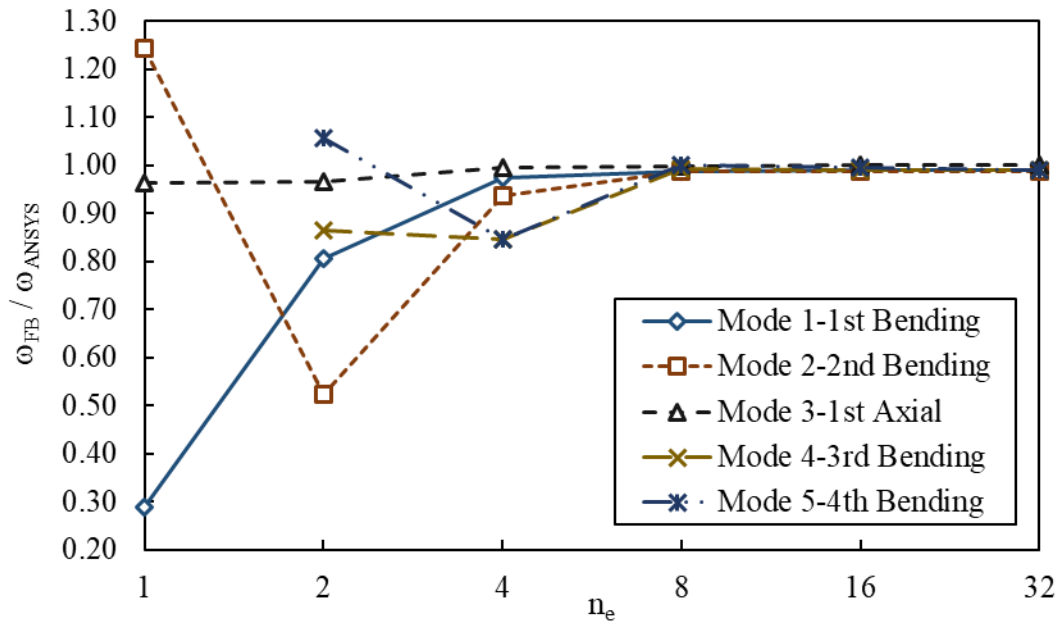


Figure 4.4 The comparison of the frequencies for the higher modes obtained using FB and ANSYS, C-F beam, material steel, aspect ratio $L/h_R = 10$, taper ratio $h_L/h_R = 3$, with increasing number of elements in the solution

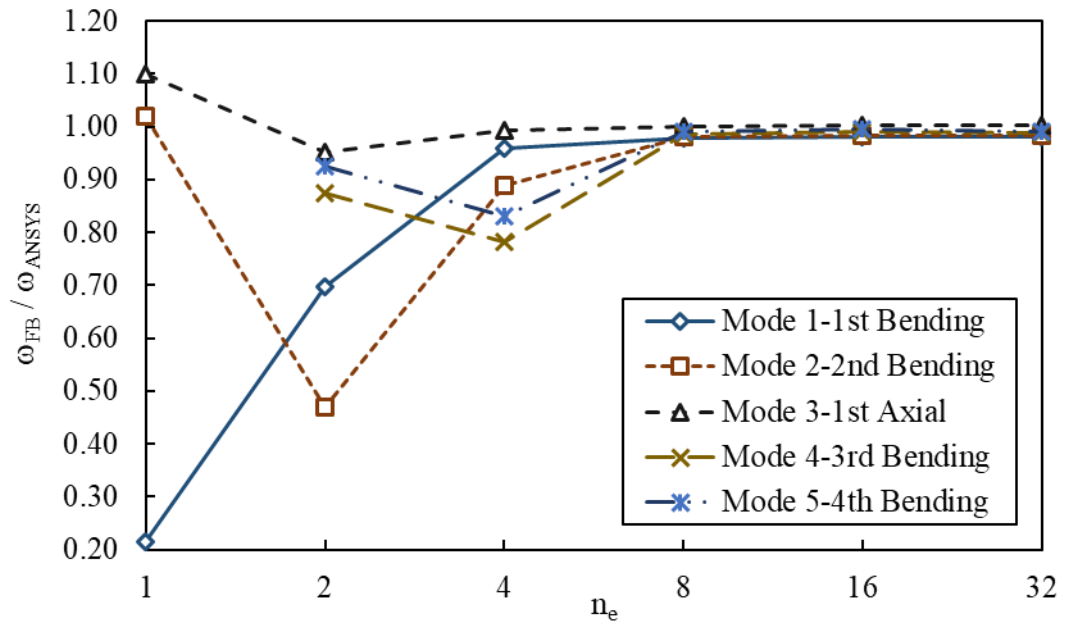


Figure 4.5 The comparison of the frequencies for the higher modes obtained using FB and ANSYS, C-F beam, material steel, aspect ratio $L/h_R = 10$, taper ratio $h_L/h_R = 4$, with increasing number of elements in the solution

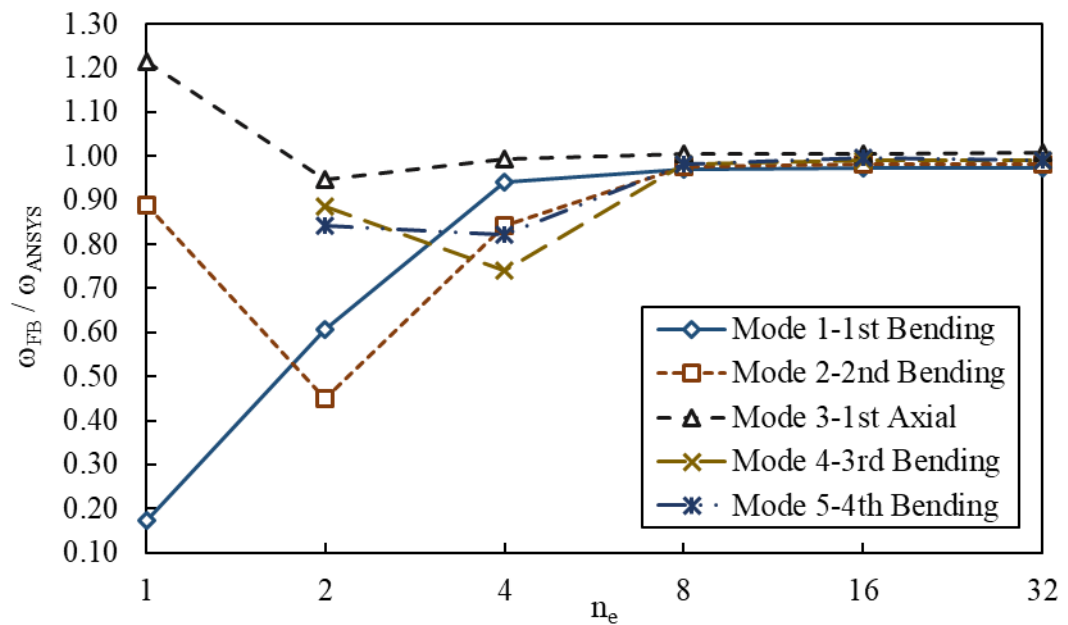


Figure 4.6 The comparison of the frequencies for the higher modes obtained using FB and ANSYS, C-F beam, material steel, aspect ratio $L/h_R = 10$, taper ratio $h_L/h_R = 5$, with increasing number of elements in the solution

From Figures 4.7 to 4.11, it is observed that the fastest convergence rate is reached when taper ratio is equal to 1 i.e. uniform geometry except for the 1st axial mode. A faster convergence with the uniform geometry case is expected compared to a varying geometry like in this example. It is seen from Figures 4.7 to 4.11 that when the taper ratio increases, the convergence rate decreases as before. When the taper ratio i.e. h_L/h_R , increases, the dimension at the clamped side increases for the C-F beam. Afterwards it behaves more like short and deep beam. Consequently, boundary condition effects become more significant which makes it difficult to catch the exact behavior, especially when the results of the proposed method is compared with the numerical results obtained from ANSYS providing better representation of the clamped boundary conditions.

In this case, mostly eight elements or in some instances four elements provide a good agreement even for the higher modes with different taper ratios. To conclude, inspection of these figures demonstrates accuracy and robustness of the proposed formulation with tapered geometry also for the higher modes when the number of elements is selected wisely.

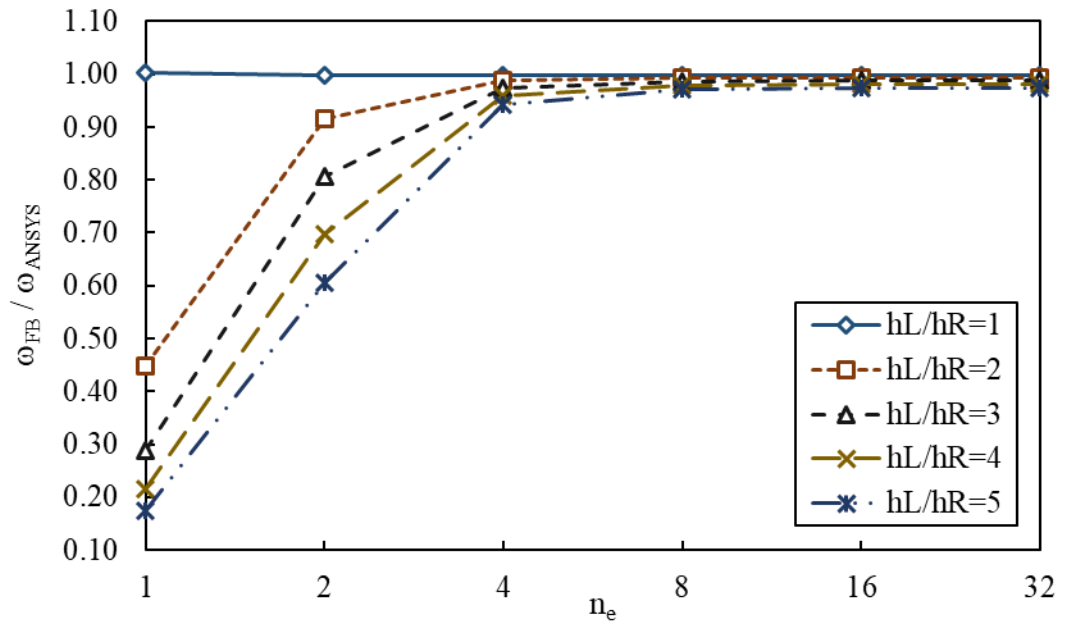


Figure 4.7 The ratio of 1st bending mode frequency obtained from FB and ANSYS, C-F beam, material steel, with increasing number of elements in the solution

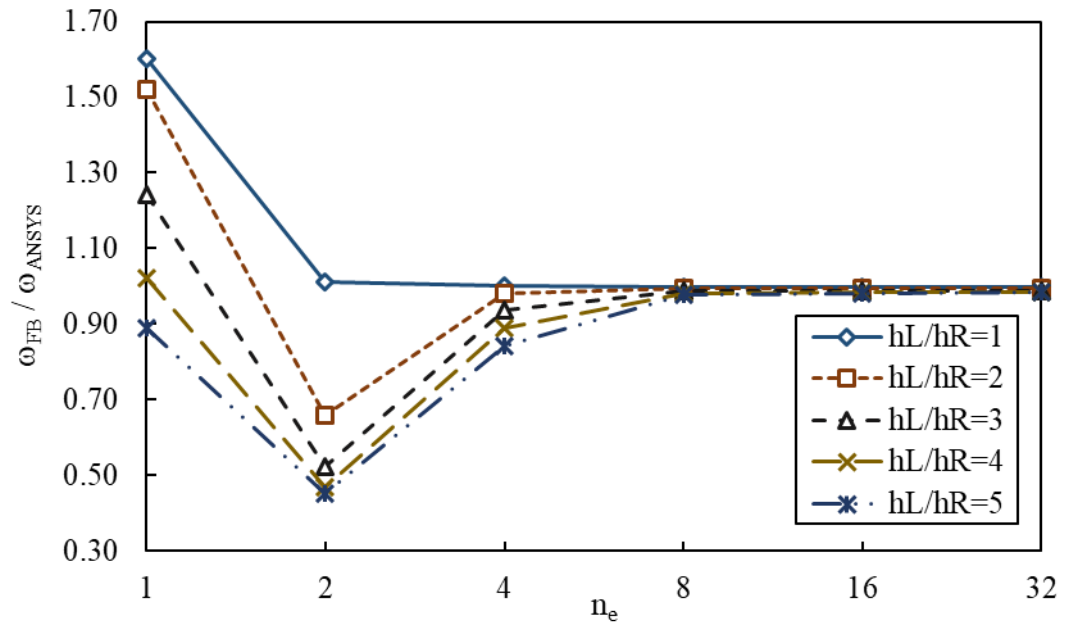


Figure 4.8 The ratio of 2nd bending mode frequency obtained from FB and ANSYS, C-F beam, material steel, with increasing number of elements in the solution

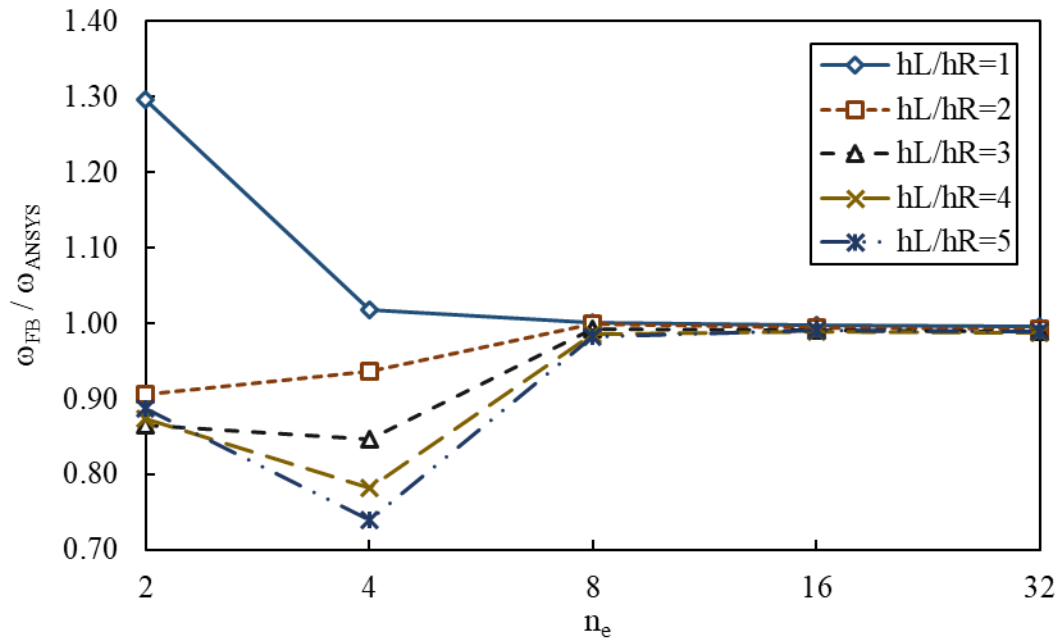


Figure 4.9 The ratio of 3rd bending mode frequency obtained from FB and ANSYS, C-F beam, material steel, with increasing number of elements in the solution

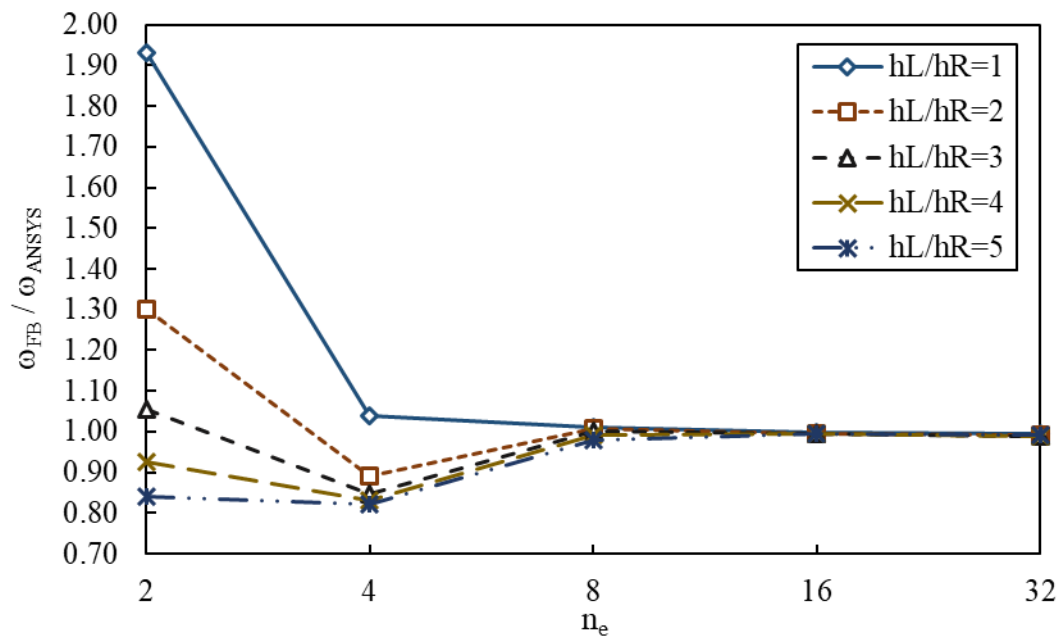


Figure 4.10 The ratio of 4th bending mode frequency obtained from FB and ANSYS, C-F beam, material steel, with increasing number of elements in the solution

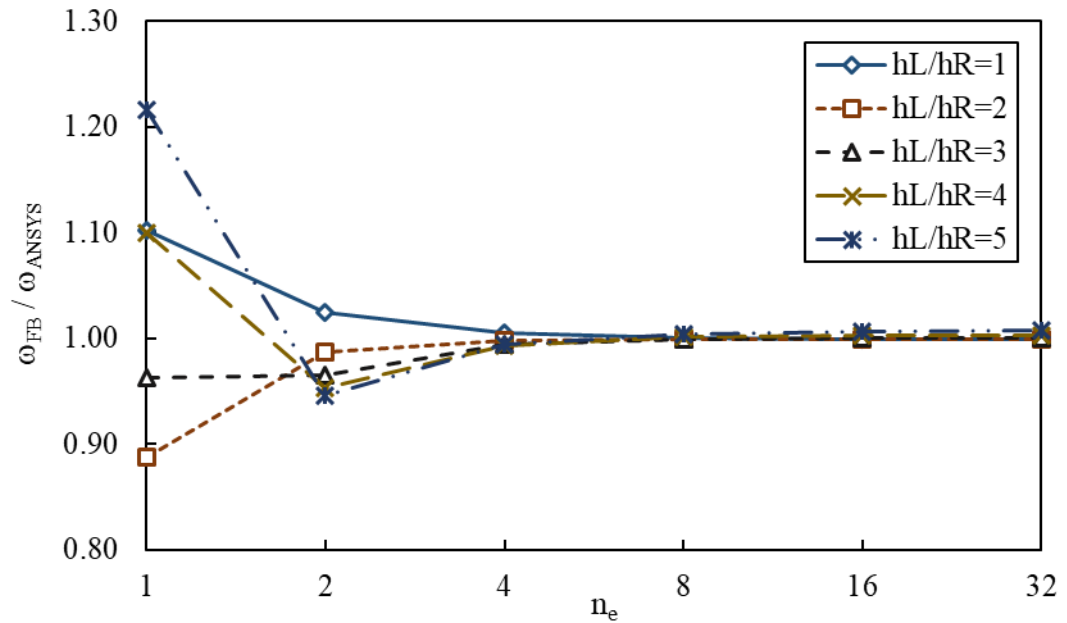


Figure 4.11 The ratio of 1st axial mode frequency obtained from FB and ANSYS, C-F beam, material steel, with increasing number of elements in the solution

In the next section, tapered geometry will be modelled with FGM instead of homogeneous material in another numerical example.

4.2.2 Tapered Geometry with Functionally Graded Materials

In this section, a power law function is used to represent continuous heterogeneous material distribution with FGM along the transverse direction of the beam. Formula for power law is outlined in Equation (2.23) where k stands for the material grading index. The effect of k on the material distribution is provided in Figure 2.7. Power law function is selected with tapered geometry instead of exponential law function because fracture mechanic problems generally prefer the latter one for material variation function e.g. in Kim and Paulino [38], Zhang et al. [39] and Ke et al. [40]. Moreover, Gruzicic and Zhao [41] outlined that from an experimental point of view, it is more applicable to use power law function to provide continuous variation with FGM.

A tapered geometry beam element with FGM in x-z plane is presented in Figure 4.12.

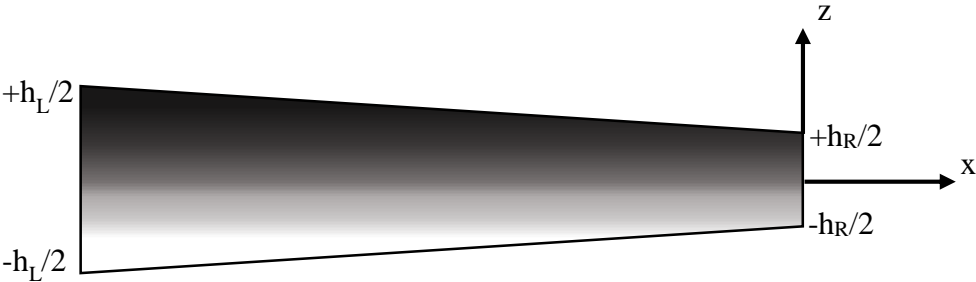


Figure 4.12 A tapered geometry beam element with FGM in x-z plane

The last numerical example on tapered beams with FGM is a novel use of the proposed mixed formulation in the literature.

4.2.2.1 The Eighth Numerical Example

In this example, the frequencies of the higher modes obtained with the proposed method are compared with the numerical results obtained from ANSYS with one boundary condition case, namely the C-F condition. The properties of FGM for the sixth numerical example are tabulated in Table 4.5 where E , ρ , ν , κ_s , k are the Young’s modulus, density, Poisson’s ratio, shear correction factor and the power law coefficient, respectively.

Table 4.5 The properties of the tapered beam element with FGM in particular at the topmost and bottommost materials

Boundary Conditions	Aspect Ratios	FGM Materials		E (GPa)	ρ (kg / m ³)	ν	κ_s
C-F	20 / 10	Top	Alumina	380	3960	0.3	5/6
		Bottom	Aluminum	70	2702		
		$k = 0.5$					

In Table 4.6, the geometric parameters of the tapered beam element with FGM are provided. In this model, the taper ratio i.e. $h_L/h_R = 2$ and the beam depth is linearly decreasing from the left to the right end. Additionally, the same taper ratio is used with two different aspect ratios i.e. $L/h_R = 10$ and 20. As can be seen from Table 4.6, the only changing dimension is the length.

Table 4.6 The geometric parameters of the tapered beam element with FGM

Length (m)	Depth (m)		Taper Ratio
	h_L	h_R	
1	0.2	0.1	2
2			

In order to see the effect of power law coefficient on material variation along transverse direction, it is strongly advised to revisit Figure 2.7. From this figure, it can be seen that the material variation is non-linear, which is more complex than linear distribution i.e. $k = 1$. Moreover, the Poisson's ratio is again taken constant value for both materials since its effect is not significant as explained for the cases with the uniform geometry.

In the modelling phase, the proposed method provides continuous material distribution exactly by the use of the power law formula given in Equation (2.23). However, it is not possible to obtain continuous material variation with ANSYS. In order to overcome this deficit, several number of laminated layers such as 4, 10, 20 are applied to the model in the ANSYS interface. In Figure 4.13, the beam element with 4 laminated layers is presented to demonstrate the variation of the material along the transverse direction of the beam.

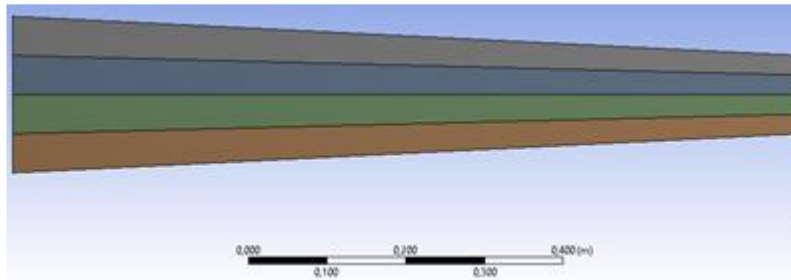


Figure 4.13 The geometric model of ANSYS with 4 laminated layers

At the midpoint of each layer, the material properties are calculated with the equation of the power law function as shown in Table 4.7. It is assumed that the material properties are constant in each layer. The same procedure is applied additionally to 10 and 20 layers; the details of the application are only given for the 4 layer case to provide a clear demonstration of the procedure.

Table 4.7 The Young's modulus and the density values along the transverse direction with $k = 0.5$

	Top	Layer 1	Layer 2	Middle	Layer 3	Layer 4	Bottom
z	75	56.25	18.75	0	-18.75	-56.25	-75
$E(z)$	380	359.978	315.077	289.203	259.835	179.602	70
$\rho(z)$	3960	3878.751	3696.536	3591.540	3472.365	3146.770	2702

During the analysis of the ANSYS model with 20 laminated layers, an error has occurred as a result of the relatively large contact surfaces between laminated layers when $L/h = 20$. This problem is solved by forming a new part from 20 surface bodies and thereupon this tool is applied for 4 and 10 laminated layers. It is noted that the node numbers and the computation times decreased after the forming of new parts.

The frequency information for the higher modes with the C-F beams and aspect ratios of 10 and 20 is tabulated in Table 4.8.

Table 4.8 The frequency information for the higher modes with L/h= 10 and 20

	C-F	
	L/h = 10	L/h = 20
	Axial: A	
	Bending: B	
Mode 1	B	B
Mode 2	B	B
Mode 3	A	B
Mode 4	B	A
Mode 5	B	B

Figures in this example are grouped into three topics. Figure 4.14 focuses on the number of the laminated layers. After this, five higher modes are compared between FB and ANSYS solutions with 20 laminated layers for L/h = 10 and L/h = 20 cases in Figure 4.15 and Figure 4.16, respectively. One of the objectives of this last example is to compare each mode with respect to the aspect ratios.

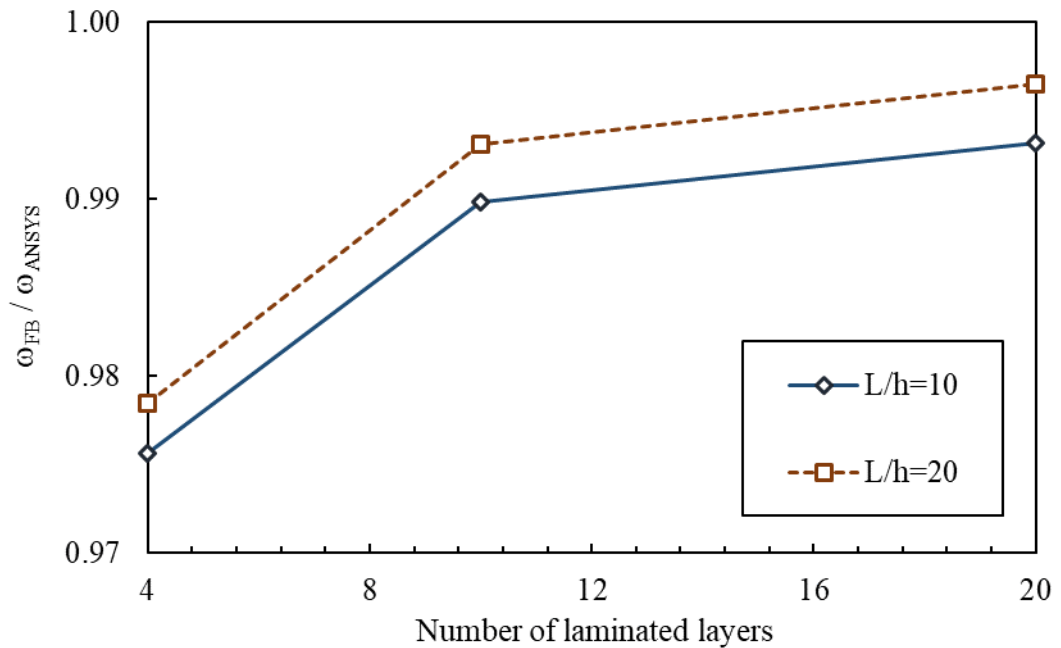


Figure 4.14 The comparison of the fundamental frequency obtained using FB and ANSYS, C-F beam, number of laminated layers 4, 10 and 20

As explained previously, in ANSYS continuous material distribution cannot be defined. As mentioned before, 4, 10 and 20 laminated layers are used in order to see whether the results converge or not. It is seen from Figure 4.14 that the ratio of FB and ANSYS solutions converge close to 1.00. From the results, it can be deduced that the convergence is not complete and if the number of laminated layers is increased in ANSYS, a better agreement would be reached. Additionally, convergence rate is faster with $L/h = 20$ than $L/h = 10$. This finding is consistent with the findings of Chapter 3.

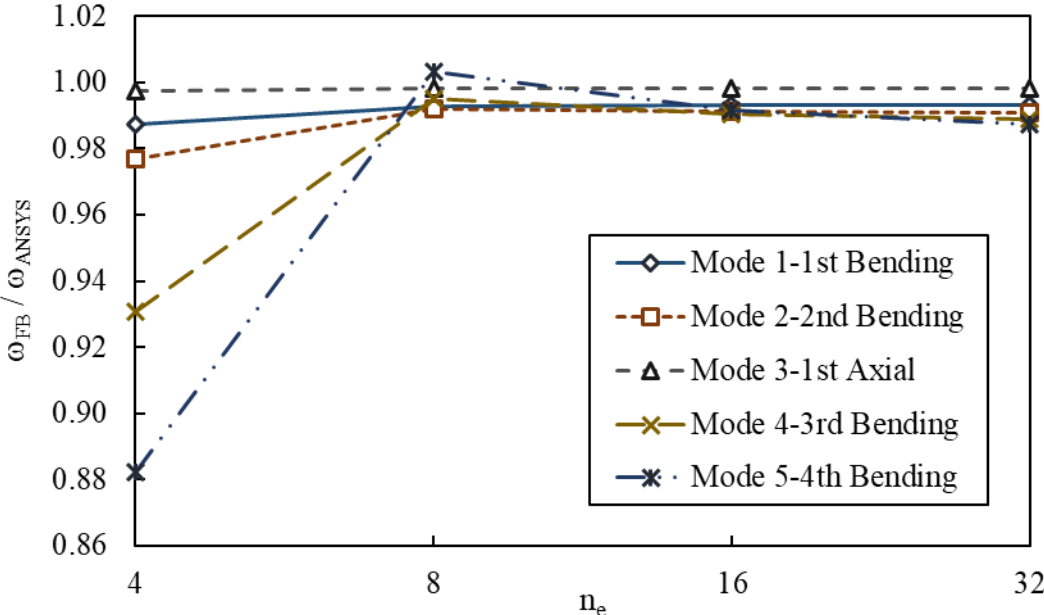


Figure 4.15 The comparison of the frequencies for the higher modes obtained by FB and ANSYS, C-F beam, aspect ratio $L/h = 10$, number of laminated layers 20

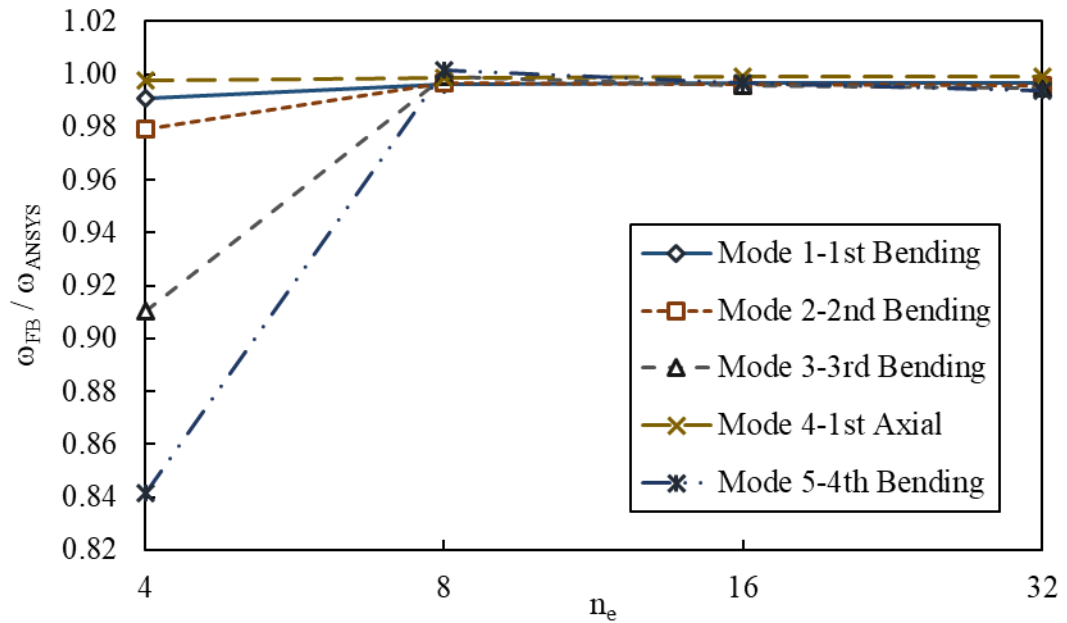


Figure 4.16 The comparison of the frequencies for the higher modes obtained by FB and ANSYS, C-F beam, aspect ratio $L/h = 20$, number of laminated layers 20

The comparison between the results of FB and ANSYS is presented separately for each mode from Figures 4.17 to 4.21. It is observed that especially for the higher modes, the ratios reach very close to 1.00 with eight elements. However, with increased number of elements, the ratios diverge slowly away from 1.00. It is more difficult to capture exact behavior for the higher modes due to the effects of the boundary conditions. Most likely the results from ANSYS are not as accurate as the homogeneous case yielding this trend in the ratios.

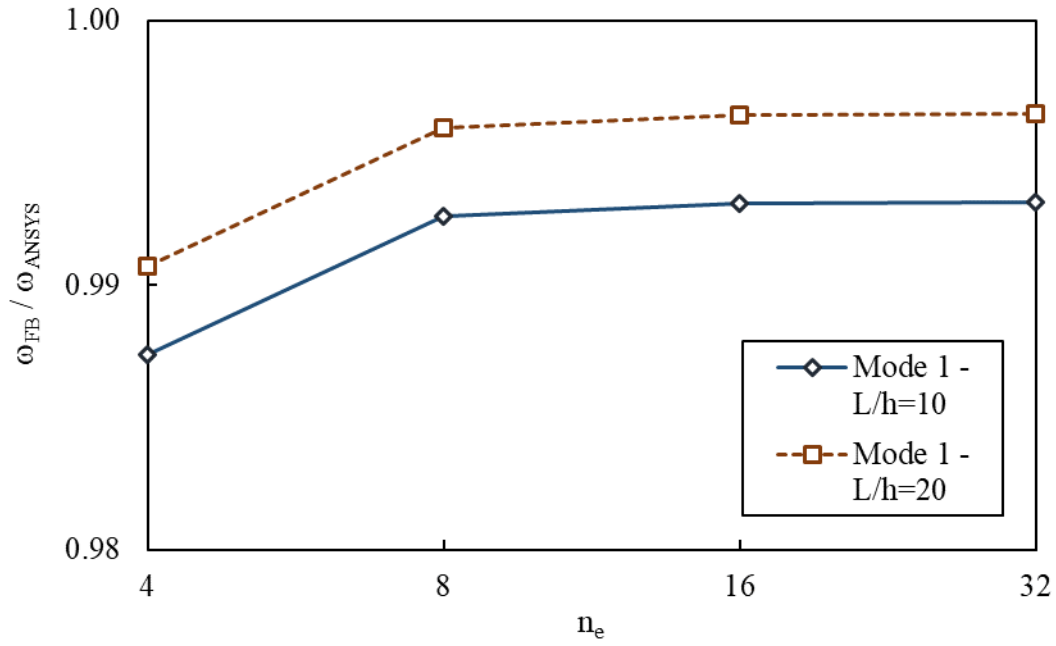


Figure 4.17 The ratio of 1st bending mode frequency obtained from FB and ANSYS, C-F beam, number of laminated layers 20

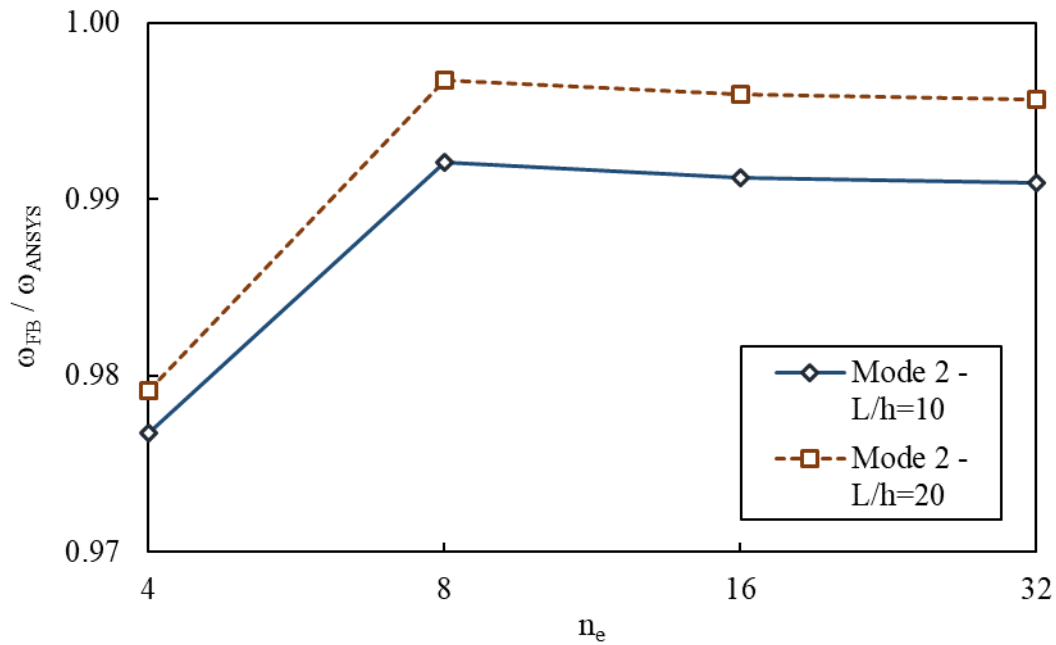


Figure 4.18 The ratio of 2nd bending mode frequency obtained from FB and ANSYS, C-F beam, number of laminated layers 20

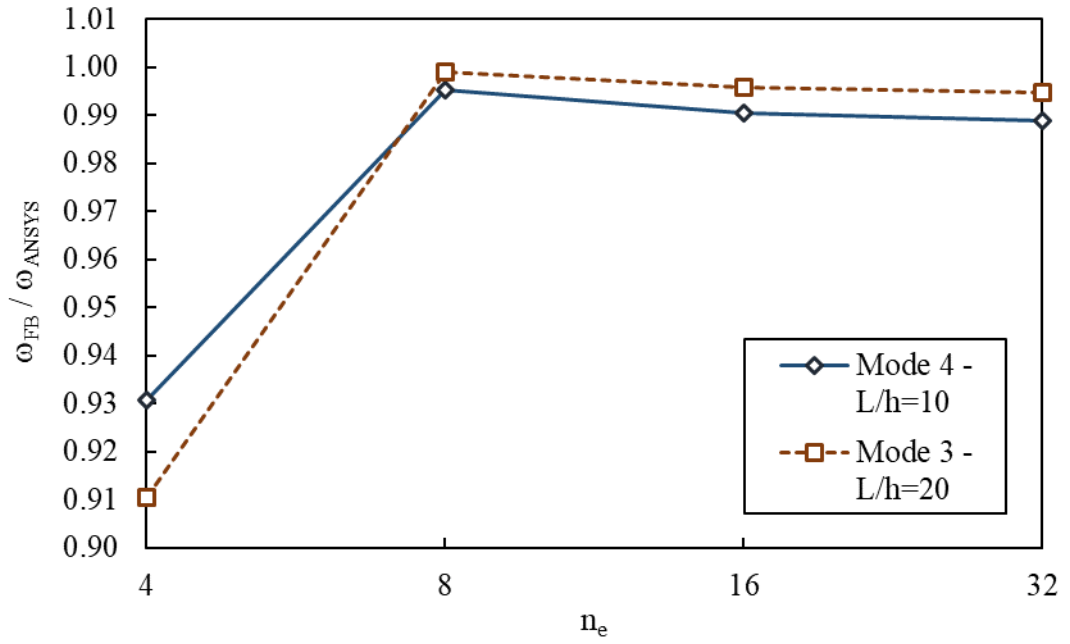


Figure 4.19 The ratio of 3rd bending mode frequency obtained from FB and ANSYS, C-F beam, number of laminated layers 20

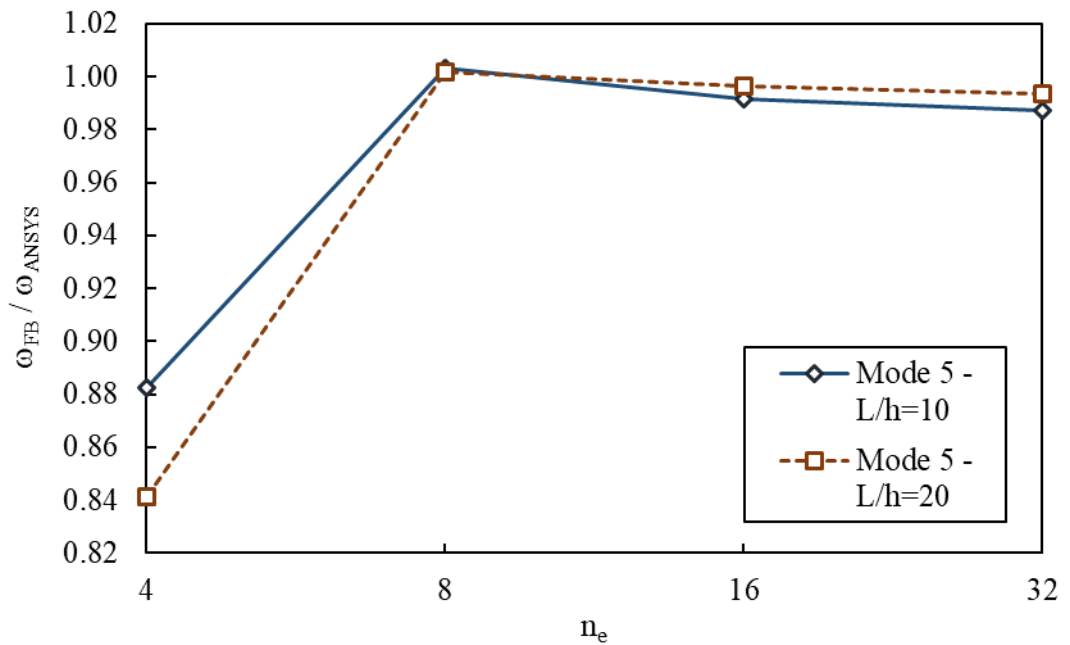


Figure 4.20 The ratio of 4th bending mode frequency obtained from FB and ANSYS, C-F beam, number of laminated layers 20

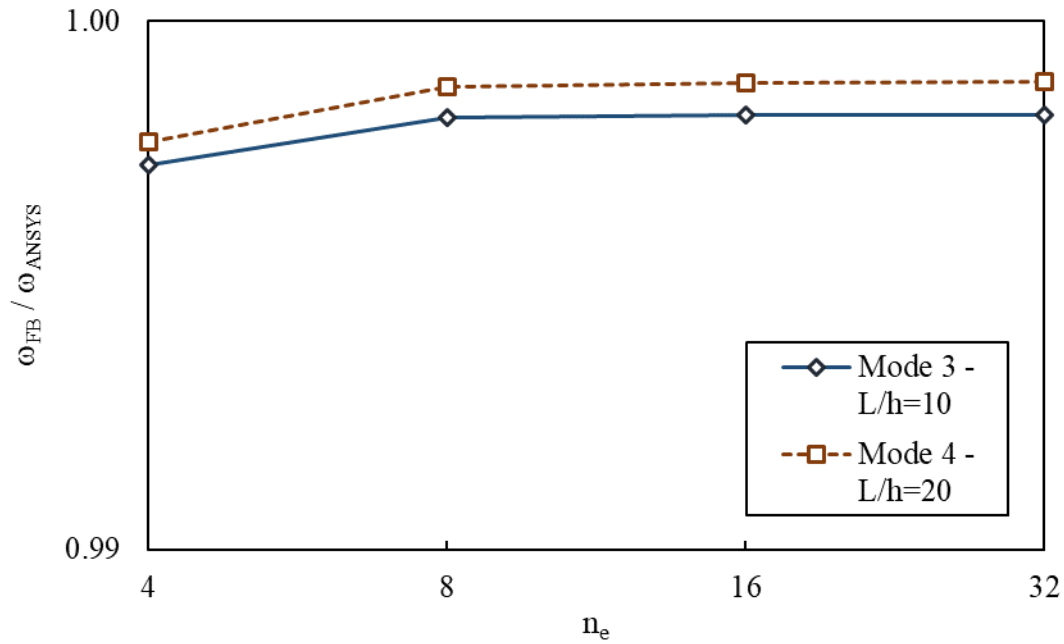


Figure 4.21 The ratio of 1st axial mode frequency obtained from FB and ANSYS, C-F beam, number of laminated layers 20

The frequencies for the first five modes obtained using FB method and ANSYS solution for the tapered geometry beam made of FGM with the C-F condition are presented for two aspect ratios 10, 20, respectively, in Table 4.9 and Table 4.10.

Table 4.9 The frequencies obtained using FB and ANSYS, C-F beam, material FGM, aspect ratios $L/h_R = 10$, taper ratio $h_L / h_R = 2$, power law coefficient $k = 0.5$

		L/h = 10							
		ANSYS			FB				
Axial: A		Number of laminated layers			Number of elements				
Bending: B		4	10	20	4	8	16	32	64
Mode 1	B	293.50	289.28	288.32	284.67	286.19	286.33	286.35	286.35
Mode 2	B	1293.50	1277.40	1273.70	1244.08	1263.60	1262.53	1262.18	1262.11
Mode 3	A	2533.40	2529.10	2528.10	2521.25	2523.51	2523.64	2523.63	2523.63
Mode 4	B	2995.80	2964.70	2957.10	2751.87	2942.77	2928.76	2924.15	2923.08
Mode 5	B	5099.90	5055.30	5044.00	4450.80	5060.50	5001.72	4980.04	4974.71

Table 4.10 The frequencies obtained using FB and ANSYS, C-F beam, material FGM, aspect ratios $L/h_R = 20$, taper ratio $h_L / h_R = 2$, power law coefficient $k = 0.5$

		L/h = 20							
		ANSYS			FB				
		Number of laminated layers			Number of elements				
Axial: A		4	10	20	4	8	16	32	64
Bending: B		4	10	20	4	8	16	32	64
Mode 1	B	74.44	73.34	73.09	72.42	72.80	72.83	72.83	72.83
Mode 2	B	348.47	343.45	342.42	335.28	341.30	341.02	340.94	340.93
Mode 3	B	867.84	855.75	853.64	777.26	852.83	850.05	849.12	848.94
Mode 4	A	1266.10	1263.90	1263.30	1260.41	1261.74	1261.84	1261.84	1261.84
Mode 5	B	1586.70	1565.50	1562.70	1314.98	1565.36	1557.19	1552.85	1551.93

CHAPTER 5

CONCLUSIONS

5.1 SUMMARY

In this thesis, force based finite element approach for beam elements with Timoshenko beam theory was verified with eight numerical examples focused on the solution of free vibration problem for beams. For verification, uniform and tapered geometries were considered separately with homogeneous material and transversely distributed FGM. The results from the proposed method were compared to two different sources including previous research results in the literature and numerical results obtained with ANSYS. Higher mode results were also compared along with the fundamental frequency. For the benchmark results; well cited works by Şimşek [32], Sina et al. [33] and Li [34], which show a wide range of results on linear elastic free vibration properties of beams with different parametric conditions including FGM cases, were used. The results of previous studies, ANSYS and the proposed formulation are all approximate values obtained by using different methods and assumptions, however, they are all compatible. MATLAB was used as a tool to perform numerical and symbolic analyses of the proposed mixed formulation.

The verification of the proposed formulation for uniform geometry as given in Soydaş [3] was considered insufficient given the benchmark cases (Leissa [5], Leissa and So [6], Leissa and Zhang [7]) were limited. In this study, additional verification of the mixed formulation beam element with tapered geometry for homogeneous material was provided by using numerical results obtained from ANSYS. A validation of the FB method has not been conducted at all for beams with FGM, especially with regards

to the accuracy of this approach compared to the benchmark results. It was validated for the first time with FGM in this study.

Various parametric studies for the beam finite element were carried out in the numerical examples for different element numbers, boundary conditions, material non-homogeneity coefficients, aspect ratios, taper ratios and different laminated layers. The outcomes of mesh refinement options in ANSYS were also investigated as another parametric study to emphasize the importance of the mesh discretization process since a model is as good as how the mesh refinement of a model represents the real life cases.

5.2 CONCLUSIONS

The following conclusions can be drawn from this thesis:

- The fundamental frequency and the frequency of the higher modes obtained by the proposed mixed formulation were compared with the numerical results available in the literature and with vibration frequencies obtained from modelling in ANSYS. The results of the proposed method for uniform or tapered geometries with homogeneous material or transversely distributed FGM were in good agreement with both results. Consequently, it was concluded that even for the most challenging scenario i.e. tapered geometry with FGM, the proposed formulation provided an accurate and robust solution when the number of elements of the proposed method was selected wisely.
- In the numerical examples, it was observed that the results with four FB finite elements compared well with respect to the benchmark cases. However, the use of eight elements provided a very good agreement with the benchmark results in general.

- The prediction of the 1st bending and 1st axial modes using the FB elements quickly converged to the benchmark values with a few number of elements, and more accurately than the frequencies of the higher modes. The higher modes were obtained with slightly higher deviation as it is much more difficult to capture the behavior of the higher modes because of the effects of boundary conditions.
- Three different boundary conditions were used in the numerical examples. The most precise results were obtained for the S-S beam condition when compared with the other boundary conditions. On the other hand, C-C beam was the case in which the least precise results were obtained, especially when the proposed method was compared with results of ANSYS. This difference stems from the fact that the aforementioned software provides the exact fixity using the clamped boundary conditions, while the proposed beam elements only applies fixity on a single point at the support. In addition to this, the constant shear deformation assumption of the Timoshenko beam theory provides an additional difficulty because the ANSYS model with multiple elements along the depth represents real beam characteristics better than the proposed method. Thus, for the short and deep beams, the results of the FB solution are somewhat less close to the ANSYS results.
- When the aspect ratio was small i.e. for the thick beams, it was difficult to catch a perfect match of frequencies with the proposed methodology. This shortcoming also occurs due to the assumption of the proposed beam element providing fixity on a single point at the end and the limitation of the Timoshenko beam theory. When thick beams are considered, the boundary condition effects become more significant. When the C-C beam condition and a small aspect ratio are considered together, the effects of boundary condition reach a maximum value.
- For tapered geometry, taper ratio, which was selected as the ratio between depth on the left side to the depth on the right side, was studied as a new parameter. C-

F was the boundary condition in the analysis. When the taper ratio increased, the beam behaves similar to a short and deep beam and therefore the convergence of the FB solution to the benchmark counterpart decreased.

- Power law coefficient that represents the change rate in FGM was also considered with three boundary conditions and different aspect ratios as another parametric study. When the number of elements were increased, the frequencies obtained using the proposed method found a good agreement with the results of ANSYS and previous research in the literature.

5.3 FUTURE RESEARCH DIRECTIONS

The following directions are suggested for future research.

- This thesis was focused on only transversely FGM. The proposed method can also be integrated with axially FGM. This will be the first use of the proposed method not only for tapered geometry but also for uniform geometry beams with axially FGM.
- In addition to the uniform geometry, tapered geometry was also analyzed in this thesis. It is also possible to extend the applications of mixed formulation to double tapered geometry or other complex cases.
- Implementation of porosity distribution in the member, instead of different material variations, along with possible inclusion of reinforcement by nanofillers as a functionally graded material can also be analyzed with use of the proposed method.

- Last but not the least, application areas of the proposed formulation can be extended to include other important mechanical problems such as beams resting on elastic foundations.

BIBLIOGRAPHY

- [1] R. M. Mahamood and E. T. Akinlabi, *Functionally Graded Materials*. Cham: Springer International Publishing, 2017.
- [2] D. K. Jha, T. Kant, and R. K. Singh, “A critical review of recent research on functionally graded plates,” *Compos. Struct.*, vol. 96, pp. 833–849, Feb. 2013.
- [3] O. Soydaş, “A Three Dimensional Mixed Formulation Nonlinear Frame Finite Element Based on Hu-Washizu Functional,” Middle East Technical University, 2013.
- [4] T. Gürol, “Finite Element Modeling of Beams with Functionally Graded Materials,” Middle East Technical University, 2014.
- [5] A. W. Leissa, “Comparisons of vibration frequencies for rods and beams from one-dimensional and three-dimensional analyses,” *J. Acoust. Soc. Am.*, vol. 98, no. 4, pp. 2122–2135, 1995.
- [6] A. W. Leissa and J. So, “Accurate vibration frequencies of circular cylinders from three-dimensional analysis,” *J. Acoust. Soc. Am.*, vol. 98, no. 4, pp. 2136–2141, 1995.
- [7] A. Leissa and Z. Zhang, “On the three-dimensional vibrations of the cantilevered rectangular parallelepiped,” *J. Acoust. Soc. Am.*, vol. 73, no. 6, pp. 2013–2021, Jun. 1983.
- [8] M. A. K. M. Dharmasiri, K. K. Wijesundara, A. J. Dammika, and P. B. R. Dissanayake, “Free vibration characteristics of a 2D tapered beam using force-based finite element formulation,” *Int. Res. Symp. Eng. Adv.*, vol. 2016, no. Irsea, pp. 8–11, 2016.
- [9] F. Tornabene, E. Viola, and D. J. Inman, “2-D differential quadrature solution for vibration analysis of functionally graded conical, cylindrical shell and annul plate structures,” *J. Sound Vib.*, vol. 328, no. 3, pp. 259–290, 2009.

- [10] P. Zhu, Z. X. Lei, and K. M. Liew, “Static and free vibration analyses of carbon nanotube-reinforced composite plates using finite element method with first order shear deformation plate theory,” *Compos. Struct.*, vol. 94, no. 4, pp. 1450–1460, 2012.
- [11] R. C. Batra and J. Jin, “Natural frequencies of a functionally graded anisotropic rectangular plate,” *J. Sound Vib.*, vol. 282, no. 1–2, pp. 509–516, 2005.
- [12] G. J. Nie and Z. Zhong, “Semi-analytical solution for three-dimensional vibration of functionally graded circular plates,” *Comput. Methods Appl. Mech. Eng.*, vol. 196, no. 49–52, pp. 4901–4910, 2007.
- [13] D. Chen, J. Yang, and S. Kitipornchai, “Free and forced vibrations of shear deformable functionally graded porous beams,” *Int. J. Mech. Sci.*, vol. 108–109, pp. 14–22, 2016.
- [14] M. Liu, Y. Cheng, and J. Liu, “High-order free vibration analysis of sandwich plates with both functionally graded face sheets and functionally graded flexible core,” *Compos. Part B Eng.*, vol. 72, pp. 97–107, 2015.
- [15] A. Saritaş, T. Gürol, and O. Soydaş, “Hybrid finite element for analysis of functionally graded beams,” *Mech. Adv. Mater. Struct.*, vol. 24, no. 3, pp. 228–239, Feb. 2017.
- [16] J. N. Reddy, “A simple higher-order theory for laminated composite plates,” *J. Appl. Mech.*, vol. 51, no. 4, pp. 745–752, 1984.
- [17] J. N. Reddy, “On locking-free shear deformable beam finite elements,” *Comput. Methods Appl. Mech. Eng.*, vol. 149, no. 1–4, pp. 113–132, Oct. 1997.
- [18] A. Saritaş and O. Soydaş, “Variational base and solution strategies for non-linear force-based beam finite elements,” *Int. J. Non. Linear. Mech.*, vol. 47, no. 3, pp. 54–64, 2012.
- [19] R. L. Taylor, F. C. Filippou, A. Saritaş, and F. Auricchio, “A mixed finite element method for beam and frame problems,” *Comput. Mech.*, vol. 31, no. 1–2 SPEC., pp. 192–203, 2003.
- [20] A. Saritaş and F. C. Filippou, “Inelastic axial-flexure-shear coupling in a mixed formulation beam finite element,” *Int. J. Non. Linear. Mech.*, vol. 44, no. 8, pp.

913–922, 2009.

- [21] C. Molins, P. Roca, and A. H. Barbat, “Flexibility-Based Linear Dynamic Analysis of Complex Structures With Curved-3D Members,” vol. 747, no. December 1996, pp. 731–747, 1998.
- [22] S. Suresh and A. Mortensen, *Fundamentals of functionally graded materials*, 1st ed. London: IOM Communications, 1998.
- [23] A. J. Markworth, K. S. Ramesh, and W. P. Parks, “Modelling studies applied to functionally graded materials,” *J. Mater. Sci.*, vol. 30, no. 9, pp. 2183–2193, 1995.
- [24] A. Chakraborty, S. Gopalakrishnan, and J. N. Reddy, “A new beam finite element for the analysis of functionally graded materials,” *Int. J. Mech. Sci.*, vol. 45, no. 3, pp. 519–539, Mar. 2003.
- [25] Y. Huang and X. F. Li, “A new approach for free vibration of axially functionally graded beams with non-uniform cross-section,” *J. Sound Vib.*, vol. 329, no. 11, pp. 2291–2303, 2010.
- [26] A. Sutradhar and G. H. Paulino, “The simple boundary element method for transient heat conduction in functionally graded materials,” *Comput. Methods Appl. Mech. Eng.*, vol. 193, no. 42–44, pp. 4511–4539, 2004.
- [27] Y. L. Chung and S. H. Chi, “The residual stress of functionally graded materials,” *J. Chinese Inst. Civ. Hydraul. Eng.*, vol. 13, pp. 1–9, 2001.
- [28] O. Soydaş and A. Sarıtaş, “Free vibration characteristics of a 3d mixed formulation beam element with force-based consistent mass matrix,” *J. Vib. Control*, vol. 23, no. 16, pp. 2635–2655, Sep. 2017.
- [29] H. F. Özel, A. Sarıtaş, and T. Tasbahji, “Consistent matrices for steel framed structures with semi-rigid connections accounting for shear deformation and rotary inertia effects,” *Eng. Struct.*, vol. 137, pp. 194–203, Apr. 2017.
- [30] “MATLAB, Release R2016b, User’s Guide.” The MathWorks, Inc.
- [31] “ANSYS Workbench, Release 17.2, Help System.” ANSYS, Inc.
- [32] M. Şimşek, “Fundamental frequency analysis of functionally graded beams by

- using different higher-order beam theories,” *Nucl. Eng. Des.*, vol. 240, no. 4, pp. 697–705, 2010.
- [33] S. A. Sina, H. M. Navazi, and H. Haddadpour, “An analytical method for free vibration analysis of functionally graded beams,” *Mater. Des.*, vol. 30, no. 3, pp. 741–747, 2009.
- [34] X. F. Li, “A unified approach for analyzing static and dynamic behaviors of functionally graded Timoshenko and Euler-Bernoulli beams,” *J. Sound Vib.*, vol. 318, no. 4–5, pp. 1210–1229, 2008.
- [35] D. N. Manik, *Vibro-Acoustics: Fundamentals and Applications*. CRC Press, 2017.
- [36] F. Delale, F., Erdoğan, “The Crack Problem for a Nonhomogeneous Plane,” *J. Appl. Mech.*, vol. 50, no. September 1983, pp. 609–614, 1983.
- [37] H. J. Xiang and J. Yang, “Free and forced vibration of a laminated FGM Timoshenko beam of variable thickness under heat conduction,” *Compos. Part B Eng.*, vol. 39, no. 2, pp. 292–303, 2008.
- [38] J.-H. Kim and G. H. Paulino, “Finite element evaluation of mixed mode stress intensity factors in functionally graded materials,” *Int. J. Numer. Methods Eng.*, vol. 53, no. 8, pp. 1903–1935, Mar. 2002.
- [39] C. Zhang, A. Savaidis, G. Savaidis, and H. Zhu, “Transient dynamic analysis of a cracked functionally graded material by a BIEM,” *Comput. Mater. Sci.*, vol. 26, no. SUPPL., pp. 167–174, 2003.
- [40] L.-L. Ke, J. Yang, S. Kitipornchai, and Y. Xiang, “Flexural Vibration and Elastic Buckling of a Cracked Timoshenko Beam Made of Functionally Graded Materials,” *Mech. Adv. Mater. Struct.*, vol. 16, no. 6, pp. 488–502, 2009.
- [41] M. Grujicic and H. Zhao, “Optimization of 316 stainless steel/alumina functionally graded material for reduction of damage induced by thermal residual stresses,” *Mater. Sci. Eng.*, vol. 252, no. 1, pp. 117–132, 1998.